UNIVERSITA' DEGLI STUDI DI TORINO

DEPARTMENT OF VETERINARY SCIENCE

RESEARCH DOCTORATE IN VETERINARY SCIENCE FOR ANIMAL HEALTH AND FOOD SAFETY

CYCLE: XXXVI

THESIS TITLE

CEREBROSPINAL FLUID AS A TOOL TO IMPROVE DIAGNOSIS AND TREATMENT IN BOVINE NEUROLOGY

THESIS' AUTHOR: DOCT. SARA FERRINI

SUPERVISOR: PROF. ANTONIO D'ANGELO

PHD PROGRAMME CO-ORDINATOR: PROF. MARIA TERESA CAPUCCHIO

ACADEMIC YEARS OF ENROLLMENT: 2020-2023

CODE OF SCIENTIFIC DESCIPLINE: VET/08 – VETERINARY CLINICAL MEDICINE

Table of Contents

ABBREVIATIONS

AC = albuminocytologic
AST = aspartate transaminase
ASV = amplicon sequence variant
ATP = adenosine triphosphate
AUC = area under curve
AUROC = receiver operating characteristicarea under curve
BAL = bronchioalveolar lavage
BLAST = basic local alignment search tool
CI = confidence interval
CK = creatine kinase
CL = confidence level
CN = cranial nerve
CNS = central nervous system
CP = choroid plexus
CSF = cerebrospinal fluid
CVO = circumventricular organs
DNA = deoxyribonucleic acid
ETC = electron transport chain
FAD = flavin adenine dinucleotide
Fn = false negative
Fp = false positive
GABA = ɤ-aminobutyric acid
GB = gradient boosting
GTP = guanosine triphosphate
H2O2 = hydrogen peroxide
ICH = immunohistochemistry
ICP = intracranial pressure
INF = infectious-inflammatory
IQR = interquartile range
KNN = k-nearest neighbors
LDH = lactate dehydrogenase
LR = logistic regression
MCT = monocarboxylate transporter
ML = machine learning
MLP = multilayer perceptron
MUO = meningoencephalitis of unknown origin
N = total subjects
NADH = reduced nicotinamide adenine dinucleotide
NAD+ = oxidized nicotinamide adenine dinucleotide
NADPH = reduced nicotinamide adenine dinucleotide phosphate
NBSM = neonatal bacterial suppurative meningitis
NBSM-ME = neonatal bacterial suppurative meningitis-meningoencephalitis
NCBI = national center for biotechnology information
NETs = neutrophil extracellular traps
NGS = next generation sequencing
NL = neurolocalization
NON INF = noninfectious-inflammatory
NSAID = non-steroidal anti-inflammatory drug
OMI = otitis media/interna
OTU = operational taxonomic unit
PCR = polymeare chain reaction
PE = paired – end
PERMANOVA = permutational multivariate analysis of variance
PL = pleocytosis
QIIME = quantitative insights into microbial ecology
RBCC = red blood cell count
RF = random forest
RI= reference interval
RNA = ribonucleic acid
ROC = receiver operating characteristic
rRNA = ribosomial ribonucleic acid
SAS = subarachnoid space
SD = standard deviation
SEM = standard error of the mean
SFR = sample-to-feature ratio
SOP = standard operating procedure
SVM = support vector machine
TCA = tricarboxylic acid
TEM = thromboembolic meningoencephalitis
Tn = true negative
TNCC = total nucleated cell count
TLR = toll-like receptors
Tp = true positive
TP = total protein
VTH = veterinary teaching hospital

Abstract

Achieving an etiological diagnosis in bovine central nervous system (CNS) infection is challenging. Cerebrospinal fluid (CSF) analysis in infection shows changes that are not specific. The timely analysis of CSF is essential, yet it is subject to operator proficiency and requires specialized facilities. Furthermore, bacterial identification in CNS infection relies on CSF culture, which lacks sensitivity. To address these limitations, pioneering approaches might hold potential. Machine learning (ML) is revolutionizing disease diagnosis. Next-generation sequencing (NGS) could bypass the need for CSF culture. CSF lactate is recognized in humans as a CNS infection biomarker. Lastly, automated CSF analysis could be an alternative to labor-intensive manual analysis.

Based on these premises, we developed 4 projects (P1, P2, P3, P4) exploiting these pioneering approaches applied to analysis of bovine CSF.

P1 compared ML models to predict the likelihood of CNS infection in cattle. We created a ML based web app for infection diagnosis. ML methods were trained on demographics, clinical findings and CSF analysis. P2 exploited 16S rRNA sequencing to compare the CSF microbial composition in cattle with CNS infection and other CNS disorders. P3 established a Reference Interval (RI) for CSF lactate and assessed its potential as a biomarker for detecting CNS infection. Statistical analysis was performed to demonstrate an association between CSF lactate levels and interpretation of CSF in sick animals. P4 assessed the Idexx ProCyte Dx® analyzer's capability in analyzing CSF in cattle. We investigated the instrument's performance in delivering total (TNCC) and differential cell count compared to the gold standard laboratory analysis.

P1: 98 cattle with CNS infection and 86 with other CNS disorders were included. All methods had high prediction accuracy (≥80%). Logistic regression had the highest accuracy (0.84) and was implemented in a web app.

P2: an infectious-inflammatory (n = 3) and a non infectious-inflammatory group (n = 3) were formed. There were no detectable differences in the CSF microbial composition of the samples from the two groups. *Pseudomonas spp*. (45%) was the most frequently expressed bacterial genus.

P3: 27 healthy and 86 sick cattle with CNS disorders were included. The RI for CSF lactate was 1.1-2.4 mmol/L. The highest lactate level was found with neutrophilic pleocytosis (median = 7; $p < .0001$).

P4: CSF was collected from 113 cattle, 76 with normal TNCC and 37 with increased TNCC. Procyte Dx® TNCC correlated well with the laboratory TNCC (rho = 0.89; $p < .01$) while could not provide a differential count.

With the thesis presented here we investigated and developed several novel methodological approaches to improve CSF analysis in infectious and non-infectious CNS disorders in cattle. We investigated the potential of novel computational and technical modalities for diagnosis including a prediction web app using ML and identification of CSF lactate as an inflammatory biomarker. Challenges such as distinguishing microbial communities in CSF and performing a complete automated CSF analysis remain, and the work described here will form the basis for future studies.

INTRODUCION

1 Ventricular system anatomy

1.1 Introduction

The ventricular system of the brain is an interconnected series of cavities filled with cerebrospinal fluid (CSF) that cushions the brain and that extend caudally into the ependymal canal, located within the spinal cord. Within this system, CSF is produced and circulates (1). Two lateral ventricles are located in the cerebral hemispheres of the telencephalon and communicate by way of two interventricular foramina with the third ventricle, a ring-shaped cavity surrounding the thalamus. The third ventricle continues caudally through a narrow canal known as the mesencephalic aqueduct or Sylvian aqueduct (1). The mesencephalic aqueduct connects the third ventricle to the fourth ventricle, positioned between the cerebellum above and pons and medulla oblongata below. The fourth ventricle continues with the ependymal canal of the spinal cord and communicates with the subarachnoid space (SAS) through two lateral recesses that leads to lateral apertures (1).

1.2 Embryogenesis

The ventricular system in the brain originates from the internal cavity of the neural tube during embryonic development. In domestic animals, this embryonic structure forms around the third week of development through the elevation and subsequent fusion of the lateral margins of the neural plate, a process known as primary neurulation. The closure of the neural tube is not simultaneous across the embryo. Fusion initiates initially at the level that will eventually form the medulla oblongata (the most caudal part of the brainstem) and progresses cranial and caudal. Initially, the neural tube closure is incomplete, leaving two openings at the cranial and caudal ends, known as the anterior and posterior neuropores, respectively (1). The rostral neuropore closes early in development while the caudal

neuropore closes later. After closure, the cranial portion of the neural tube dilates to form the three primitive brain vesicles: prosencephalon, mesencephalon, and rhombencephalon. The caudal portion gives rise to the spinal cord. The neural tube is initially lined with pseudostratified columnar neuroepithelial cells. Subsequently, these cells undergo mitotic reproduction, resulting in the formation of a multilayered tube with three concentric layers. The innermost layer consists of ependymal cells, which remain in contact with the central lumen of the neural tube and act as the lining for the future ventricular system and ependymal canal. Some of these ependymal cells migrate outward and transform into two types of precursor cells: neuroblasts and glioblasts. Neuroblasts give rise to neurons and form the mantle layer, which ultimately contributes to the formation of the gray matter in the central nervous system (CNS). These neuroblasts extend cytoplasmic extensions laterally, creating the marginal layer, which plays a crucial role in the development of the white matter of the neural tube. Conversely, glioblasts differentiate into astrocytes and oligodendrocytes. Astrocytes are present in both the mantle and marginal layers, while oligodendrocytes are more concentrated in the marginal layer (2). Subsequently, the primitive brain vesicles differentiate into definitive brain regions: the prosencephalon divides into the telencephalon and diencephalon, the mesencephalon remains undivided, and the rhombencephalon divides into the metencephalon and myelencephalon. Concurrently, the internal cavities of these structures develop into the ventricular system. To complete their development, the formation of choroid plexuses (CPs) at the level of the lateral, third, and fourth ventricles is crucial. These CPs will be the primary sites of CSF formation. From an embryonic standpoint, these structures originate through the invagination of the choroidal tela. This invagination arises from the adhesion between the pia mater, the meningeal layer adjacent to the brain and spinal cord, and a thin layer of ependymal cells, along with their associated blood capillaries (1).

1.3 Lateral Ventricles

The lateral ventricles are two c-shaped cavities, one on each side of cerebral hemisphere. Each ventricle can be divided into three distinct regions: a central body that communicates with the third ventricle via an interventricular foramen or Monro foramen, a rostral horn that extends as a narrow duct towards the olfactory bulb via the olfactory peduncle, and a ventral or temporal horn that develops within the corresponding lobe (Figure 1-2) (3).

1.4 Third Ventricle

The third ventricle is a median structure separating the right and left halves of the diencephalon. When viewed laterally, its shape appears irregularly circular as it develops around the interthalamic adhesion and contains several recesses. In the ventral portion, three recesses can be identified: the optic recess, between the optic chiasm and the lamina terminalis; the infundibular recess, located within the infundibulum of the neurohypophysis; and the infra-mamillary recess, rostroventral to the mamillary bodies (3). Two additional recesses, the suprapineal and pineal recesses, are found on the vault of the third ventricle, located respectively rostrally and caudally to the pineal gland (4). The rostral wall of the third ventricle is formed by lamina terminalis while the roof is formed by tela choriodea that gives rise to CPs (3). The third ventricle communicates caudally with the mesencephalic aqueduct and bilaterally with the lateral ventricles through the interventricular foramina. The mesencephalic aqueduct is a tubular structure that is narrower cranially and wider caudally, running longitudinally through the midbrain and connecting the third ventricle to the fourth ventricle (Figure 1-2) (1,3).

1.5 Fourth Ventricle

The fourth ventricle is a rhomboid-shaped chamber that develops above the pons and the medulla oblongata. The floor of the fourth ventricle, also known as rhomboid fossa, has a

ventral longitudinal groove called the median sulcus. Bilaterally, a sulcus limitans marks the transition from floor to wall. The fourth ventricle's roof is formed by the tela choroidea, called "tenia of the fourth ventricle". This structure extends rostrally with the rostral medullary velum and caudally with the caudal medullary velum, where the CPs of the fourth ventricle develop (3). The majority of the CSF present in the fourth ventricle flows outward to the SAS, exiting the fourth ventricle bilaterally through a lateral recess that leads to a lateral aperture. The recess and aperture are located immediately caudal to the caudal cerebellar peduncle. Only a small fraction of CSF enters the ependymal canal (Figure 1-2) (3).

Figure 1: Ventricular system of the brain. The direction of the arrows indicates the flow of cerebrospinal fluid (from "Veterinary Neuroanatomy and Clinical Neurology" by de Lahunta A, Glass E, Kent M, 2021).

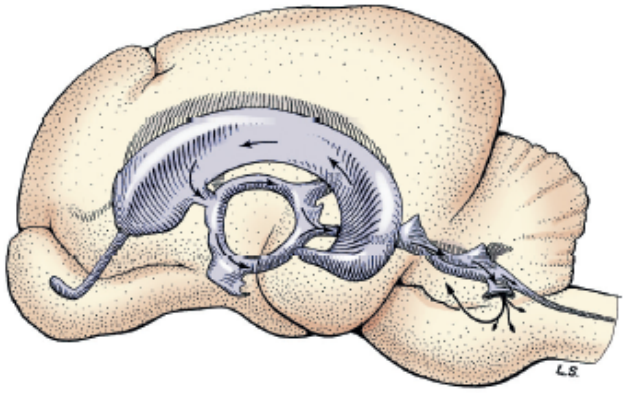

Figure 2: Ventricular system, dorsal-ventral view (from "Veterinary Neuroanatomy and Clinical Neurology" by de Lahunta A, Glass E, Kent M, 2021)

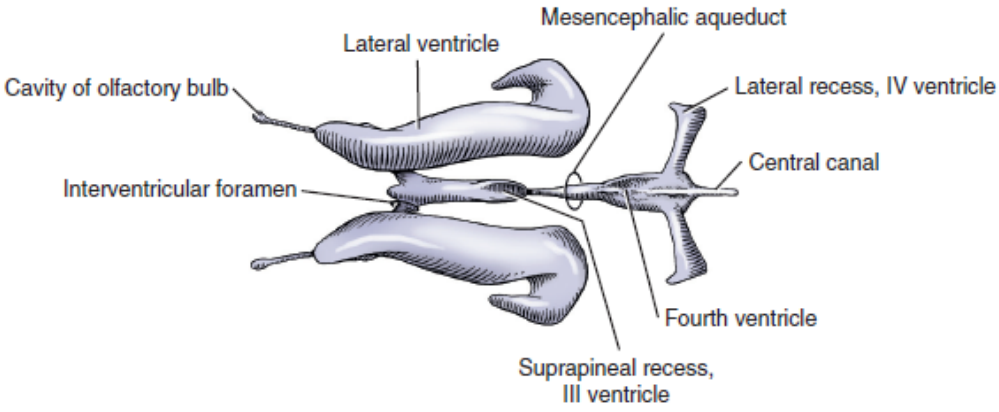

1.6 Choroid Plexuses (CPs)

In specific regions lining the ventricles, nervous tissue is absent, allowing the pia mater to directly contact the ependyma. This combined tissue, known as the tela choroidea, comprises a portion of the lateral ventricles' floor and the third and fourth ventricles' roofs. When combined with a capillary plexus, the tela choroidea gives rise to the CP. Each CP projects into a ventricle as a band of clustered villi. Each villus of a CP features microvascular proliferation and cuboidal ependymal cells (choroidal epithelium). The choroidal epithelium comprises simple cuboidal cells that are held together by tight junctions on the apical side. These cells are continuous with the ependymal cells that line the ventricles internally. The blood capillaries that constitute the CP are fenestrated and lack tight junctions between endothelial cells, forming a semi-permeable membrane that selectively allows certain substances to pass between the blood and the CSF (1,3). The CP of each lateral ventricle extends into the third ventricle through the interventricular foramen. As a result, two choroid plexuses are present on the roof of the third ventricle. The roof of the fourth ventricle also contains paired choroid plexuses, each extending into the SAS by protruding through the lateral recess and aperture of the fourth ventricle (3).

1.7 Circumventricular organs

Circumventricular organs (CVOs) are midline structures located around the third and fourth ventricle, characterized by an increased blood supply, the absence of the blood-brain barrier, and the presence of ependymal cells that function as baroreceptors and chemoreceptors. Additionally, these areas contain specialized ependymal cells called tanycytes that are responsible for active secretion of CSF.

Within the third ventricle the subcommissural organ is located ventrally to the caudal commissure and is composed of thickened secretory ependyma; the subfornical organ is situated caudally to the interventricular foramina and it controls salt intake.

Furthermore, an additional CVO called the area postrema is located at the caudal end of the fourth ventricle. This area consists of densely vascularized gray matter and serves as emetic center (3).

2 CSF

2.1 Definition and composition

CSF is an ultrafiltrate of blood plasma that surrounds and permeates the entire CNS and therefore protects, supports, and nourishes it. In general, CSF is produced within the ventricles of the brain by the CPs, circulates to the SAS, and is absorbed into the venous sinuses. The SAS is found at varying depths, following the irregularities of the cerebral surface, and contains dilations known as cisternae (3). The most significant cisterna is the cerebellum-medullary cistern, also referred to as the cisterna magna, located in the atlanto-occipital region. Additionally, there is the lumbar or lumbosacral cistern situated caudally near the cauda equina.

Physiologically, CSF is clear and transparent. Microscopically, it is nearly acellular, with nucleated cells typically measuring less than 10 cells/µL according to literature reports for cattle (5). However, different cutoffs have been reported in the literature (range 3 to 10 cells/µL) (5–7). It should also not contain red blood cells (7). The leukocyte population naturally present in the CSF mainly consists of mononuclear cells, particularly lymphocytes, while neutrophils are rarely observed (8). Regarding the protein fraction of CSF, which primarily consists of albumins, it is of lower concentration compared to levels in the blood. In bovine species, the reference limit value is approximately <40 mg/dL, although slight variations may exist depending on the specific literature source considered (5,6,8). In addition to albumins, which are not synthesized within the CNS but derived from the blood, CSF also contains a small amount of globulins as part of its physiological composition (9).

The albumin quotient, a measure of blood brain barrier (BBB) permeability is defined with following equation:

$$Albumin\ quotient = \frac{CSF\ albumin}{serum\ albumin}\ x\ 100$$

The IgG index instead, a measure of intrathecal production of IgG, is calculated as follows:

$$IgG\ index = \frac{CSF\ IgG}{serum\ IgG}\ x\ \frac{serum\ albumin}{CSF\ albumin}$$

It has been observed that the protein concentration in CSF can vary depending on the sampling site. Specifically, it tends to be higher in samples obtained from the lumbar cistern compared to those from the cisterna magna. However, this finding has only been demonstrated in dogs (10), and studies conducted in small ruminants have not found significant differences in protein concentration between the two sites in health (11). No similar studies in bovine species are currently available. This difference in concentration could be attributed to the normal cranio-caudal flow of CSF (12).

Glucose is also physiologically present in the CSF, typically at concentration equivalent to 60-80% of blood glucose concentration. Glucose enters the CSF through facilitated transport with specific carriers or, in minor quantities, through diffusion. Its concentration in the CSF depends on blood glucose concentration, the rate of glucose transport into the CSF, and the metabolic rate of the CNS (13). CSF glucose normal range in healthy cattle is 35-70 mg/dL (6).

In terms of the ionic composition of CSF, potassium and calcium are present in lower concentrations compared to blood, while chloride, magnesium, and sodium, are more abundant in CSF compared to blood (14). Sodium is the most abundant ion in CSF, and its concentration closely correlates with blood levels. CSF sodium concentration in cattle are reported to range between 132 and 144 mmol/L, with lower values in calves and higher values in adult cattle. On the other hand, potassium, with a concentration of approximately 3 mmol/L (range 2.7-3.2 mmol/L), plays a crucial role in neuronal function and

neurotransmitter release. Changes in plasma potassium concentration have little effect on CSF potassium levels, because its transport across the BBB is limited. Calcium, with a physiological range in CSF of 1-1.5 mmol/L, is secreted by the CPs, and thus its concentration in CSF is independent on blood concentration (13). Magnesium and chloride in CSF play an important role in neuronal conduction. Magnesium concentration in healthy cattle is reported to range between 1.7 and 2.7 mmol/L, while chloride between 121 and 125 mmol/L (6,15).

Several enzymes, such as aspartate transaminase (AST), creatine kinase (CK), and lactate dehydrogenase (LDH), are present in CSF. The concentration of CK in CSF is usually independent of that in serum and its elevation in CSF may reflect nervous system disease. Elevations in AST and CK concentration could be indicative of significant myelin degeneration within the CSF, as observed in extensive studies (16). However, CK concentration might be falsely increased by contamination of CSF with epidural fat or dura during CSF collection (17). Increased LDH activity has been shown in CNS lymphoma and CNS inflammatory conditions (13).

Additionally, neurotransmitters such as ɤ-aminobutyric acid (GABA), the primary inhibitory neurotransmitter in the CNS, and glutamate, the primary excitatory neurotransmitter in the CNS, are also present in the CSF (13).

2.2 Production and Absorption

The majority of CSF is produced in the CPs of the ventricles, with approximately 35% produced in the third and lateral ventricles and 23% in the fourth ventricle. The remaining CSF (42%) is mainly produced at the SAS level (14).

The methods of CSF production are a selective ultrafiltrate from blood plasma and active transport mechanisms that utilize energy. Sodium–potassium ATPase in the membrane of the choroidal epithelial cells plays an important role in that: sodium is actively transported

out of the choroidal epithelial cell into the ventricular cavity, with water molecules and chloride and bicarbonate ions following through by way of facilitated transport.

CSF production is relatively constant, although the rate varies among species. The complete volume of CSF is both generated and reabsorbed approximately 3 to 5 times each day. The rate of CSF production is independent of the hydrostatic pressure of the blood but is influenced by the osmotic pressure of blood, with hyperosmolarity reducing its production and hypo-osmolarity increasing it (13).

Once produced, CSF circulates within the ventricular system and the ependymal canal, moving caudally towards the cauda equina. It follows a specific pathway: from the lateral ventricles, it passes through the interventricular foramina into the third ventricle. From there, it travels along the mesencephalic aqueduct to reach the fourth ventricle. At this level, the majority of CSF enters the SAS through the lateral apertures, and a small amount enters the ependymal canal and runs in a cranio-caudal direction, reaching the cauda equina (3).

In the SAS a significant portion of CSF passes dorsally over the cerebellum, and then over the cerebrum, where it has access to the venous sinuses. CSF covers almost the entire external surface of the brain and spinal cord, where it can penetrate the parenchyma along with the larger blood vessels in their perivascular spaces. These spaces are extensions of the SAS to the point where the pia mater blends with the adventitia of the blood vessel (14).

The flow of CSF is influenced by various factors, including the pulsations of blood within the vessels of the CPs and cerebral arteries following cardiac systole, as well as the movement of cilia on the external surfaces of the ependymal cells (14). Other determinants of CSF flow are the variation in intra-thoracic and intra-abdominal pressures associated with the respiratory cycle. Additional pressure changes that induce currents in CSF flow include physical activities like running, jumping, changes in posture (standing up or lying down), and coughing (3).

To maintain a nearly constant CSF volume despite continuous production, the CSF must be reabsorbed into the bloodstream. The primary site of reabsorption occurs at the level of arachnoid villi, which collectively form arachnoid granulations located within the intracranial venous sinuses and cerebral veins. The arachnoid villus is a prolongation of the arachnoid membrane and SAS into the lumen of the venous sinus covered by the endothelium of the vessel wall: at this level blood and CSF are separated by a single layer of endothelial cells (14). The villi function as one-way valves, allowing CSF to pass into the bloodstream when CSF pressure exceeds that of the blood sinuses. Conversely, when pressures are reversed, the structure collapses, closing the spaces and preventing blood from entering the CSF (18). Other sites of CSF absorption include the venous and lymphatic vessels associated with the spinal nerve roots and cranial nerves (CN), particularly the drainage associated with CN I (olfactory CN), II (optic CN), and VIII (vestibulocochlear CN). Lastly, the parenchymal vessels absorb the minimal amount of CSF that reaches the interstitial spaces of the cerebral parenchyma (14).

2.3 Functions

The CSF fulfills crucial functions for the CNS. Firstly, it serves as the fluid medium in which the CNS is suspended, providing mechanical protection by acting as a cushion against potential impacts (14). CSF also helps regulate the intracranial pressure (ICP). Cardiac function, respiratory activity, variations in posture and physical exercise can induce natural fluctuations in the volume of blood and CSF inside the cranial cavity. However, these fluctuations do not lead to an alteration of ICP due to the communication between these two fluid compartments. An increase in the volume of one compartment automatically corresponds to a decrease in the volume of the other (13). This mechanism also applies to pathological increases in ICP caused by elevated cerebral blood volume. For instance, conditions associated with poor tissue oxygenation and resulting hypercapnia can trigger

vasodilation of cerebral arteries, leading to increased blood flow to the brain (14). In response to sudden pressure increases, the body employs a compensatory mechanism involving temporary accumulation of CSF within the cervical SAS.

CSF is a source of nourishment as it transports metabolites and nutrients between blood and the CNS parenchyma. It also serves to transport neuroendocrine cells and neurotransmitters within the parenchyma. CSF plays a role in maintaining the ionic balance necessary for neuronal function serving as a chemical buffer for the neural tissue. This control is achieved through various active transport mechanisms and systems that selectively determine the inclusion or exclusion of specific substances in the composition of CSF. Moreover, it is responsible for eliminating catabolites derived from neuronal metabolism, proteins, foreign particles (such as cells and bacteria), by transporting them to the arachnoid villi and subsequently into the venous system. Additionally, these substances can be eliminated by passing from the CSF into the lymphatic vessels associated with the roots of CN and spinal nerves (13).

2.4 Collection and preservation in bovine species

CSF collection is a common ancillary procedure performed in veterinary medicine for both companion animals and farm animals when neurological signs raise suspicion of a CNS pathology (8).

CSF sampling can be conducted either at the level of the cerebellum-medullary cistern, or at the level of the lumbar or lumbosacral cistern depending on the species. Generally, sampling at the lumbosacral cistern is preferred in cattle and other farm animals. This is primarily because sampling at the cerebellum-medullary cistern often requires general anesthesia to ensure proper patient positioning, which is challenging to implement in farm animals, particularly under field conditions (8). Additionally, studies have shown that, except for protein concentration, which might be higher in samples obtained from the lumbosacral

region compared to those collected at the atlanto-occipital level, there are no significant differences between CSF samples obtained from these two sites, especially in the absence of a focal compressive lesion of the spinal cord (11). Therefore, choosing the lumbosacral cistern as the sampling site in large animals is further justified. In adult cattle capable of walking, lumbosacral sampling is performed with the animal in standing position, adequately restrained. Sedation is generally not required for CSF sampling, although it may be necessary in the case of particularly nervous animals, using xylazine at a dose of 0.05-0.1 mg/kg body weight. In animals already in forced recumbency and in calves, sampling can be performed with the animal in sternal recumbency, with the limbs flexed and hind limbs extended forward along the sides. This positioning allows for a slight opening of the lumbosacral intervertebral space, facilitating access. Lateral recumbency is also mentioned as a possibility for calves and lambs, although it can make landmark identification more challenging (8).

The insertion point of the needle is identified using a series of landmarks. The lumbosacral intervertebral space is located on the midline between the last lumbar vertebra (L6) and the first sacral vertebra, as well as between the tubers sacrale on either side. Within this space, a depression can be palpated. Within this depression, the needle insertion point is identified at the intersection of two imaginary lines, one connecting the tuber coxae and one connecting the caudal edge of the spine of L6 and the cranial edge of the spine of the second sacral vertebra. The latter is more prominent and easier to feel than the spine of the first sacral vertebra (Figure 3) (7,8,14).

Figure 3: Placement of the spinal needle for performing lumbosacral CSF collection. The image represents the procedure performed in horses but is analogous in cattle. Triangle: second sacral spine, cranial edge; square: tubers sacrale; cross: spine of L6, caudal edge; circle: tubers coxae (from "Veterinary Neuroanatomy and Clinical Neurology" by de Lahunta A, Glass E, Kent M, 2021).

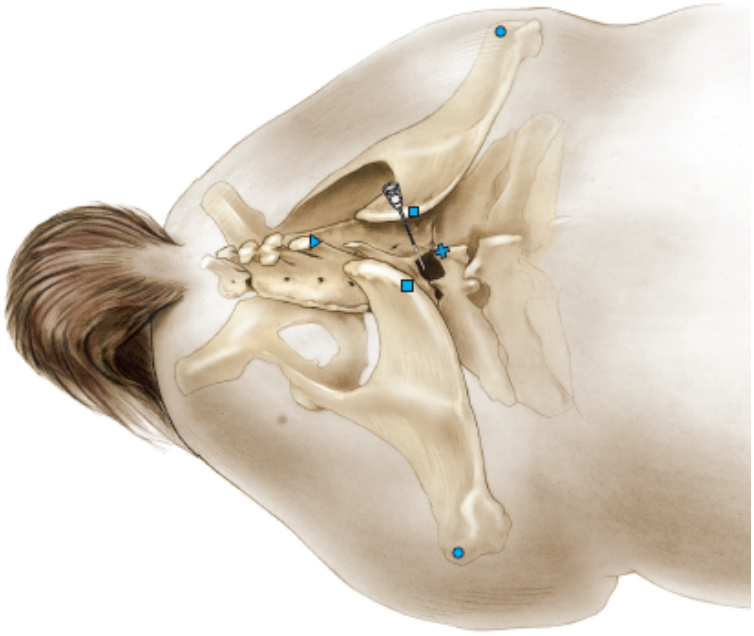

The site should be clipped, surgically prepared, and the operator should wear sterile gloves. Subcutaneous injection of 1-2 mL of procaine hydrochloride might be performed. For CSF collection, an appropriate-length and diameter spinal needle is used based on the size of the animal. In adult cattle, a 90-100 mm and 18G spinal needle with fitted stilette is typically used. For calves, a 50 mm and 20-21G needle can be used without an internal stilette (7,8). The needle should be inserted perpendicular to the dorsum of the animal, with the bevel of the needle pointing cranially. It should be advanced slowly through the skin, subcutaneous tissue, inter-arcuate ligament, or ligamentum flavum. A slight loss of resistance should be perceived when passing through the ligamentum flavum and entering the epidural space. When the dura-arachnoid is penetrated, there may be a slight movement of the tail, flexion of the pelvic limbs, or contraction of the axial muscles. This indicates that the needle is now in the dorsal SAS. At this stage, if there is a stilette, it can be taken out and the needle

should be advanced gradually, observing for CSF flow at intervals of 1 mm. The goal is to aspirate CSF from the SAS situated dorsal to the spinal cord. However, CSF may not always flow at this point, and in some cases, it might be necessary to cautiously guide the needle through the caudal sacral segments and meninges (known as the filum terminale), reaching the floor of the vertebral canal. From there, the needle can be slowly retracted dorsally into the ventral SAS. The CSF can be allowed to flow spontaneously into the collection test tube. In approximately 1-2 minutes, an adequate volume (around 1-2 mL) should be obtained for further analysis. Compression of the external jugular veins may aid in the flow of CSF in difficult patients. Rotating the needle may also help to free the needle tip from obstruction by meninges or spinal nerve roots. Alternatively, a syringe can be connected to the needle hub, taking care not to cause movement that could damage the underlying spinal cord or result in meningeal hemorrhage. A gentle aspiration should be performed (8).

CSF sample should be collected in sterile plain tubes, while EDTA tubes should be avoided for routine sampling, as the additive can falsely elevate the total protein (TP) concentration. Ideally CSF should be analyzed within one hour as delayed processing may lead to significant distortions in cell structure and a decrease in total nucleated cell count (TNCC) due to cell lysis (19). This susceptibility to damage might be influenced by the low concentration of CSF protein, the lipid concentration, and tonicity, all of which typically contribute to the stabilization of cell membranes in other fluids (20). This hypothesis is also supported by the fact that a previous study in dogs showed that CSF samples with TP concentrations ≥50 mg/dL were less susceptible to cell deterioration than those with lower protein concentrations (19).

If processing is delayed for more than 1-hour, cellular changes might occur, including nuclear pyknosis, cytoplasmic and nuclear membrane lysis, and disintegration, with discordant information in literature regarding the most susceptible cell type (19,21,22).

The rapid degradation of the sample often poses practical challenges in situations where, for example, the analysis laboratory is located more than an hour away from the collection site, or the collection is performed during the laboratory off-hours. To address these challenges, numerous studies have been conducted over the years on samples collected from both companion and farm animals to assess the effectiveness and impact of exogenous stabilizing agent on the sample.

Studies conducted on canine and feline CSF (both in health and disease) have shown that the addition of autologous serum at concentration of 11%, the addition of bovine fetal serum at concentration of 20%, and the addition of hetastarch (hydroxyethyl starch) at 1:1 concentration with CSF, allows for sample analysis after 24 to a maximum of 48 hours, without significantly altering cell degradation affecting the final interpretation (19,23).

Similar studies have been conducted in cattle. In these studies, autologous serum was used at a final concentration of 11%, and the samples were analyzed within one hour and after 24 hours of refrigerated storage (4°C). In healthy animals, no significant differences were found that could compromise the clinical-diagnostic interpretation between fresh and stored samples (24). However, discordant results were obtained in subjects with neurological disorders, with a significant difference in both TNCC, which was significantly decreased in stored samples, and in differential nucleated cell count, where a significant increase in lymphocytes and a significant decrease in monocytes was observed with storage (21). In conclusion, the recommendation remains to analyze the samples within one hour of collection. However, if this is not feasible, the use of stabilizing agents such as serum (autologous or bovine fetal serum) and hetastarch can be considered. The addition of serum results in a change in TP concentration and in general any added stabilizing agent causes a dilution effect that must be taken into account when interpreting the results. Therefore, if one of these preservatives is chosen, it is recommended to send two aliquots to the laboratory: one aliquot should be placed in a tube containing the stabilizing agent and can

be used for cytological evaluation and cell counts. The other aliquot, placed in an empty tube, can be used for TP concentration determination and possibly antibody titer analysis (25).

2.5 Analysis and interpretation in bovine species

CSF analysis is a common ancillary examination performed in ruminants presenting neurological signs. However, it is possible for the CSF to show no detectable alterations even in the presence of a morbid lesion. Additionally, different lesions can result in similar alterations, which may not necessarily correlate with the severity of the disease or the prognosis (25). Therefore, it is crucial to assess and interpret CSF analysis results in conjunction with clinical signs, medical history, general physical examination, neurological examination, and other tests conducted within the context of the individual case (25).

CSF routine analysis involves macroscopic and microscopic evaluation of the sample.

Macroscopic analysis involves evaluating the color and turbidity of the sample. Under normal conditions, CSF is colorless and transparent. A pink or red color suggests the presence of blood pigments, which is often iatrogenic due to meningeal vessel rupture during the sampling procedure. In such cases, the sample might not be uniformly reddish and after centrifugation, the supernatant should appear clear as intact red blood cells settle. However, if the presence of blood is due to an ongoing pathological process, the sample will be uniformly reddish, and the supernatant will have a yellowish or yellow-orange color known as xanthochromia. Xanthochromia results from the release of oxyhemoglobin and methemoglobin during the degradation of erythrocytes. It typically appears a few hours after subarachnoid hemorrhage and persists for about 10 days (26) or up to 2-4 weeks according to other sources (8).

Blood contamination within CSF could lead to CSF dilution, causing falsely elevated TNCC and TP concentration readings, this being due to blood components transferring into the

CSF. However, conflicting information is present in the literature regarding the influence of blood contamination on CSF analysis. A reported threshold for identifying a sample as contaminated is red blood cell count (RBCC) > 500 cells/μL. Correction formulas are reported in order to adjust TNCC and PT concentration according to RBCC (12), though their use is debated and it is advisable to interpret CSF samples with blood contamination cautiously.

A yellow-green coloration associated with increased turbidity might indicates an ongoing purulent process, such as septic meningitis, accompanied by an increase in the TNCC within the CSF. Turbidity itself might depend on an increase in cellularity of the sample (above 500 cells/μL) (25) such as high protein concentrations (8).

The concentration of TP can be evaluated. As previously mentioned, CSF has an extremely low protein content (expressed in mg/dL) relative to serum (expressed in g/dL), requiring a spectrophotometric method for protein determination, while the evaluation of TP concentration in CSF using a refractometer is not accurate. The most accurate spectrophotometric technique utilizes the red Pyrogallol reagent (27). Urine test strips are reported as a screening test to estimate CSF TP concentration. A value of 2+ or higher in the urine protein reagent indicates an increase in proteins in the analyzed CSF sample (8). However, it is highly specific for albumin detection but less specific for globulin detection, and it is therefore suitable only for initial approximate quantification (28). On the other side, for a rapid estimation of globulin concentration, the Pandy test can be employed. A few drops of CSF are added to 1 mL of Pandy reagent (10% carboxylic acid). If the solution becomes cloudy, it indicates the presence of globulin and has a sensitivity of approximately 50 mg/dL (25). However, these methods lack validation in ruminant CSF; thus, it is advisable to confirm results through spectrophotometric assessment. The main protein component in CSF is albumin, which derives entirely from the plasma and is produced exclusively by the liver. The ratio between albumin concentrations in CSF and plasma, known as albumin

quotient (see Chapter 2.1), remains constant in healthy animals. Therefore, an increase in the albumin quotient, reflecting elevated levels of albumin in the CSF, can be considered an indicator of BBB damage (25). On the other hand, an increase in the globulin component might be the result of intrathecal production and is associated mainly with infectious-inflammatory conditions affecting the CNS. In lesions directly damaging the BBB (such as neoplastic extradural and intramedullary compressive lesions, trauma, vasculitis, ischemic necrosis, non-suppurative viral encephalomyelitis), a normal TNCC may be accompanied by an elevation in TP concentration, referred to as albuminocytologic (AC) dissociation (25). Cytological examination of the CSF involves the total and differential cell count and the morphological evaluation of cells present in the sample. These procedures are performed placing the CSF into a hemocytometer chamber and observing it under an optical microscope. The standard operating procedure (SOP) of the laboratory service of the Veterinary Teaching Hospital (VTH) of the University of Turin provides the following procedure: for TNCC, a Nageotte hematocytometer is used (Figure 4). The Nageotte contains two gridded counting areas each containing 40 rectangular areas. 100 µL of CSF are diluted 1:1 with Turk's solution (aqueous methylene blue) to lyse erythrocytes. This mixture is placed in both counting areas of the hemocytometer. A coverslip is positioned over the counting areas of the chamber before introducing the CSF. Cell counting occurs after the cells settled within the hemocytometer chambers. This settling is facilitated by allowing the hemocytometer to rest in a humidified Petri dish for 5 minutes before initiating the cell count. Using an optical microscope (at 400X magnification), nucleated cells present in 8 rectangles (4 in each counting area) are counted, which correspond to a total volume of 10 µL. The cumulative count of cells must be divided by 5 (due to the 1:2 dilution with Turk's solution), resulting in the cell count per 1 µL.

Figure 4: Nageotte counting chamber (Image from the SOP of the Clinical Medicine Laboratory at the VTH of the University of Turin).

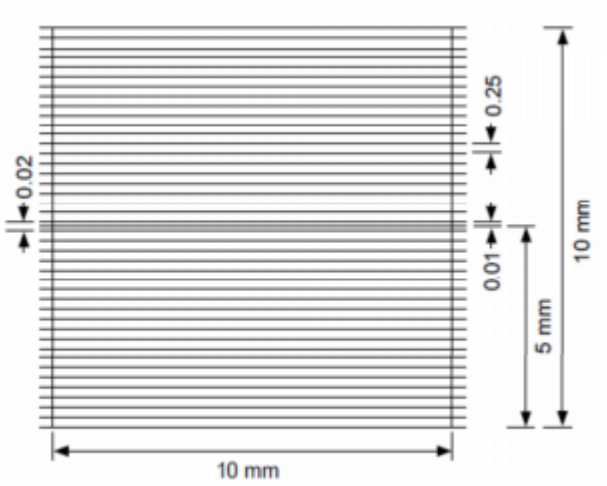

For RBCC, a drop of undiluted CSF is placed in both counting areas of a Burker haemocytomether (Figure 5), covered with a coverslip. Within each counting area a grid of 9 smaller squares is present. Using an optical microscope (at 200X magnification) erythrocytes are counted in 1 small square for each counting area. The resulting mean is then multiplied by 10. The final count corresponds to the number of cells present in 1 µL.

Figure 5: Burker counting chamber (Image from the SOP of the Clinical Medicine Laboratory at the VTH of the University of Turin).

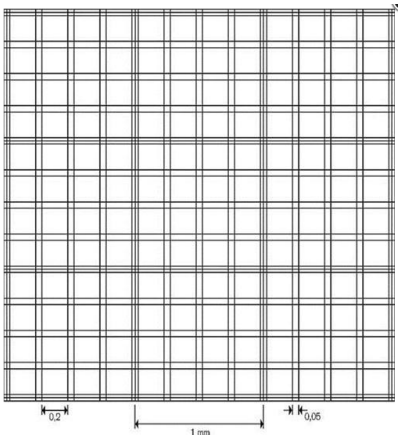

Differential nucleated cell count and morphological evaluation of cells are typically carried out on concentrated CSF samples (200-250 µL per sample) on smears prepared with a cytocentrifuge (Cytospin2, Shandon). Cytocentrifugation is performed at 150 g for 6 minutes to preserve cell morphology. Alternatively, sedimentation chambers can be used. These chambers can be commercially obtained or custom-built using easily accessible materials (12). Once concentrated, the sample is air-dried and subsequently stained using May-Grunwald Giemsa technique. Table 1 provides an overview of traditional and alternative techniques for CSF microscopic evaluation.

Table 1: CSF microscopic evaluation techniques. RBCC = red blood cell count; TNCC = total nucleated cell count; TP = total protein. Detailed information on these techniques can be found in the text above.

CSF microscopic evaluation		Traditional techniques	Alternative techniques
	TP	Spectrophotometry with red Pyrogallol reagent	Pandy test; urine test strip
	TNCC	Microscopy (hemocytometer chamber)	
	RBCC	Microscopy (hemocytometer chamber)	
	Cells morphology	Microscopy (cells cytocentrifugation)	Microscopy (cells sedimentation)

When an increase in TNCC beyond the reference values is observed in the CSF, it is referred to as pleocytosis (PL). PL can be classified based on severity (e.g. mild if <50 cells/µL, moderate if 51-100 cells/µL or marked if >100 cells/µL) (29) or based on the prevalent cell type (i.e. neutrophilic, mononuclear, or mixed, which refers to the presence of both mononuclear cells and neutrophils; more rarely eosinophilic) (8,26).

Infectious diseases will often lead to CSF PL and increased TP concentration. The cell types present vary significantly, but generally, bacterial diseases are associated with a predominance of neutrophils, often degenerated and with toxic changes, while viral diseases show more smaller mononuclear cells. As an exception, listeriosis, despite being bacterial, usually shows a mild to moderate mononuclear PL. Fungal and protozoal diseases typically cause mixed cell responses. Protozoal infections and helminth parasite infestations can result in an eosinophilic and neutrophilic response in the CSF, as well as hemorrhage. In chronic inflammatory states in which significant CNS tissue necrosis is present, the CSF may contain numerous large mononuclear cells or macrophages (7). With traumatic injury to the CNS, microscopical analysis of CSF may reveal pathological hemorrhage signs including erythrophagia, haemosiderophages or haematoidin crystals. Erythrophagia denotes reactive macrophage ingestion of erythrocytes, which are visible within the cytoplasm of the immune cell. Haemosiderophages are reactive macrophages containing round to oval particles of dark blue-green haemosiderin pigment. These particles vary in size and show positive staining for iron with Prussian blue. The iron originates from metabolized hemoglobin. Bilirubin is another product of haemoglobin metabolism; it forms golden, rhomboid or rectangular haematoidin crystals. Moreover neutrophils, not showing toxic changes, followed by macrophages, will usually appear in the CSF in response to hemorrhage (12).

With most CNS malformations and in metabolic/toxic disorders, the CSF analysis will be normal. Pathological findings in the CSF in these diseases may be secondary to trauma in

case of deformations that result in progressive traction injury to CNS neural tissues, or in case of considerable tissue destruction, such as lead poisoning, sodium salt/water intoxication and polioencephalomalacia in ruminants where a mild mononuclear PL can be seen.

CNS degenerative disorders do not typically cause any changes in CSF constituents (7). The most frequent CSF change in patients with neoplasia is a mild AC dissociation as these lesions behaves like space occupying lesions. Atypical lymphocytes can be detected in CSF from cattle with CNS lymphosarcoma (7). In the presence of a vascular disorder, protein leakage and the pathological hemorrhage signs previously described are common (7).

Additional evaluations, beyond routine analysis, can be performed on CSF samples. When a bacterial agent is suspected to be the cause of a CNS disease, both aerobic and anaerobic bacterial cultures of CSF may be performed. However, positive bacterial culture results in confirmed cases of bacterial CNS infections are extremely uncommon. The occurrence of false negatives may be due to previous use of antibiotics, low microbial concentration, or to the presence of slow-growing and fastidious microorganisms (30,31). An alternative to culture, particularly when dealing with microorganisms that cannot be cultured or samples with low microbial concentration, is the polymerase chain reaction (PCR). PCR can detect the presence of specific infectious agents by amplifying their DNA (deoxyribonucleic acid) (25). Furthermore, in cases where an infectious CNS pathology leads to intrathecal production of immunoglobulins, the antibody titer for the suspected infectious disease might be evaluated. Although widely used in human and companion animal medicine, these techniques are not commonly employed in farm animal medicine, with limited application in research studies (25,32).

Additional evaluation conducted on ruminant CSF, including glucose, electrolytes (such as sodium and magnesium), and enzyme measurements, presently do not yield clinically valuable diagnostic insights. Low glucose concentration has been observed in animals with

bacterial meningoencephalitis, as both microorganisms and neutrophils rely on glucose for metabolism (9). Measuring magnesium concentration proves significant in suspected hypomagnesemia tetany cases, as both CSF and blood magnesium concentrations bear a significant correlation to the clinical manifestation of this condition (33). Furthermore, sodium concentration elevation has been noted in instances of sodium chloride poisoning (5).

Concerning enzymatic activity assessment, increased CK activity has been observed in neurological pathologies linked to substantial white matter damage. Yet, this increase lacks specificity as it can also be influenced by sample blood contamination or extradural fat presence (16). In the context of CSF lactate evaluation, known to be highly beneficial in human medicine for diagnosing CNS bacterial infections, this topic will be comprehensively reviewed in Chapter 6.

3 Neurological pathologies of bacterial etiology in bovines

3.1 Definition and prevalence

Bacterial infection of the CNS poses a clinical challenge and is a leading cause of neurological disorders in cattle (29).

The nomenclature of CNS infections depends on the implicated anatomical structures. Meningitis is ascribed when one or multiple meningeal layers are engaged, while during meningoencephalitis the pathological process extends to the cerebral parenchyma. Meningoencephalomyelitis arises when the spinal cord is also involved. Terms like meningo-ventriculitis and ependymitis denote involvement of ventricular linings, while choroid plexitis designates an inflammatory process affecting the CPs. Encephalitis and myelitis respectively pertain to the brain and spinal cord parenchyma. These descriptors can be further refined by defining the stage of disease (acute/chronic), etiological factors (bacterial/viral/parasitic, etc.), and histopathological lesion types (e.g. suppurative/non-

suppurative). To indicate involvement of gray matter, white matter, or both, the prefixes polio-, leuco-, and pan- are employed, respectively (34).

The prevalence of distinct neurological infection of the CNS varies worldwide.

Viral CNS infections, notably rabies in cattle, are more frequently documented in Latin America, Africa, and Asia, while bacterial infections tend to predominate in more developed regions. In particular, two studies in the United States (29,35) highlight that suppurative bacterial meningoencephalitis linked with sepsis and listeriosis constitute the principal cause of neurological signs in cattle. Two additional studies—one from Switzerland (36) and the other from the United Kingdom (37) —align more closely with Italy's epidemiological context, where comparable studies are lacking. In the Swiss study, bacterial infections of the CNS were the most prevalent, primarily manifesting as cases of suppurative meningoencephalitis. In the UK, the most common inflammatory neurological pathologies are identified as listeriosis and vertebral osteomyelitis.

3.2 Classification

The subsequent sections describe the most common bacterial-induced neurological pathologies in bovine species. Particular emphasis is placed on those prevalent in European literature and grounded in the expertise of the author.

3.2.1 Sepsis and Neonatal bacterial suppurative meningitis-meningoencephalitis (NBSM-ME)

Sepsis is a significant health issue in calves under two weeks of age and is linked to a considerable fatality rate (38,39). Inadequate or unsuccessful transfer of passive immunity and exposure to virulent pathogens are critical factors predisposing to sepsis development. In ruminants, the placenta does not permit the transfer of antibodies during pregnancy. Consequently, newborn calves lack antibodies capable of defending them against microorganisms commonly present in their living environment, and the development of

active individual immunity requires time. The intake of colostrum within the first hours of a calf's life is crucial to ensure the acquisition of an adequate quantity of immunoglobulins that can traverse the intestinal barrier and establish an effective immune system, thereby safeguarding the calf against potential infections (40). The primary causative agent of sepsis in calves is most frequently *Escherichia coli* (39,41,42), followed by *Salmonella spp.*, *Campylobacter spp.*, *Klebsiella spp*., *Staphylococcus spp.*, and *Streptococcus spp*. (39,43). Neonatal bacterial suppurative meningitis-meningoencephalitis (NBSM-ME) often arises as a consequence of sepsis (34,42). Bacteria can travel through the bloodstream to the leptomeninges, although the exact mechanism of pathogen entry remains unclear (39,44). Possible mechanisms could involve the establishment of a prolonged and intense presence of bacteremia in the highly perfused dural venous system and CPs, adherence of bacterial fimbriae, phagocytosis of the pathogens by circulating monocytes, and endocytosis through the microvascular endothelial cells. However, these are not the only possible mechanisms; indeed, bacteria can also access the meninges through contiguity following middle/inner ear infections, sinusitis, or infections of cranial bones resulting from trauma (34).

Bacteria proliferate within the CSF. Complement activity is essentially absent within the CSF, and in conjunction with low levels of specific antibodies, this results in insufficient opsonization of pathogens within the meninges. Despite an early influx of leukocytes into the CSF during bacterial meningitis, the host's defense system remains suboptimal due to deficient opsonic activity (39). The consequences of meningitis are linked to the damages caused by the direct invasion of tissues by bacteria (which are sometimes also capable of toxin release) and those resulting from the release of pro-inflammatory cytokines (39). Following bacterial penetration into the tissues, an inflammatory process is initiated, involving the recruitment of leukocytes from the blood and an increase in vascular permeability, leading to edema. In severe cases, edema can progressively lead to an

elevation in ICP, resulting in reduced perfusion of the cerebral parenchyma and ischemic/hypoxic injuries (45).

Clinical signs are usually nonspecific and primarily attributable to the primary site of infection and/or septicemia. These signs may include fever, diarrhea, swelling and redness of the umbilical stump, joint swelling, dysorexia/anorexia, hyperemia of the episcleral vessels, dehydration, and loss of suckling reflex (39). Additionally, calves may exhibit lethargy, ataxia, difficulty maintaining quadrupedal stance, tremors, hyperesthesia, and head and neck extension (46). Strabismus, nystagmus, blindness may be observed. As the condition progresses, recumbency may occur, along with severe sensory depression leading to coma, seizures, and death (6).

Blood tests may reveal neutrophilia or, in cases of septicemia, neutropenia (46) but are overall relatively inconclusive as they reflect concurrent conditions such as septicemia, diarrhea, and dehydration. Macroscopically, CSF can appear white-yellowish (or greenish in severe cases) and turbid due to the high cellular and protein content, occasionally containing pus or fibrin flocculi (47). Microscopic analysis usually shows a marked neutrophilic PL in acute bacterial forms, whereas mononuclear cells prevail in chronic cases (6,46). TP concentration is also markedly increased. Intra or extracellular bacteria may also be observed (6,48). However, for precise etiological diagnosis, CSF culture may be conducted, although literature reports suggest that this test yields positive results in only 50-60% of cases (6,49).

At necropsy, lesions related to sepsis are often present in various body regions. The meninges typically appear opaque, thickened, and petechiae are present. Meningeal vessels are congested, and CSF within the ventricles may be turbid and contain fibrin flocculi. Microscopically, a purulent inflammatory process with infiltration of neutrophils and lymphocytes in nervous tissue is observed, along with disseminated hemorrhages,

inflammation of meningeal vessels, and bacterial colonies around blood vessels of the meninges and cerebral parenchyma (6,45,47).

NBSM-ME cases often have a rapid course and poor prognosis; a retrospective study on 32 calves reported a survival rate of 16% (48). Thus, immediate antibiotic therapy is initiated based on clinical suspicion which may be adjusted based on culture and sensitivity results (34). The choice of antibiotic is influenced by various factors:

- Chemical and physical characteristics affecting its ability to cross the BBB (which is often compromised in meningitis, resulting in increased permeability).
- Spectrum of activity: Molecules with broad-spectrum activity effective against both Gram-negative and Gram-positive bacteria are generally chosen, or alternatively, a combination of products is used to cover the spectrum.
- Avoidance of newer-generation drugs to minimize the development of drug resistance.
- Authorization for use in bovine species.
- Formulation.
- Cost.

Dosage is typically maximized to achieve sufficient concentration in nervous tissue. However, it should be noted that in very young subjects, renal and hepatic functions responsible for drug secretion and detoxification are not fully efficient, potentially causing side effects at lower dosages compared to adult subjects (6). The first-line antimicrobial choices comprise the sulfonamides and tetracycline, while penicillin may also be considered (50). Anti-inflammatory therapy is often combined with antibiotic treatment to improve the overall condition of the animal and counteract secondary effects of inflammation (39).

Considering the high mortality rate, prevention is crucial, emphasizing the provision of adequate colostrum, proper umbilical stump hygiene and disinfection, and excellent hygiene conditions in the calving area for all newborns (49).

3.2.2 Thromboembolic meningoencephalitis (TEM)

Thromboembolic meningoencephalitis (TEM) is a septic, thromboembolic, suppurative, and necrotic meningoencephalitis predominantly of cattle caused by *Histophilus somni*, previously known as *Haemophilus somnus* (46). The disease involves a complex pathogenesis rooted in the bacterium's role as a significant respiratory pathogen within the bovine respiratory disease complex. The process initiates with the dissemination of *H. somni* into the circulatory system, triggering a sequence of events that significantly impacts the vascular and neural compartments. Upon reaching the endothelial surfaces, the bacteria start organizing in biofilms, which determines the expression of tissue factor activity and the disruption of intercellular junctions, instigating a cascading effect that culminates in intravascular coagulation and the consequential thrombosis of small cerebral vessels. Persistence of *H.* somni's within lesions is further increased by its intrinsic capacity to evade intracellular destruction by phagocytic cells of the immune system. Key virulence factors and mechanisms that contribute to this intricate pathogenesis include membrane lipooligosaccharide, the induction of host cell apoptosis, intraphagocytic survival strategies, and the presence of immunoglobulin Fc-binding proteins (34).

This disease is primarily seen in feedlot cattle in the weanling to young adult stage, with stress from transport, introduction to a new environment, and sometimes a new group, being predisposing factors due to compromised immune defenses. Although cases typically exhibit low morbidity and high mortality rates, severe outbreaks of TEM with elevated morbidity and mortality levels can occur. Respiratory signs may appear 7-14 days before the onset of neurological signs (34). Lateral recumbency, profound depression, and closed to semiclosed eyelids giving the animal a sleepy look (the disease is also known as Sleeper syndrome) are frequent. Blindness may or may not be present and could be unilateral or bilateral. An animal in lateral recumbency may progress to opisthotonos and seizures. If the animal is able to stand, ataxia and weakness are present. Dysfunction of multiple CN may

be evident on closer neurologic examination. A high fever is observed frequently. The course is rapid, and death usually occurs within 24-36 hours from the onset of neurological signs in the absence of treatment (34).

Presumptive diagnosis relies on history, clinical and neurological examination, blood, and CSF analysis. The main differential diagnoses for encephalopathy in feedlot cattle are TEM, polioencephalomalacia, lead poisoning, and water intoxication. Definitive diagnosis is often based on post-mortem examination. Peripheral blood abnormalities are nonspecific and may include neutropenia or neutrophilia with left shift. CSF characteristics reflect a bacterial infectious process associated with hemorrhage, showing often neutrophilic PL, increased microprotein concentration, and elevated RBCC with macroscopic xanthochromia (6,8,34,46).

At necropsy, disseminated suppurative lesions can be observed in various organs, including myocardium, pleura, genitourinary and respiratory tracts with lung consolidation, laryngeal and tracheal mucosal ulcers, and formation of diphtheritic membranes (6). Necropsy findings related to the nervous forms are hemorrhagic infarcts in the brain and spinal cord. The lesions are most often multiple and of various sizes, with some being visible macroscopically. Histologically, vasculitis, thrombosis, and neutrophil infiltrates are the signature of the disease (34).

Treatment of an affected animal should be attempted only if the animal is believed to be in the early stages of the disease and antibiotic therapy combined with non-steroidal anti-inflammatory drugs (NSAIDs) and supportive care is advisable. *H. somni* is generally susceptible to a majority of conventionally employed antimicrobial agents (6). Furthermore, concerns regarding antibiotic penetration are minimal due to the compromised endothelial integrity and infarcts leading to the disruption of the BBB (34). For commercial livestock, the administration of parenteral oxytetracycline stands as the most commonly recommended

therapeutic approach. Treatment is not recommended if the animal presents in recumbency, indicating an advanced stage where antibiotic therapy is ineffective (46).

Following a case of TEM, it is advisable to monitor animals in the same group as the affected individual to promptly intervene in case signs appear (34).

3.2.3 Otitis media and otitis interna (OMI)

Otitis media/interna (OMI) is a common bacterial-origin pathology in ruminants, especially in cattle, causing significant economic losses (51). Both sporadic cases and outbreaks have been reported (52). The condition is more frequent in calves aged 1 week to 18 months, particularly during the weaning period(53). Males might be predominantly affected (54), especially in cases of *Mycoplasma bovis* infections (55). Beef cattle are generally more affected, though there has been an increase in cases in dairy cattle in recent years (56). Incidence of the condition may increase in winter months and during extreme climatic periods (57).

In most cases, OMI is a consequence of an upper respiratory tract infection and bacteria ascend through the Eustachian tubes from the nasopharynx to reach the middle ear. Therefore, commonly involved bacteria are those responsible for respiratory infections in cattle, such as *Mycoplasma spp*, *Mannheimia haemolytica*, *Pasteurella multocida*, *Corynebacterium pseudotuberculosis*, and *Histophilus somni* (6,58). *M. bovis* is becoming the primary etiological agent of OMI in dairy cattle, but its exact prevalence is difficult to determine due to the challenge of culturing these microorganisms and the presence of non-pathogenic species within the same genus in healthy ears (56). *Trueperella pyogenes*, is frequently isolated in chronic forms (56). Other microorganisms from the genera *Streptococcus*, *Staphylococcus*, and *Neisseria* have been isolated in conjunction with the aforementioned respiratory bacteria, but that these microorganisms can also be present in the external ear of healthy cattle (59). More rarely, OMI could result from an external ear

infection that breaches the tympanic membrane or from septicemia. Hematogenous spread can usually be ruled out if there are no clinical signs of septicemia (6,59). When the infection arises from the external ear, it is often secondary to parasitic infestation. This possibility is rare in Europe and more typical of tropical and subtropical environments, where the involved parasites are usually nematodes. In temperate zones, though rare, a similar situation could arise due to infestation with *Raillietia auris* (56).

OMI, if left untreated, can spread to the CNS, causing subdural abscesses, meningoencephalitis, or brain abscesses. Dissemination to the CNS is rare, however (6).

Clinical signs vary depending on the structures involved. Considering that the infectious process is usually unilateral and involves both the middle and inner ear, peripheral vestibular signs with involvement of the CN VII and the CN VIII can be observed. These may include head tilt towards the side of the lesion, horizontal nystagmus with the rapid phase that goes away from the lesion, and vestibular ataxia with a tendency to drift and circle toward the side of the lesion. CN VII involvement is due to its close proximity to the tympanic bulla, resulting in ipsilateral deficits including drooping eyelid, pendulous ear, and flaccid lip and nostril (6,56). Sometimes, before the onset of vestibular signs, reduced appetite, fever, and persistent head shaking due to the discomfort from the ongoing inflammatory process may be noticed (60).

In cases of involvement of the external ear, discharge from the ear, generally purulent, may be observed (59). Finally, in cases where the inflammatory process disseminates to the CNS, animals might develop subtle or pronounced signs of brain disease (6).

The presumptive diagnosis of OMI is primarily based on medical history and clinical examination, and the main differential diagnosis is listeriosis. Based on neurological examination, the two conditions can be distinguished, as animals with OMI maintain a normal and alert level of consciousness and the disease does not involve CN other than CN VII and CN VIII (59). Definitive diagnosis requires additional investigations. Blood analysis

may show only an inflammatory leukogram not being therefore very indicative. CSF analysis is usually normal unless there is CNS involvement (46).

For a definitive diagnosis, otoscopic examination or imaging techniques such as X-rays or CT scans can be used to visualize the tympanic bullae. Aural discharges can be cultured or tested by PCR for the presence of *Mycoplasma spp.* or other bacteria.

Post-mortem necropsy examination can reveal characteristic lesions such as erythema and swelling of the tympanic membrane, edema or thickening of the mucosa of the auditory system, exudate in the tympanic cavity, rupture of the tympanic membrane with exudate accumulation in the external auditory canal, destruction or sclerosis of bony structures inside and around the ear, and replacement of bony structures with granulation tissue. Histopathological examination may reveal a suppurative inflammatory process in the tympanic cavity and surrounding bony structures, osteolysis, and perineural inflammation of CN VII and VIII (56,59).

Treatment varies depending on the etiological agent causing the OMI. Parasitic otitis requires external ear lavage and topical antiparasitic therapy with ivermectin (59). For bacterial otitis, antibiotic therapy is indicated. Ideally, antibiotics should be chosen based on culture and sensitivity, but this is often not feasible. Given the frequent involvement of multiple bacterial species, a broad-spectrum therapy is often chosen (56). *Mycoplasma* organisms, which lack a bacterial cell wall, are often involved, making the use of β-lactams ineffective in these cases (6). In a study from 2015, a combination therapy of tulathromycin, oxytetracycline, and carprofen was found to be effective in calves with early diagnosis of OMI (54). Another study identified complete response to enrofloxacin administration (52). Overall acute cases often exhibit complete remission of clinical signs, while chronic cases, which are often refractory to treatment, may have persistent neurological deficits even after complete resolution of the infectious-inflammatory process (6,59).

3.2.4 Encephalitic listeriosis

Neurologic disease produced by pathogenic serotypes of *Listeria monocytogenes* is common in adult cattle. Listeriosis is a disease with zoonotic potential, raising public health considerations when its occurrence is evident. In most cases, human infection occurs following the consumption of inadequately pasteurized milk, cheeses made from such milk, or meat-based products. Less commonly, infection may result from contact with infected animals (46,59).

Listeria monocytogenes is a motile, gram-positive bacillus with the remarkable ability to inhabit and replicate within macrophages and various other cell types. This bacterium infiltrates the brainstem, specifically targeting CN V and CN VII, and potentially other CNs. Research strongly suggests that the entry of the organism into the CNS commonly occurs through breaches in head tissues, in regions such as the face and oral cavity. Migration of *Listeria* occurs along CNs, primarily the trigeminal branches, ultimately reaching the pontomedullary region of the brainstem, thereby initiating the development and dissemination of meningoencephalitis. Another possible route of CNS infection is reported to be via the bloodstream. Bacterial infection manifests as diffuse microabscesses and a meningitis characterized by the inflammatory response's evolution from neutrophilic dominance to a prevalence of mononuclear cells.

Feeding of silage, most particularly when it has not been rendered totally anaerobic during processing, is the main risk factor for listeriosis. Thus, animals being fed silage, often indoors in winter, that have teeth erupting or are predisposed to facial and mouth injury by access to coarse straw are overrepresented with the disease.

Encephalitic listeriosis is characterized by mental state depression, often accompanied by a gradual or sudden onset of head tilt and circling behavior. These animals may also display a tendency to isolate themselves from the herd, drawing attention to ocular and nasal discharge, food retention in the oral cavity, excessive salivation, teeth grinding, and

abdominal bloating, which are readily noticeable to farmers and owners. Upon neurological examination, head tilt and turn, circling, as well as paresis and ataxia affecting all limbs are consistent findings. Several CNs are often involved:

- CN V: loss of tone and drooping jaw, inability to eat due to paresis/paralysis of the masticatory muscles, and loss of sensitivity in the head.
- CN VII: drooping ear, loss of lip tone and ptosis (which cause drooling on the same side), absence of the menace response and palpebral reflex (which can lead to secondary exposure keratitis).
- CN VIII: vestibular signs such as head tilt, pathological nystagmus and vestibular ataxia.

As the infection spreads to the midbrain, progressive obtundation sets in, culminating in a semicomatose state, and the disease is fatal without treatment. It is noteworthy that, during the early stages of the disease, forebrain-related signs such as seizures, aggressiveness, and blindness are usually absent, a characteristic that differentiates listeriosis from various other meningoencephalitis observed in ruminants.

The diagnostic suspicion of listeriosis is based on the history (particularly indicative information such as silage consumption) and neurological signs, supported by characteristic findings in CSF analysis. A venous blood gas analysis can identify metabolic acidosis resulting from excessive bicarbonate loss due to salivation (59). CSF analysis usually reveals increased TP concentration and moderate mononuclear PL. The extent of CSF alterations is not correlated with the severity of the disease or prognosis (6,8). *L. monocytogenes* rarely reaches the ventricular system, hence both culture and PCR from CSF frequently yield negative results (61). A definitive diagnosis of encephalitic listeriosis is made at necropsy (59). Isolation of *L. monocytogenes* can be successful from biopsy samples of nervous tissue, especially if stored at refrigeration temperature (4°C), as the

bacteria can multiply under such conditions (6,46). Immunohistochemistry (IHC) for *listeria* antigens results more effective than culture for detecting the pathogen (56). At necropsy, lesions are present throughout the brainstem. Macroscopic findings include mild to marked congestion of meningeal vessels. Microscopic lesions are more characteristic and include multifocal asymmetrical brainstem microabscesses with areas of malacia and intense perivascular cuffing with mononuclear cells, and meningoencephalitis. Other findings are multifocal gliosis, axonal degeneration and swelling and neuronophagia (6,56). Within necrotic areas, macrophages prevail, while neutrophils are more prominent in microabscesses. The aforementioned microscopic lesions are sufficient for diagnosing listeriosis even in the absence of microorganism isolation (59). Therapeutically, administration of antibiotics over an extended period of generally 2-4 weeks or more is recommended. Commonly used antibiotics include tetracyclines (oxytetracycline), penicillin, and ampicillin (6,56,59). Supportive therapy to rehydrate the animal and restore proper acid-base and electrolyte balance is crucial alongside antibiotic treatment. The use of anti-inflammatory therapy remains under discussion; in dehydrated animals, potential adverse effects of NSAIDs, such as renal toxicity and gastrointestinal ulcerations, may be exacerbated (56,59). Similarly, steroid anti-inflammatory agents like dexamethasone might inhibit cell-mediated immune response (56).

3.2.5 CNS abscesses and empyema

Suppurative processes of the CNS often create considerable necrosis. The accumulation of necrotic tissue localized within a tissue (e.g. the brain), is an abscess. When this purulent accumulation occurs in a pre-existing cavity or between adjacent tissues, it is referred to as empyema. Basilar empyema is an accumulation of purulent material at the level of the basisphenoid bone surface, involving also the carotid rete mirabile and the pituitary gland (62). Brain abscesses or empyema are a relatively rare condition of mainly adult cattle, with

two possible pathogenic mechanisms proposed as causes: either the expansion of a localized purulent process involving other structures of the skull (such as chronic frontal sinusitis) or the dissemination through the bloodstream. For basilar empyema there is often a history or evidence of processes such as nose ringing (46). Organisms isolated from brain abscesses or empyema in ruminants include *Trueperella pyogenes* in the majority of cases, *Corynebacterium pseudotuberculosis*, *Fusobacterium*, *Streptococcus spp*, *Acinetobacter spp*, *Pseudomonas spp*, and *E. coli*. (46,49). Brain abscesses fall under the category of "space-occupying lesions", and their clinical manifestations primarily arise from the compression they exert on brain tissue, varying according to the location of the lesion. Typically, the clinical signs are asymmetric and exhibit a gradual onset. Commonly observed signs include altered sensorium, behavioral changes, ataxia, tetraparesis, blindness (unilateral or bilateral), compulsive walking, circling, head pressing, and head tilt. When an abscess is located near the brainstem, it can lead to deficits in several cranial nerves (6,46,49). In more advanced stages of the disease, signs may include decerebrate rigidity posture and seizures (6). Additionally, severe conditions like brain herniations, where the cerebellum descends through the foramen magnum, exerting pressure on the medulla oblongata, can be lethal.

Suspecting a brain abscess in cattle relies on clinical presentation and CSF analysis, which may vary from normal to significantly altered, with elevated TP concentration and severe PL (8). This variation depends on the location of the abscess, either extradural or intradural. In some cases, contrast MRI and CT have been employed to confirm the diagnosis in bovine patients. However, the latter are not practical in routine clinical settings and definitive diagnosis often requires postmortem investigations. During necropsy, macroscopic examination may reveal flattened convolutions, cerebellar herniation, and telencephalic asymmetry. Predominantly, lesions are found in the cerebral cortex, characterized by yellowish, purulent material encapsulated by a thin whitish layer. The inflammatory infiltrate

is prominent, with both healthy and degenerated neutrophils. Abundant bacteria, a delicate fibrous lining, neovascularization, and perivascular infiltrates of lymphocytes and plasma cells are also observed (62). While treatment involving antimicrobials and anti-inflammatory drugs may yield a slight, albeit temporary, improvement, the prognosis remains extremely poor (46).

3.2.6 Vertebral suppurative arthritis, osteomyelitis and discospondylitis

Pyogenic organisms can infect vertebrae and associated structures, leading to a range of pathological changes that ultimately compress the spinal cord. This process is commonly observed in colostrum-deprived neonates and may coincide with other pyogenic diseases caused by various bacteria such as sepsis and NBSM-ME. Clinical signs often include reluctance to move, stiffness, pain, paresis, and other neurological deficits. The involvement of different segments of the spinal cord can lead to specific neurological deficits, such as flaccid pelvic limb paresis/paralysis and hyporeflexia in case of L4-S2 spinal cord lesion. Coexisting problems like diarrhea, polyarthritis, localized sepsis, or other abscesses may be present. Diagnosis involves imaging (X-rays, CT, MRI), and CSF analysis, which can vary from normal to mononuclear PL or AC dissociation. CSF culture is only rarely positive while culture from samples obtained by direct aspiration from vertebral and paravertebral lesions has proven useful in identifying the bacterial agent. Treatment includes prolonged antimicrobial, although the prognosis remains generally poor (46).

3.2.7 Septic aortic thrombosis

Diarrhea and sepsis caused by *E. coli* can precede the development of septic thrombosis in the descending aorta and iliac arteries, leading to subsequent paralysis in neonatal or preweaning calves. This condition results in significant motor neuron impairments, particularly affecting the pelvic limbs, tail, and perineum, ultimately culminating in flaccid paraplegia (46,63).

3.3 Knowledge gaps in bacterial infection of the CNS

Achieving an etiological diagnosis in case of CNS infection is paramount, enabling precise treatment and effective control and prevention strategies. Doing so can be challenging however because clinical signs and hematological changes often are nonspecific.

While advanced diagnostic imaging is less feasible for larger animals, CSF collection can be easily and safely performed in the field. CSF analysis in the diagnosis of infection usually shows a moderate to marked increase in TNCC and TP concentration which are not specific for CNS infectious diseases, however (26). Additionally, as outlined in Chapter 2.4, the timely analysis of CSF is essential, yet it is subject to operator proficiency and requires specialized facilities that may not be readily accessible on-site. Furthermore, the current approach for identifying the causative agent behind bacterial CNS infection relies on bacterial detection through Gram staining or CSF culture isolation and this method is burdened by delayed diagnosis and suboptimal sensitivity (8,29).

To address these limitations, pioneering approaches might hold potential. Machine learning (ML) techniques, have shown promise in revolutionizing disease diagnosis (64). By analyzing complex patterns and correlations within datasets, ML algorithms can potentially discern subtle nuances that elude human observation, leading to more accurate and rapid diagnoses. These algorithms could be trained on large datasets including different clinical and laboratory information, supporting the diagnostic process of bacterial infection of the CNS. Another frontier lies in the utilization of next-generation sequencing (NGS) technologies (65). NGS offers unparalleled insights into microbial diversity, enabling the detection of even rare and elusive pathogens. By sequencing bacterial genomes present in CSF samples, NGS can provide a comprehensive view of the pathogenic landscape, allowing for targeted treatment strategies and real-time monitoring of therapeutic efficacy. Moreover, the quest for novel biomarkers holds significant promise in transforming diagnostic paradigms (66). The discovery of specific molecules associated with bacterial

CNS infections could offer rapid and reliable diagnostic tools. These biomarkers could be detected in CSF samples, offering a fast and specific means of identifying CNS bacterial infections. Lastly, the validation and exploration of automated CSF analyzers could serve as a viable alternative to the labor-intensive manual analysis, offering more prompt and operator-independent outcomes (67).

In conclusion, the accurate diagnosis of bacterial CNS infection in cattle is an imperative yet challenging endeavor. While traditional diagnostic approaches rely on clinical reasoning and CSF standard analysis, the integration of innovative approaches like ML, microbial DNA sequencing, biomarker identification and automated CSF analysis holds the potential to revolutionize the field. These cutting-edge methodologies could provide timely, accurate, and specific diagnoses, thereby facilitating more effective treatment and management strategies for bacterial CNS infection in cattle.

The upcoming sections will provide an overview on the current landscape of ML techniques integrated into clinical decision-making, advancements in bacterial DNA sequencing methods, the exploration of lactate as a potential bacterial infection marker and the current use of automated analyzers for CSF analysis.

4 ML in medicine and scientific research

The use of ML in medicine and scientific research has gained significant attention recently (68). Advanced technologies have led to the rapid accumulation of diverse patient data, including medical images, -omics profiles, clinical records, and social media data. These health datasets are often high-dimensional, containing numerous features per observation (64). Moreover, datasets are typically sparse, noisy, and lack statistical power, complicating traditional data analysis methods that focus on single variables or simple correlations. Additionally, integrating diverse data types for a comprehensive understanding of diseases exacerbates these challenges (64). To address this, advanced ML models are increasingly

applied to biomedical and healthcare data. In contrast to conventional statistical analysis, which depends on predefined rules and follows a hypothesis-driven approach, ML learns insights directly from input data, enabling predictions in new scenarios. These approaches help tackle high-dimensional data by reducing analyzed features and integrating data sources to increase statistical power (64). ML techniques are broadly divided into three categories: supervised, unsupervised, and reinforcement learning methods. Among these, supervised ML is the most frequently employed for disease-related data and needs a labeled dataset for training. These labels often require manual curation, like a radiologist labeling MRI scan images or a pathologist categorizing post-mortem patient samples. The ML algorithm constructs a model based on the relationship between input features (e.g., brain region size from an MRI scan) and the label (e.g., diagnostic category) from this labeled dataset. Subsequently, the algorithm can predict the label for new, unlabeled datasets using this model. Classification and regression are two subsets of supervised learning. Classification predicts categorical outputs (diagnostic categories) for each data sample (patient), while regression predicts continuous variables (e.g., functional impairment degree on a continuous scale). In contrast, unsupervised ML does not require labeled data and is useful for clustering data samples or simplifying complex datasets. For instance, gene expression datasets can be analyzed using unsupervised clustering algorithms to identify patient clusters with shared molecular characteristics.

Reinforcement learning employs “rewards” or “punishments” to achieve desired outcomes. For instance, an algorithm might explore a new medication regimen based on the medical history of patients, with rewards for improvements and punishments for adverse reactions. Although rapidly explored, reinforcement learning is less prevalent in the disease research field compared to supervised and unsupervised learning (Figure 6) (64,69).

Figure 6: Categories of Machine Learning (from “Applications of machine learning

to diagnosis and treatment of neurodegenerative diseases", by Myszczynska et al. 2020)

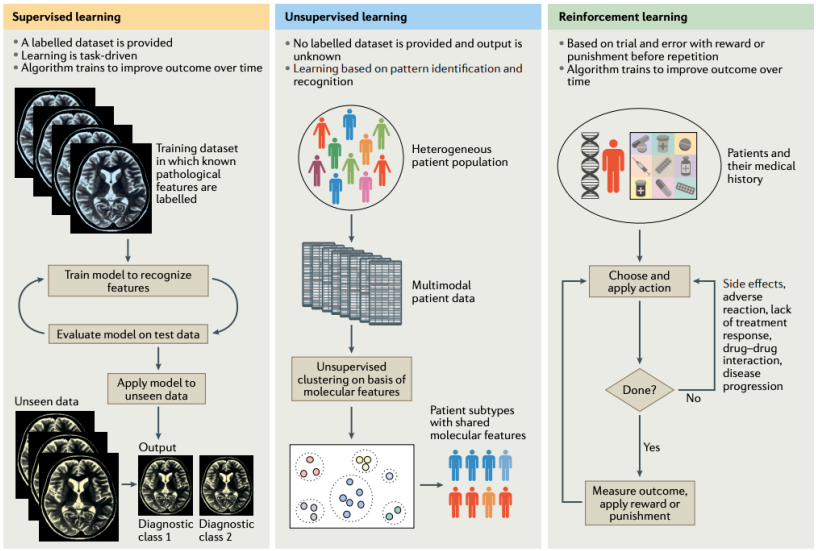

Numerous ML algorithms exist and choosing the right one for specific data is crucial. When focusing on supervised learning, modality (data form) and volume (data sample count) play vital roles in algorithm selection. For data with a low sample-to-feature ratio (SFR) (SFR <10:1), algorithms struggle to learn effective 'featurization' and classification. Featurization means identifying and extracting characteristics or 'features' that differentiate data points into classes. A higher SFR facilitates better feature identification. For limited datasets, constrained models like hierarchical Bayesian models simplify the task by learning a few parameters. Larger datasets commonly employ support vector machines (SVM) or random forests (RFs). SVMs map datasets to maximize the separation of categories (e.g. healthy and diseased). In contrast, RFs construct numerous independent decision trees, each providing a classification, and the algorithm selects the most common prediction from these trees to mitigate overfitting seen with a single decision tree.

A comprehensive review (70) has underscored the widespread utilization of ML methods in human medicine field. The review identified 44 articles that applied ML techniques to improve human disease diagnosis within the period 2015-2020, primarily concentrated in the fields of cardiology, endocrinology, infectious diseases, and pulmonology.

Compared to human medicine, the utilization of ML methods in veterinary medicine has been considerably limited. Specifically, when applying ML to clinical decision-making and diagnosis, only a few studies have explored its potential role. Examples include predicting the likelihood of survivability and the necessity for surgery in horses diagnosed with acute abdomen (71), as well as predicting the occurrence of chronic kidney diseases in cats (72). Additionally, ML has been employed for disease classification using MRI data in dogs (73,74).

In light of these findings, it is evident that ML holds substantial promise for advancing veterinary medicine, offering opportunities to enhance clinical decision-making, diagnosis, and disease classification. Future investigations in this realm are warranted.

5 NGS for microbial community analysis

NGS technology has advanced our understanding of microbial communities within diverse environments (75). NGS technology enables the simultaneous sequencing of millions of DNA fragments, providing unprecedented insights into the genetic composition and functional potential of complex ecosystems and bypassing the need for microbial culture (75). This approach has now applications in diverse fields and is advancing in veterinary and human medicine, aiding diagnostics in challenging cases (76).

Sequenced based microbiome studies can be divided into metagenomic sequencing (i.e. shotgun sequencing) and metataxonomic or metabarcoding sequencing (i.e. 16S gene sequencing). Shotgun sequencing involves sequencing all DNA present in a sample, while 16S gene sequencing focuses specifically on a universal gene (16S gene) highly conserved among bacteria. Shotgun sequencing provides more information than 16S gene sequencing. In particular, shotgun sequencing is better suited for exploring various microbial kingdoms, including not just bacteria but also viruses and fungi. Additionally, shotgun metagenomic sequencing has the potential to identify bacteria and other microorganisms at

the species level (e.g., Bifidobacterium longum), and in some cases, even down to the strain level. In contrast, 16S gene sequencing typically identifies bacteria at the genus level (e.g., Bifidobacteria). Furthermore, unlike 16S gene sequencing, shotgun sequencing offers insights into microbial gene content and functions. Nevertheless, despite the fact that 16S gene sequencing cannot directly profile microbial genes/functions, some bioinformatic tools are available to predict microbiome function with 16S gene data. Furthermore, innovative approaches to 16S gene sequencing have recently been introduced to enhance the depth of taxonomic classification, reaching the species level for a majority of identified bacteria (75). Adding to this, a significant advantage of 16S gene sequencing in bacterial community investigation lies in its reduced likelihood of amplifying and sequencing 'host' DNA. In contrast, shotgun metagenomic sequencing involves sequencing all DNA within a sample, potentially leading non-microbial reads to obscure microbiome results. This distinction is especially crucial in microbiome studies on samples where microbial biomass could be low while host DNA is abundant. Based on these premises, 16S gene sequencing might be better suited for investigating bacterial CNS infection in cattle. The following sections will describe workflow and application on microbiome analysis, focusing on 16S gene sequencing.

5.1 16S gene PCR and sequencing workflow

Irrespective of the chosen sequencing technique, the fundamental stages of investigating microorganisms in a sample are quite similar. This process starts with sample collection and preservation, which can vary based on context and sample type. Sterile conditions are recommended during collection to ensure patient well-being and prevent contamination that could impact analysis outcomes. A significant challenge lies in distinguishing between encountered microorganisms as potential pathogens or contaminants when interpreting

sequencing data (77). This distinction becomes particularly crucial when sequencing samples with low biomass (78).

Given the vulnerability of nucleic acids to environmental enzymes or host action, sample preservation is critical, and the sample should be frozen upon collection at -80°C, being cautious not to undergo repeated freeze-thaw cycles which could release endogenous nucleases and degrade nucleic acids (79) If immediate freezing is not possible, various preservation media that stabilize or fix bacterial DNA for sample storage are being developed (80).

The sample processing begins with the extraction of DNA. Extraction can be manual or automated depending on the laboratory, and a variety of commercial kits are available based on the chosen method and the type of biological sample (75).

The subsequent steps involve creating DNA libraries. Library preparation will vary according to the technique of sequencing. 16S library preparation is based on the following steps:

- Amplicon PCR: the 16S rRNA (ribosomial ribonucleic acid) gene regions are selectively amplified using PCR with universal primers targeting conserved regions. This step generates amplicons specific to the 16S gene across diverse microorganisms. Usually the 16S targeted regions are the V3 and V4 regions, however different protocols have been suggested in the literature (75,81).
- PCR clean up: this step purifies the 16S V3 and V4 amplicon away from free primers and primer dimer species.
- Index PCR: this step attaches dual indices and sequencing adapters. These adapters contain sequences that enable the samples to be multiplexed and that will be recognized by the sequencing machine. Ligation involves binding the adapters to the ends of the DNA fragments.
- PCR clean up 2: This step cleans up the final library before quantification.

- Library Quantification, Normalization, and Pooling: the purified library is then quantified and normalized to ensure equal representation of each sample before pooling. For quantification a fluorometric method that uses dsDNA binding dyes is recommended (e.g. Qubit Fluorometer). Moreover, the library size should be verified by means of a Bioanalyzer that provides quantitative and precise information about the size distribution of the library fragments. This is crucial for ensuring the success of the sequencing experiment (82).

The sequencing process itself is automated and executed by sequencers, specialized machines designed to determine the order of nucleotide bases that constitute DNA chains. Sequencers come in various types, each with its unique mechanism. The outcomes produced are referred to as reads, which are sequences of bases corresponding to sections or complete DNA fragments (77). These reads are also described as the base sequences of individual DNA molecules (77,83). Diverse NGS platforms are available from different manufacturers, each incorporating distinct technologies and capabilities. Illumina platforms are the most prevalent, with a range of instruments such as MiniSeq, MiSeq, NextSeq, NovaSeq, and HiSeq models.

The sequencing results require analysis and interpretation, typically accomplished through specialized software and pipelines. Commonly used pipelines include QIIME (quantitative insights into microbial ecology), USEARCH and DADA2 (84,85). The first step of analysis is to convert the raw reads into a feature table. These raw reads are typically in paired-end (PE) 250 bases mode. The process begins with the grouping of raw amplicon PE reads based on their barcode sequences, a procedure known as demultiplexing. Subsequently, the PE reads are merged to generate amplicon sequences, with the removal of barcodes and primers. It is common to include a quality control step to eliminate low-quality amplicon sequences. A crucial aspect of amplicon analysis involves selecting representative sequences to serve as proxies for species identification. There are two primary methods for

representative sequence selection: clustering into Operational Taxonomic Units (OTUs) or denoising to generate Amplicon Sequence Variants (ASVs). The UPARSE algorithm is utilized for sequence clustering, grouping sequences with 97% similarity into OTUs. However, this method may fail in detecting subtle differences among species or strains. A more precise denoising algorithm called DADA2 has been developed, which produces ASVs as highly accurate representative sequences. This denoising approach is accessible through various tools such as 'denoise-paired/single' by DADA2, 'denoise-16S' by Deblur in QIIME 2 and '-unoise3' in USEARCH. Finally, a feature table, referred to as the OTU/ASV table, is generated by quantifying the frequency of these feature sequences in each sample. Concurrently, the feature sequences can be assigned taxonomy, typically at various hierarchical levels, including kingdom, phylum, class, order, family, genus, and species. This taxonomic assignment provides a means of dimensionality reduction in the analysis of microbiota data (84).

In general, 16S gene sequencing is primarily employed to gather information about the taxonomic composition of microbial communities. However, several software packages have been developed to predict potential functional information. This prediction is based on linking the 16S gene sequences or taxonomy information with functional descriptions found in the scientific literature (84).

Figure 7 illustrates the workflow of commonly used methods for 16S rRNA gene sequencing (referred to as “amplicon”) (A) and metagenomic (B) sequencing.

Figure 7: Workflow of commonly used methods for 16S rRNA gene sequencing (A) and metagenomic (B) sequencing (from “A practical guide to amplicon and metagenomic analysis of microbiome data”, by Liu et al. 2021)

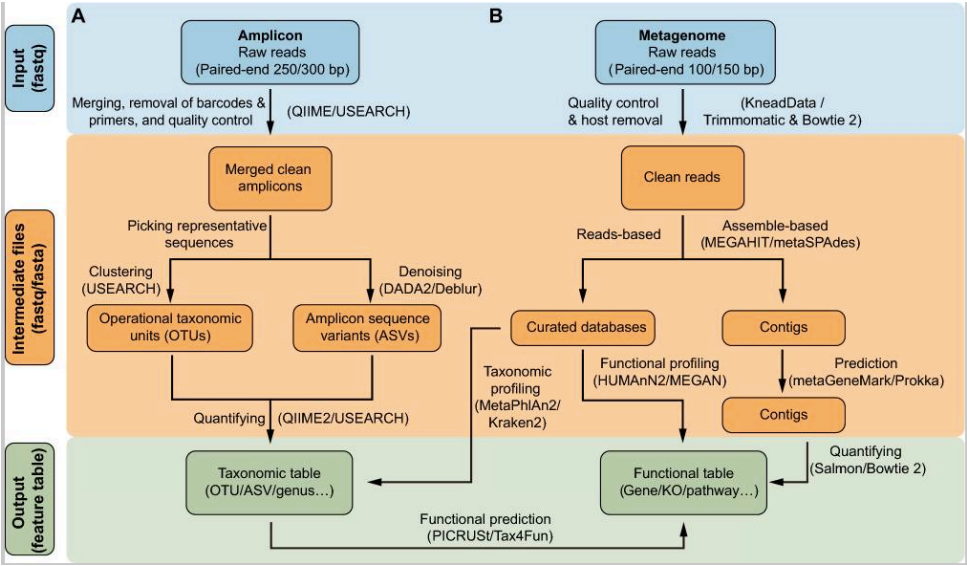

5.2 Applications in human CSF

Bacterial CNS infections in human occur mostly in children, elderly and immunocompromised individuals. Meningitis can also develop after neurosurgical procedures like craniotomy, or during the insertion of devices like ventriculostomy tubes. It is also observed in cases of spinal surgery and among patients who have experienced head injuries (86).

Over the last decade, advanced sequencing technologies have greatly improved the capacity to detect the causative agents of infectious diseases of the CNS in clinical human samples, where conventional methods are often burden by delayed diagnosis and lack of sensitivity (65). In particular, several studies focused on the application of NGS techniques on CSF and both metagenomic and metataxonomic sequencing techniques have been applied (87,88). However, studies demonstrate varying sensitivity and specificity of NGS methodologies due to different extraction methods and databases used for comparison. Despite the benefits, challenges in result interpretation, identification of commensal vs. pathogenic microbes, and technical limitations persist, warranting further research to establish NGS as a diagnostic gold standard for CNS infections (78). Moreover, NGS's potential to investigate the CNS microbiome, once considered sterile, is emerging as a

groundbreaking avenue of research. Recent studies have explored the presence of microbes within CSF and brain tissue, with varying results and implications for understanding neurological health and disease (89,90).

5.3 Applications in veterinary medicine

Unlike human medicine, in the veterinary field, there have been 3 published studies so far, where CSF was analyzed with NGS technology. These were conducted in dogs and aimed to evaluate the presence of potential causative agents in subjects with meningoencephalomyelitis of unknown origin (MUO) using shotgun sequencing. Their analyses did not identify potentially pathogenic microorganisms, supporting the hypothesis that MUO might be immuno-mediated (91–93). Another study aimed to assess the prevalence of neurologic infectious diseases in the Swiss cattle population and used metagenomic sequencing on RNA and DNA extracted from brain tissue to diagnose viral infections (36).

Concerning the use of 16S sequencing in cattle, several studies have been performed on substrates different from CSF. In particular, they focused on characterizing the rumen and fecal microbiome (94,95), the respiratory system microbiome (96,97), and the skin microbiome (98), both in health and disease.

In summary, a wide range of applications for NGS exists within the field of farm animal medicine. However, applications of NGS on CSF to investigate diagnosis of CNS infection in veterinary patients are lacking.

5.4 Experimental considerations in Low-Biomass research

Samples can be categorized as having high microbial biomass (e.g., stool), low microbial biomass (e.g., respiratory tract samples), and zero-to-low microbial biomass (e.g., placental

and fetal tissues, brain tissue, and CSF). In the latter, the existence of microorganisms is not established (78).

Contamination presents an ongoing challenge in microbiological research, especially concerning low or zero-to-low biomass samples. The issue has been highlighted by recent reports of human tissues, such as blood, brain and cancers, which were previously thought to contain no, or very little, bacterial biomass, but apparently contain diverse microbial communities. These discoveries carry implications for human health and disease. However, in investigations involving low biomass, distinguishing meaningful signals from contamination-induced noise is complex. Contamination may lead to misinterpreting sterile tissues as non-sterile or vice versa, thereby obscuring genuine microbial signals. Contaminants can originate from microbial DNA present in various sources such as reagents, labware, tools, and DNA extraction kits. Additionally, cross-contamination can occur between PCR tubes or wells, sequencing runs, and sequencing lanes (99–101).

Commonly used negative controls are imperfect, as they only capture a limited subset of sample-processing stages or are unevenly distributed across batches. Relying excessively on such negative controls often leads to the identification of false positive signals attributed to contaminant detection. Even with proper controls in place, distinguishing authentic signals from low-abundance contaminants proves challenging, as sporadic appearances of signals in both samples and negative controls are possible. Conversely, potentially genuine signals associated with samples can sometimes erroneously emerge in negative-control samples due to cross-contamination during DNA extraction, PCR or sequencing stages (78,101).

Given the limitations of sequencing approaches, confirmation through alternative methods, such as 16S FISH, bacterial culture, 16S qPCR, or ICH for bacterial components (e.g., LPS), is necessary (78).

6 Lactate

6.1 Introduction

Lactate is a metabolite produced by various metabolic reactions within the body. For a long time, it was considered a simple byproduct of anaerobic metabolism, but its importance has now been significantly reevaluated, and its fundamental role in cellular bioenergetics is recognized. Moreover, both in human and veterinary medicine, lactate proves to be a potentially crucial diagnostic, prognostic, and therapeutic target, particularly in emergency and intensive care conditions (102).

6.2 Definition

Lactate and lactic acid are not synonymous. Lactic acid, with a chemical formula of CH3CH(OH)COOH, is a strong acid with a pKa of 3.8, which is not produced in vivo. At physiological pH, lactic acid is nearly completely dissociated into the lactate anion, C3CH(OH)COO-, and H+ protons (103). Lactate exists in the form of two enantiomers, due to its asymmetric C2 atom: L-lactate and D-lactate. Under physiological conditions, L-lactate is the predominant enantiomer in the mammalian body, accounting for 95-99% of total body lactate (103,104). D-lactate is produced in significantly lower quantities through the glyoxalase metabolic pathway and the degradation of glucose and carbohydrates by commensal bacteria in the gastrointestinal tract of mammals (105). L-lactate can potentially be produced by all cells in the body, and subsequently, it can be either utilized directly by the producing cell for further metabolic pathways or released from it, accumulating in the blood and many other body fluids, including CSF, synovial fluid, interstitial fluids, and effusions (106).

6.3 Biochemistry of L-lactate

Under physiological conditions, L-lactate is primarily produced by skeletal muscle (40-50%), the brain (13%), and adipose tissue (in varying amounts) (107). Other L-lactate-producing tissues and cells include the renal medulla, erythrocytes, leukocytes (mainly neutrophils), platelets, skin, and the gastrointestinal tract (106). Erythrocytes, lacking mitochondria, produce 80% of blood L-lactate (108). However, under pathological conditions such as sepsis, there is a marked increase in L-lactate production by phagocytic immune cells (neutrophils and macrophages) and therefore by organs rich in phagocytes like the liver, spleen, intestines, and lungs (109).

The most significant metabolic pathway leading to L-lactate production is represented by anaerobic glycolysis. Glycolysis is the primary degradation pathway of glucose, consisting of a cascade of enzymatic reactions occurring in the cell's cytosol. Starting from one molecule of glucose, it produces two molecules of pyruvate, two molecules of (adenosine triphosphate) ATP, and two molecules of reduced nicotinamide adenine dinucleotide (NADH). This process requires a constant supply of oxidized nicotinamide adenine dinucleotide (NAD+) for ATP production, occurring in the absence of oxygen. Subsequent phases take place in the mitochondria and only in the presence of oxygen. The pyruvate produced via anaerobic glycolysis is decarboxylated to Acetyl Co-A within the mitochondria, a reversible reaction catalyzed by the enzyme complex pyruvate dehydrogenase. Acetyl Co-A then enters the tricarboxylic acid (TCA) cycle, generating carbon dioxide, NADH, flavin adenine dinucleotide (FADH2), and guanosine triphosphate (GTP). The protons generated from reduced cofactors NADH and FADH2 create a proton gradient enabling ATP production through the electron transport chain (ETC). This combination of glycolysis, the TCA cycle, and the ETC yields approximately 36 final ATP molecules from the oxidation of one glucose molecule (110).

Under physiological conditions, around 10% of the pyruvate produced by glucose, is converted to L-lactate in the cytoplasm through a reversible reaction catalyzed by the

ubiquitous enzyme LDH (Figure 8) (111). LDH exists in five different isoenzymes, separable through electrophoresis: LDH1, LDH2, LDH3, LDH4, LDH5. Each isoenzyme is a tetramer composed of variously combined H and M subunits. Thus, each organ has a distinct pattern of LDH isoenzymes based on its metabolic needs. Within the CNS, LDH1 and LDH2 are the most expressed isoenzymes (112). When cellular oxygen availability decreases, NAD+ reserves deplete, pyruvate and NADH accumulate in the cytosol, and LDH increases its activity, resulting in more L-lactate production (113). L-lactate formation reduces cytoplasmic pyruvate and H+ concentrations, while replenishing NAD+. This way, through glycolysis, the cell continues to produce ATP (114). While ATP production under anaerobic conditions is significantly reduced (only 2 moles of ATP are produced per mole of glucose metabolized to lactate), compared to aerobic metabolism, it allows a certain amount of energy to be generated, sustaining cellular metabolism (105). When oxygen supply is restored, LDH converts L-lactate back to pyruvate, which can enter the TCA cycle or be utilized in gluconeogenesis. Hence, L-lactate formation serves as a protective mechanism, consuming pyruvate and H+ ions, alleviating acidosis (115). L-lactate serves as a readily transportable energy accumulation molecule, a form of energy currency that can be exchanged and transferred to meet metabolic demands (116).

6.4 Lactate transport

Lactate is primarily transported across cell membranes through facilitated passive transport facilitated by proton-linked monocarboxylate transporters (MCT) and sodium-coupled MCTs. There are around 14 identified MCTs, with MCT1 and MCT4 being the most significant in mammalian tissues. These MCTs exhibit variable expression across different tissues and are relatively non-specific, moving various substrates including lactate, pyruvate, acetate, propionate, butyrate, acetoacetate, and beta-hydroxybutyrate. MCTs also have a crucial role in "lactate shuttles," which facilitate energy exchange between distinct

cells and tissue types. Lactate shuttles have been observed in the brain, striated muscles, liver, kidneys, and myocardium, serving as the primary means for lactate transportation across cells, particularly among tissues with varying energy requirements (Figure 8) (117).

6.5 Biochemistry of D-lactate

D-lactate is produced in minimal concentrations in mammals, primarily through the glyoxalase metabolic pathway and fermentations carried out by commensal bacteria located in the gastrointestinal tract. Additionally, exogenous administrations of sodium lactate, lactate Ringer's solution, some solutions used for peritoneal dialysis, and propylene glycol administration can lead to the formation of D-lactate (106). It is also reported that the consumption of certain foods by humans, such as milk, yogurt, pickles, apples, molasses, tomatoes, beer, and wine, can represent a minimal exogenous source of D-lactate (106).

The glyoxalase metabolic pathway is a biochemical process that results in the conversion of methylglyoxal (a reactive and toxic substance produced in small amounts during the metabolism of carbohydrates, fats, and proteins) into D-lactate and glutathione. This reaction is catalyzed by two enzymes: glyoxalase I and glyoxalase II (118). This is a ubiquitous reaction that can occur in the cytosol or mitochondria. Generally, the amount of D-lactate produced through this metabolic pathway is extremely small (on the order of micro- or nanomoles) and therefore is rare to have a condition of D-lactic acidosis. D-lactate is normally produced in the organs of the gastrointestinal tract where fermentations occur (rumen, cecum, colon), mainly by *lactobacilli* and *bifidobacteria*. Under physiological conditions, the D-lactate produced in this way is not a threat to the body's acid-base balance because it is rapidly converted by gut microbiota into acetate and other short-chain fatty acids, such as propionate and butyrate (119). Once absorbed, propionate is eliminated by the liver and converted into glucose, triglycerides, and carbon dioxide, while butyrate is oxidized by colon mucosal cells for ATP production (120).

Another possible metabolic pathway for D-lactate is its further conversion to pyruvate by the enzyme D-α-hydroxy acid dehydrogenase and D-lactate dehydrogenase. The latter was initially thought to be present only in lower organisms, but subsequent studies have shown its presence in mammalian mitochondria. Specifically, these enzymes might be located on the inner face of the mitochondrial membrane (121). However, there are contrasting theories in the literature regarding the metabolism and excretion of D-lactate in mammals. The most widely shared opinion is that D-lactate is not efficiently metabolized by mammals (119).

D-lactic acidosis is a metabolic condition that rarely occurs in mammals and is defined as metabolic acidosis accompanied by an increase in serum D-lactate ≥ 3 mmol/L (122). In humans it is occasionally observed as a consequence of short-bowel syndrome. It also occurs in ruminants after grain overfeeding, inappropriate ruminal fermentation of milk, and as a sequela to diarrhea in neonatal calves (103). An increase in D-lactate concentration has also been documented in cats with diabetic ketoacidosis (123), propylene glycol intoxication (124), exocrine pancreatic insufficiency (125), and gastrointestinal disorders (126).

6.6 The Warburg Effect

The Warburg effect, also known as “aerobic glycolysis”, is a biological metabolic phenomenon first observed in cancer cells. These cells show a tendency to prioritize glycolysis, even under oxygen-rich conditions. This metabolic choice results in the generation of lactate as a secondary product and contrasts with the predominant energy production method of normal cells, which heavily rely on oxidative phosphorylation within the mitochondria, especially in the presence of oxygen. Despite the comparatively lower energy yield of glycolysis, cancer cells persistently utilize this pathway to fulfill their energy demands. The Warburg effect is named after Otto Warburg, who first described this metabolic alteration in 1923. The exact reasons behind why cancer cells exhibit this

metabolic shift are complex and not completely understood yet. Some theories suggest that the Warburg effect may provide advantages to cancer cells by supporting rapid growth, providing biosynthetic precursors, and helping them cope with the unique metabolic challenges of their environment. Moreover, tumor cells are not the only ones exhibiting this distinctive metabolic pathway: naive immune cells, including neutrophils, dendritic cells, and macrophages, switch their metabolism from oxidative phosphorylation to aerobic glycolysis when activated using toll-like receptors (TLR) ligands or pro-inflammatory cytokines, in a manner similar to tumor cells. Furthermore, in the brain, lactate production, primarily driven by astrocytes, also occurs via this metabolic pathway (127).

6.7 Lactate in blood

6.7.1 Introduction

In both human and veterinary medicine, lactate, is a metabolite measured and evaluated primarily in blood. An increase in blood lactate has been significantly correlated with the severity, morbidity, and mortality of numerous pathological conditions such as shock, heart failure, acute liver failure, severe sepsis, neoplasia, seizures, poisonings, and pharmacological therapies (128).

Hyperlactatemia is defined as an increased concentration of lactate in blood beyond the reference range. In dogs, normal lactate values range from 0.3 to 2.5 mmol/L (129); in cats, the reported normal range in the literature is 0.30 – 1.69 mmol/L (130). In cattle, normal blood lactate values reported are 0.31–1.51 mmol/L (131).

When collecting blood for lactate concentration evaluation, there are numerous factors to consider to accurately interpret the results. Some studies show, for instance, that if an animal becomes agitated and moves during the blood sampling, a temporary state of hyperlactatemia can occur due to muscular activity (130); even prolonged occlusion of the vessel from which the blood is collected can increase lactate concentration (132), however,

the vessel momentary occlusion during routine blood sampling should not lead to this kind of alteration (133). Regarding the sampling site, lactate measured in arterial blood seems to be a better balance between lactate production and extraction by all body tissues compared to venous lactate (129). However, the difference between arterial and venous lactate is minimal (unless severe hypoperfusion is present) and lactate is usually measured in venous blood due to ease of collection (102). Lactate can be measured in whole blood, plasma, or serum. Measuring lactate in serum is not recommended as the time needed for sample preparation can lead to a significant increase in metabolite concentration, however (134). Lactate measured in whole blood should represent the average of plasma and intra-erythrocytic concentration after red blood cell lysis, while plasma lactate represents only the plasma portion. Nevertheless, most lactate analyzers, both laboratory-based and portable, use whole blood as the sample but do not perform erythrocyte lysis, so the lactate value they provide is actually the plasma value; this allows for much quicker results, as there is no need to wait for the time required for centrifugation and sample separation, and the provided value is still reliable (116). Understanding the machine's operation and reported value type is crucial for comparing results with reference ranges and literature (116). Finally, concerning sample handling, it is advised not to use tubes containing sodium citrate as it interferes with lactate measurement in the sample and leads to falsely lower results (134).

6.7.2 Classification of hyperlactatemia

As previously mentioned, when a blood lactate value exceeds the physiological range, it is termed hyperlactatemia. Hyperlactatemia is divided into two broad categories: type A, resulting from insufficient oxygen supply, and type B, where oxygen supply appears to be maintained. Patients can exhibit both type A and type B simultaneously. Furthermore, type A hyperlactatemia can be relative, due to an increased oxygen demand, or absolute, due to inadequate oxygen supply. Type B hyperlactatemia is further divided into three

subcategories: B1, associated with underlying pathology; B2, associated with drugs and toxins; and B3, caused by congenital metabolic disorders (102).

Relative type A hyperlactatemia is induced by a sudden increase in the oxygen demand of the body and is primarily associated with physical activity or seizures. In both cases, however, the increase is moderate and temporary, as the lactate concentration rapidly decreases (in about 20-60 minutes) when muscular activity stops (135).

Absolute type A hyperlactatemia is due to reduced oxygen supply and is observed in cases of shock, local and systemic hypoperfusion, severe anemia, severe hypoxemia, and carbon monoxide poisoning (116). Among these, shock is the most common cause in veterinary medicine. It has been observed that hyperlactatemia occurs independently of the type of shock (hypovolemic, cardiogenic, obstructive, distributive) (136). Specifically, it develops when shock becomes decompensated: this is when oxygen extraction is maximized, leading to tissue hypoxia and activation of anaerobic metabolism to support cellular energy production. Therefore, hyperlactatemia serves as an indicator of hypoperfusion (102).

Also type B1 hyperlactatemia, associated with the underlying pathology, is quite common in veterinary medicine. Common causes include sepsis, which induces a hypermetabolic state and damages microcirculatory components, leading to altered blood flow, mismatched capillary perfusion, and unbalanced oxygen delivery to tissues (137). Malignant neoplasms can interfere with lactate-related metabolic pathways via the Warburg effect (see Chapter 6.6), as can diabetes mellitus due to dysregulated glycolysis, compromised gluconeogenesis, reduced pyruvate dehydrogenase activity, and decreased oxidative metabolism (106). Studies suggest that dogs with diabetes mellitus have statistically higher plasma lactate concentrations compared to healthy dogs (138). Liver and kidney diseases can also alter lactate elimination mechanisms (116). Additionally, thiamine deficiency, hypothyroidism, cellular respiration disturbances, microcirculation alterations, or adrenergic

stimulation leading to catecholamine release can contribute to type B1 hyperlactatemia (116).

Type B2 hyperlactatemia, associated with drugs and toxins, is well-documented in human medicine, with limited studies in veterinary medicine. Glucocorticoids, used at anti-inflammatory or immunosuppressive doses, have been shown to increase blood lactate concentration in animals. They alter carbohydrate metabolism, promote amino acid conversion to pyruvate, inhibit pyruvate dehydrogenase, and enhance the hyperlactatemic effect of catecholamines (139). Acetaminophen intoxication is associated with hyperlactatemia due to mitochondrial respiration disruption and liver dysfunction, leading to reduced lactate elimination (140). Significant increases in blood lactate have also been reported in cases of ethylene glycol intoxication. Ethylene glycol is converted to toxic metabolites such as glycolic acid, oxalate, and glyoxylic acid. This process elevates the NADH/NAD+ ratio and inhibits pyruvate metabolism, promoting lactate formation (141). However, it is known that ethylene glycol metabolites can be mistakenly measured as lactate by some portable analyzers, leading to wrongly measured increases (142). Finally, intoxication with propylene glycol (a substance widely used as a preservative in cosmetics, food products, and pharmaceuticals) is reported to cause hyperlactatemia. However, these cases are sporadic in veterinary medicine, and the pathogenesis is not fully elucidated (143). Lastly, type B3 hyperlactatemia, resulting from congenital metabolic errors, is extremely rare in animals. Possible congenital defects associated with this condition include pyruvate dehydrogenase complex defects, defects in the TCA cycle, gluconeogenesis defects affecting pyruvate carboxylase, phosphoenolpyruvate carboxykinase, fructose 1,6-bisphosphatase, or glucose 6-phosphatase (106).

6.8 Lactate in other body fluids

Both in human and veterinary medicine, several studies have been conducted to assess the concentration of lactate in other body fluids besides blood.

6.8.1 Abdominal effusion

In veterinary medicine, the increase in lactate concentration in peritoneal fluid has been observed primarily in the presence of bacterial septic effusions, neoplastic effusions, and strangulating intestinal obstructions. For instance, a study demonstrated that a lactate concentration > 2.5 mmol/L was significantly correlated with septic peritonitis in both dogs and cats (144). Another study found significantly increased lactate concentrations in abdominal effusion in dogs with neoplastic effusion (145). Experimental studies in dogs have also shown that in the presence of strangulating intestinal obstruction, lactate concentration in peritoneal fluid rapidly and significantly increases, while it tends not to increase in non-ischemic intestinal obstructions (146). Similar results have been obtained in studies carried out in horses: horses with strangulating intestinal obstructions also had significantly higher lactate concentrations in peritoneal fluid (specifically ≥ 4 mmol/L) compared horses with non-strangulating obstructions (147). Additionally, another study showed that in horses, a ratio of lactate concentration in peritoneal fluid to blood > 1 significantly correlated with the need for abdominal surgery (148); however, this result remains controversial as it was not confirmed by other studies (149).

6.8.2 Pericardial effusion

In dogs, the concentration of lactate in pericardial effusion has been evaluated to determine whether it could be used as a marker to differentiate neoplastic effusions from effusions of other origins in this location. Despite the median lactate concentration values in neoplastic effusions being significantly higher than that of non-neoplastic effusions, the too wide overlap between the two groups prevented lactate to be a useful diagnostic tool (150). No similar studies were conducted in other animal species.

6.8.3 Bronchoalveolar lavage (BAL) and pleural effusion

In human medicine, increased lactate concentration has been observed in bronchoalveolar lavage (BAL) during inflammation (151). Additionally, numerous studies have been conducted to assess the concentration of lactate in pleural effusion highlighting that low lactate values exclude an ongoing septic process, while elevated values are more likely to be associated with sepsis or neoplastic conditions (152). In veterinary medicine, there are currently no studies that have investigated this parameter in pleural effusion.

6.8.4 Synovial fluid

Studies conducted in human medicine demonstrate that a low concentration of lactate in synovial fluid allows for the exclusion of septic arthritis, while elevated lactate levels can be associated with different forms of inflammatory arthritis (153,154). In veterinary medicine, studies have been carried out in dogs and horses, while research on other species is lacking. In dogs, higher lactate concentration in synovial fluid is associated with septic arthritis compared to immune-mediated inflammatory arthritis (155). Conversely, in horses, such conclusion is less unequivocal, with considerable overlap in lactate values observed between infected cases and their healthy controls (156,157).

6.9 Lactate in CSF

6.9.1 Introduction

Lactate in the CNS is produced primarily by astrocytes in response to neuronal activity by “aerobic glycolysis”. This metabolic pathway is specific to astrocytes and is regulated by a gene expression profile that promotes lactate production from pyruvate rather than its utilization in the TCA cycle (Warburg effect, see Chapter 6.6). Once produced, lactate exits astrocytes and can be taken up by neurons, as both cell types possess MCTs that facilitate lactate transport via the lactate shuttle. Neurons can utilize lactate as an alternative energy

substrate to glucose (which remains the preferred energy substrate), thereby continuing to generate a certain amount of ATP crucial for neuronal survival (Figure 8) (158).

Figure 8: Simplified representation of lactate production within astrocyte and astrocyte-neuron lactate shuttle model (created with Biorender). GLUT: glucose transporter; MCT: monocarboxylate transporter; LDH: lactate dehydrogenase.

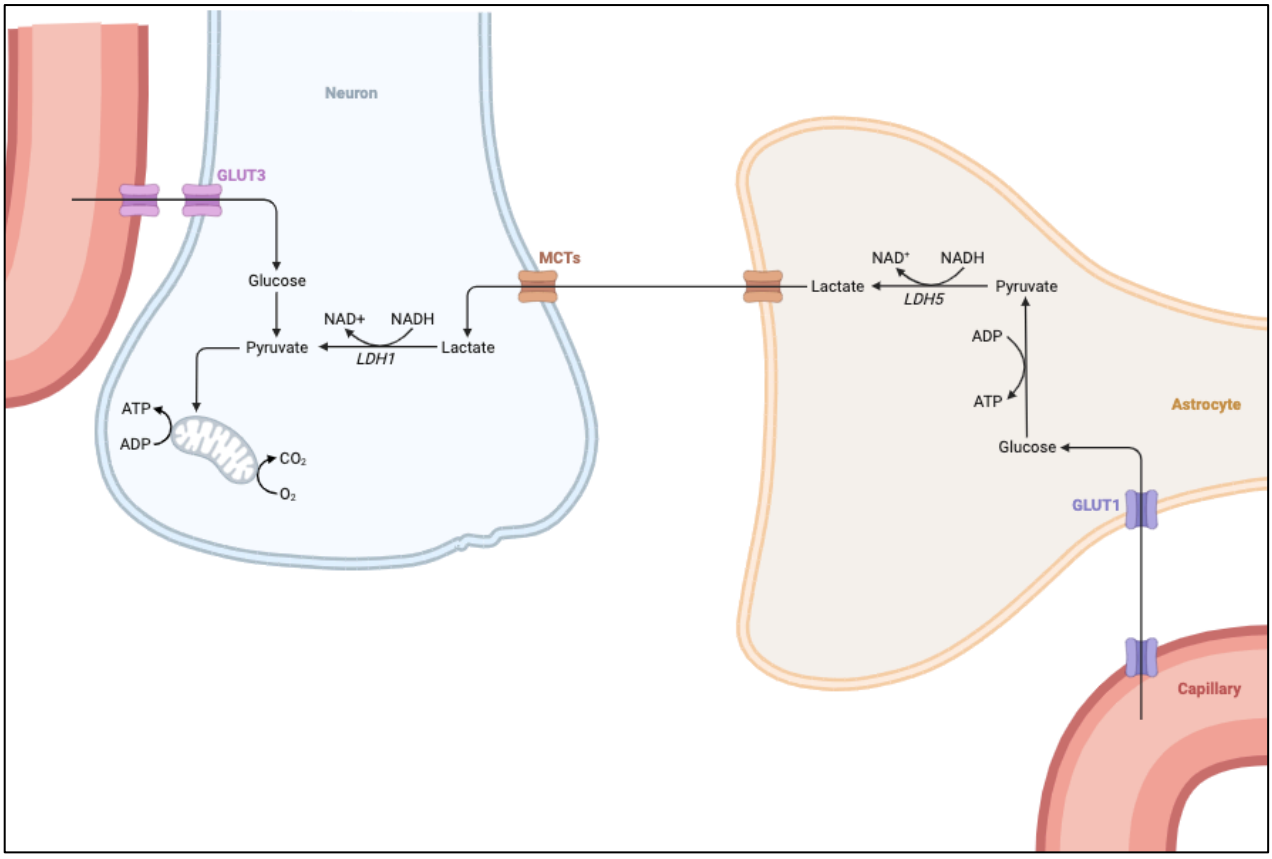

Numerous studies have underscored the physiological significance of lactate in ensuring neuronal survival and functionality, especially under specific conditions such as hypoglycemia and hypoxia (159). While lactate plays a neuroprotective role within certain limits, a marked increase in its production by neural tissue, leading to elevated CSF concentration, is indicative of neural distress and altered metabolism. This could result from various CNS pathologies such as infections, seizures, strokes, mitochondrial disorders, traumas, subarachnoid hemorrhages, and many others (160).

It is important to emphasize that the concentration of lactate measured in CSF can be regarded as a specific marker of the metabolic state of the CNS, as it is independent of blood lactate levels. This arises from lactate's full ionization at physiological pH, resulting in slow BBB permeation. Multiple studies confirm this concept (161,162). However, under pathological conditions, the integrity of the BBB could be compromised, leading to a partial impact of blood lactate concentration on CSF lactate concentration (163,164).

6.9.2 Measurement techniques

The traditional measurement of lactate usually involves enzymatic or chromatographic methods. Enzymatic techniques for lactate detection utilize enzymes to catalyze reactions that generate detectable signals corresponding to lactate concentrations in a sample. Lactate oxidase, a commonly used enzyme, reacts with lactate in the presence of oxygen, producing pyruvate and hydrogen peroxide (H_2O_2) as byproducts. The enzymatic reaction's detection can be interpreted through various approaches including colorimetric detection, amperometric detection, fluorometric detection, and electrochemical detection. On the other hand, chromatographic methods for lactate detection involve separating and quantifying lactate molecules within a sample using chromatography techniques. Once the lactate molecules are separated, they can be analyzed using a mass spectrometer. This device quantifies the separated lactate molecules based on their distinctive signals (165).

Portable lactate analyzers find frequent use in both human and veterinary medicine. These include devices like Lactate Plus©, StatStrip Xpress©, Accutrend©, Lactate Pro©, Lactate Scout©, and iSTAT©. These analyzers rely on enzymatic methods to measure lactate concentration. Specifically, Accutrend© and Lactate Plus© have been applied in veterinary medicine for measuring lactate concentration in CSF (166,167).

Lactate Plus©, is part of the same family as StatStrip Xpress© (Nova Biomedical, Waltham, MA, USA) and has been previously validated for canine CSF analysis (166). It quantifies L-lactate concentration using an enzymatic amperometric system. This approach involves utilizing a lactate oxidase electrochemical biosensor to detect the production of hydrogen peroxide resulting from the enzymatic reaction. This process generates an electric current that directly corresponds to the lactate concentration. This instrument requires about 0.6-0.7 µL of the sample and provides results within 13 seconds (166).

The advent of these low-cost, user-friendly devices that provide reliable data in extremely rapid times is at the core of the growing interest in lactate as a potential prognostic and diagnostic marker in various pathological conditions, both in human and veterinary medicine. The minimal amount of sample required for conducting the analysis is another advantage of these tools, as the majority of laboratory analyzers require a volume of at least 100 µL of sample (166).

6.9.3 Effect of blood contamination

The impact of blood contamination on CSF lactate concentration remains a topic of debate in the literature. Erythrocytes can generate lactate through anaerobic glycolysis, potentially leading to increased CSF lactate levels when present in samples, especially if analysis is not conducted promptly after collection (168,169). However, recent consensus suggests that blood contamination does not significantly affect CSF lactate concentration (170–174).

6.9.4 Clinical utility of lactate in CSF

6.9.4.1 Human Medicine

Lactate in CSF has been extensively studied in human medicine, revealing elevated concentration in various CNS-related pathologies. The physiological range for this metabolite in humans is 1.2 - 2.1 mmol/L (175).

The most promising diagnostic efficacy of CSF lactate is observed in the context of identifying bacterial meningitis and effectively distinguishing it from aseptic/viral presentations.

Bacterial meningitis is uncommon (incidence 0.4-5%) yet serious, with mortality rates of 20-40% (176). Early diagnosis is hindered by nonspecific clinical signs, concurrent infections, and challenging CSF interpretation. Numerous studies have demonstrated an increase in CSF lactate concentration during bacterial meningitis in the attempt to establish a cut-off (range, from 2.1 to 4.44 mmol/L) that can differentiate bacterial meningitis from aseptic inflammation of the CNS (177–180).

CSF lactate, rapidly measurable especially with portable analyzers, has exhibited superior diagnostic utility compared to other CSF parameters (TNCC, TP concentration, glucose concentration, CSF-to-blood glucose ratio) as a diagnostic aid in bacterial infection of the CNS (176). The underlying mechanism of this elevation in lactate concentration remains not fully elucidated, though it may be linked to lactate generation by immune cells recruited during infection. Specifically, neutrophils are the first cells to be recruited to the site of infection where they participate in anti-microbial host defense as regulators of both innate and adaptive immunity. Activated neutrophils display diverse effector mechanisms, including phagocytosis, activation of NADPH (reduced nicotinamide adenine dinucleotide phosphate) oxidase, release of granular contents, and release of neutrophil extracellular traps (NETs). These NETs consist of DNA, histones, microbicidal peptides, and antimicrobial enzymes and are associated with lactate formation via the Warburg effect (127,181,182). Additional

hypotheses include lactate production through anaerobic glycolysis within nervous tissue due to reduced blood flow and cerebral hypoxia, or lactate synthesis by the infecting bacteria.

Elevated CSF lactate concentration has also been documented in other neurological disorders, such as prolonged seizures. Patients experiencing status epilepticus due to various causes exhibited significantly higher CSF lactate concentration. Furthermore, this rise seems to correlate with prognosis, as patients with unfavorable outcomes displayed elevated CSF lactate levels compared to those who achieved successful recovery (183). Lactate alterations occur in neurodegenerative disorders like multiple sclerosis and Alzheimer's disease, both linked to mitochondrial dysfunction and increased anaerobic metabolism (184–186). Aneurysmal subarachnoid hemorrhage is characterized by the presence of blood in the SAS resulting from the rupture of intracranial aneurysms. Increased CSF lactate levels detected within the initial 10 days of clinical signs onset are associated with an adverse prognosis, potentially related to hyperglycolytic cerebral metabolism (187). Primary mitochondrial dysfunctions affecting the CNS are associated with increased CSF lactate level. Mitochondrial disorders prevent cells from using pyruvate as an energy substrate, leading to anaerobic metabolism and lactate production. CSF lactate concentration, as well as the lactate/pyruvate ratio, significantly differ in mitochondrial disease patients compared to controls (188).

6.9.4.2 Veterinary Medicine

In the field of veterinary medicine, numerous studies have been conducted to investigate CSF lactate diagnostic or prognostic utility in conditions affecting the CNS (163,164,167,173,174,189). Most of these studies focus on companion animals, particularly dogs, while there is a limited number of studies conducted on farm animals (15). In canines, a recently established normal range for CSF lactate, using the portable analyzer Lactate

Plus©, is reported to be 1.02 – 2.49 mmol/L (166). CSF lactate concentration above 3.6 mmol/l has been reported to be indicative of encephalitis in cattle but a normal range for this species has not been established (15).

With regards to the role of CSF lactate in seizures, there is still limited definitive information available. Initial studies conducted in the 1960s demonstrated a modest increase in CSF lactate concentration in dogs immediately after inducing chemically induced seizures (190). Similar results were later obtained in laboratory rat studies, which showed increased lactate concentration in brain tissue following experimental seizures (191,192). On the other hand, a recent study conducted on a population of dogs with various types of seizures and diverse etiologies showed that CSF lactate concentration was minimally affected by seizure activity in dogs and increased concentrations were more likely associated with the underlying disease process, in particular with neoplastic and inflammatory conditions (174). The difference in these results compared to human clinical data and experimental animal studies might arise from the routine inclusion of general anesthesia and oxygen supplementation during CSF collection in dogs during clinical procedures. Consequently, elevated blood oxygen levels could mitigate potential effects of seizures on CSF lactate concentration (174). Interestingly, a recent study assessed CSF lactate concentration in dogs under two different anesthetic protocols (propofol and isoflurane) and found that the anesthetic agents themselves can impact mitochondrial energy metabolism, leading to fluctuations in lactate concentration (193).

CSF lactate concentration was found to be increased in cats after experimentally induced spinal cord injury, although not correlating with trauma severity or prognosis (194). This increase was partly attributed to decreased blood flow through the injured spinal cord segment (resulting in hypoxia) and edema-induced compression of the parenchyma and vascular component. On the other hand, a recent study that examined CSF lactate

concentration in dogs with acute thoracolumbar intervertebral disc herniation did not discover any elevation in CSF lactate level (195).

Animals studies have also explored the relationship between CSF lactate concentration and CNS inflammation. In particular, studies have been conducted concerning CSF lactate in cases of MUO and an elevated CSF lactate concentration was detected in comparison to reference values (167,173). However, no significant differences in lactate values emerged among diagnostic subgroups of MUO and discordant results were obtained in terms of survival. Higher lactate concentrations were observed in dogs with marked lymphocytic PL and in cases where intense perivascular lymphocytic proliferation was observed during necropsy, suggesting that elevated CSF lactate might be associated with lymphocyte activation in the CNS (173,196).

Additional research conducted on companion animals has demonstrated elevated CSF lactate concentration in instances of head trauma, subarachnoid hemorrhage, and senile dementia (170,197,198).

Regarding bovine species, one recently published article explored the role of CSF lactate in cattle with neurological disorders. The study detected higher CSF levels in cattle with encephalitis compared to health, but it failed to distinguish between bacterial meningitis and other neurological disorders (15).

In summary, several veterinary studies have investigated the potential of CSF lactate concentration as a diagnostic or prognostic marker for various CNS pathologies, primarily in companion animals. However, none of the studies were able to elucidate the role of CSF lactate in bacterial CNS infections in animals.

7 Automated CSF analyzers

Traditionally, cell counting in CSF involves manual microscopic methods, employing hemocytometer chambers as described in Chapter 2.5. This process is time-consuming,

labor-intensive, and necessitates skilled laboratory personnel. Furthermore, this method has high intra-and inter-operator variability and shows insufficient precision (199). While automated hematology analyzers are now a fundamental component of clinical laboratories standard equipment, replacing the use of microscopic counting chambers for blood cell analysis, microscopic techniques remain the gold standard for CSF analysis. This is primarily because existing hematology analyzers are not optimized for evaluating low-cell concentrations (67).

Automated analyzers for CSF are currently studied in human medicine as an alternative to the gold standard manual analysis, and these methods serve as alternatives to manual techniques (67,200,201). In the field of veterinary medicine, limited research has explored the application of hematology analyzer for CSF in dogs (199,202,203) and demonstrated that automated CSF analysis can be performed in canine species. Some limitations were observed, particularly in samples with low cellularity and in the differential cell count analysis. Among the available hematology analyzers, the Idexx ProCyte Dx® (IDEXX Laboratories, Inc.) is considered the most accurate and comprehensive complete blood counting (CBC) testing available. It is currently in use at numerous veterinary hospitals, including the VTH of Turin. A recent study assessed the ProCyte Dx® Hematology Analyzer's performance in analyzing CSF in dogs (199). The findings revealed a strong correlation between the analyzer and the gold standard laboratory analysis in detecting TNCC, but suggested software modifications to improve sensitivity in detecting smaller cell increments. Overall, the diagnostic field of CSF cytology could benefit from an automated system for CSF cell counting that would meet the following requirements: the ability to count accurate small numbers of cells with particular emphasis on the differentiation between normal TNCC and increased TNCC; the ability to differentiate between polymorphonuclear and mononuclear cell populations; a rapid turnaround time and the use of small sample volumes.

EXPERIMENTAL SECTION

PROJECT 1 - A novel machine learning-based web application for field identification of infectious and inflammatory disorders of the central nervous system in cattle

1 Introduction

CNS infections in cattle are a major cause of economic loss, mortality, and decreased productivity (34,62). Certain neurological infections also may be zoonotic (35). Achieving an etiological diagnosis may allow for accurate treatment and appropriate control and prevention measures. Doing so can be challenging however because clinical signs and hematological changes often are nonspecific. CSF can be easily and safely collected in the field for diagnosis. It is the most direct antemortem method of diagnosing CNS disease, because advanced diagnostic imaging is much less feasible in large animals (26).

Some nervous diseases are related to age, neuroanatomical localization often is associated with specific infectious disorders and CSF analysis for diagnosis of inflammation usually shows a moderate to marked increase in TNCC and protein concentration (29,49,56). In the field, tentative diagnosis in a patient referred for neurological signs is arrived at by clinical reasoning and history taking for age, clinical findings including vital signs, clinical course, neuroanatomical localization, and CSF analysis. However, the cause of neurological signs rarely is confirmed without post mortem examination.

On the other hand, techniques based on artificial intelligence are gaining widespread application in a large variety of predictive tasks both in human and veterinary medicine, as well as in medical imaging interpretation and the clinical decision-making process (71,204,205). The ability to accurately predict the presence of an infectious or inflammatory disorder would be of considerable benefit for clinicians in selecting appropriate treatment.

Based on these premises, our primary objective was to develop and compare ML models that, based on demographic data and clinical and diagnostic findings, are able to predict the likelihood of a CNS disorder of infectious or inflammatory origin in neurologically-impaired cattle. Our secondary aim was to develop a user-friendly web application derived from the ML model that could be easily applied in clinical settings for the diagnosis of CNS disorders of infectious or inflammatory origin.

2 Materials and methods

2.1 Study population

The medical records of cattle presenting with signs suggestive of a CNS disorder to the neurology service of the VTH of Turin between July 2007 and March 2022 were reviewed. All animals underwent general and neurological examination by a board-certified specialist in neurology (ADA), CSF and blood analysis, and post mortem examination when possible. The medical records were evaluated for data on age, sex, breed usage, neuroanatomical localization of the CNS disorder, CSF analysis (TNCC, TP concentration, final CSF interpretation), and final diagnosis expressed as the VITAMIN D mnemonic (206). The final diagnosis was based on signalment, neurological examination, blood and CSF analysis, response to treatment, and necropsy histopathology when performed. Missing medical record data dictated exclusion from the study. Two groups were formed according to the final diagnosis: patients with infectious or inflammatory disease of the CNS (INF group) and patients with a CNS disorder of other origin (i.e., anomalous, vascular, neoplastic, degenerative, traumatic, or metabolic-toxic disorder; NON INF group). This retrospective study was conducted in accordance with current animal welfare regulations (Directive 98/58/EC and Italian Decree Law 146/2001). Samples were collected during routine diagnostic evaluation. Written informed consent had been obtained from the owners before veterinary assessment and treatment of their animals.

2.2 Descriptive statistical analysis

Standard descriptive statistics were performed using commercially available software (Phyton version 3.8.8; Excel version 16.27). Continuous variables were tested for normal distribution using the Shapiro-Wilk test (alpha .05) and found to be not normally distributed. Standard descriptive statistics are reported as median and interquartile range (IQR) for continuous variables and percentage and frequency for categorical variables.

2.3 Machine learning

Predicting a patient's classification in a diagnostic class (INF group or NON INF group) can be interpreted as a supervised binary problem. Within this framework, several ML models were trained and tested for their ability to detect the diagnostic class based on demographic and clinical and diagnostic data. A validation strategy then was applied to render the models generalizable for achieving accurate prediction in patients outside of the training set.

2.3.1 Data preprocessing

Table 1 presents the variables and their measurements. Three were numerical (age, CSF TNCC, CSF TP concentration) and 4 were categorical (sex, breed usage, clinical neurolocalization [NL], CSF interpretation). The numerical measurements were transformed by scaling each feature x to a range between 0 and 1 as follows:

$$x_{scaled} = \frac{x - x_{min}}{x_{max} - x_{min}}$$

Nonbinary categorical covariates were encoded using the one-hot encoding scheme (https://scikit-learn.org/stable/modules/preprocessing.html#preprocessing-categorical-features). The final preprocessed dataset included 20 features. Finally, because there were no missing values, no imputation of features was necessary.

Table 1: Demographic, clinical and diagnostic attributes of the dataset. AC = albuminocytologic; CSF = cerebrospinal fluid; NL = neurolocalization; PL = pleocytosis; TNCC = total nucleated cells count; TP = total protein.

Attributes		**Details**
Demographic data	Age	In months
	Sex	Male or female
	Breed aptitude	Beef, dairy or duplex aptitude
Clinical findings	NL	Forebrain, brainstem, central vestibular system, cerebellum, spinal, multifocal, diffuse intracranial
Laboratory findings (CSF)	TNCC	Number of cells/uL
	TP concentration	Mg of microprotein/dL
	Interpretation	Unremarkable, mononuclear PL, neutrophilic PL, mixed PL, lymphocytic PL, AC dissociation

2.3.2 Validation strategy

The dataset was randomly divided into training and test sets in a proportion of 75% to 25%. The training set was used to train the models and perform 10-fold cross-validation. In general, K-fold cross-validation works by randomly splitting a dataset into K equally-sized subsets. The K-1 subsets are used for training the model, whereas the remaining subset is used as an internal test to measure a model's capabilities. This process is repeated until every subset has been employed in the validation phase. Finally, the K performances are averaged to obtain a unique cross-validation score. This procedure was applied to each possible set of hyperparameters to select those corresponding to the best cross-validation performance. Finally, the model presenting optimal hyperparameters was retrained on the entire training set and final performance was calculated on the blind test set. We repeated the experiment 100 times with different random seeds of the training test split to prevent anomalies in dataset division and obtain a statistically robust evaluation. The average $\pm$ standard error of the mean (SEM) of the results are reported.

2.3.3 Classification algorithms

The ML algorithms for diagnosis prediction were logistic regression (LR), SVM, RF, multilayer perceptron (MLP), K-nearest neighbors (KNN), and gradient boosting (GB). Briefly, LR is a statistical model that estimates the probability of an event occurring (which in our case is the INF vs NON INF diagnosis), based on a given dataset of independent variables (the clinical features). Because the outcome is a probability, it is bounded between 0 and 1. SVM predicts the outcome by identifying the curve that best separates samples belonging to the 2 classes in the data points space, where each sample is a data point for which the axes are the clinical features. The curve is required to be as distant as possible from data points of both classes. RF is an ensemble of decision trees (ie, tree-like structures in which each internal node represents a test on a feature, each branch represents the outcome of the test, and each leaf node represents a class label [INF vs NON INF]). MLP is a type of artificial neural network. This model can find complex relationships among clinical features by learning nonlinear functions to predict outcome. K-NN algorithm, similar to SVM, maps the samples into their features' space. However, instead of finding the best separator of the 2 classes, it labels a sample on the basis of the class of the nearest samples. The GB algorithm combines simple models, called weak learners, into a single strong learner in a multistep fashion. The idea of GB is that, for each step, the weak learner learns to fix the errors of the previous learner, and this procedure is repeated for a certain number of stages. The analyses were performed using the Scikit-Learn package (version 1.0.2) in Python 3.8.

2.3.4 Metrics and model comparison

The standard ML metrics to measure algorithm performance on the test set were: accuracy, recall (sensitivity), precision (positive predictive value), and F1 score. The receiver operating characteristics area under the curve (AUROC) was calculated for each ML model. Accuracy refers to the ratio between correctly identified cases and the total number of cases (Equation 1). For our study, accuracy is a measurement of the model's capability to determine whether

the CNS disorder is of infectious or inflammatory origin or not by assigning equal importance to both classes. Recall, also named sensitivity, is the ratio between correctly identified positive cases and the total number of positive cases (Equation 2). It measures the percentage of correctly identified infectious or inflammatory cases. Precision, or the positive predictive value, refers to the number of animals correctly predicted as having an infectious or inflammatory disorder out of the total number predicted (Equation 3). The F1 score (Equation 4) is the harmonic mean of precision and recall. It is particularly useful in imbalanced datasets (when the number of cattle with infection or inflammation of the CNS is not comparable to the number of cattle with a noninfectious inflammatory disorder). The ROC curve is a probability curve that plots the true positive rate against the false positive rate at various classification thresholds. The AUROC provides an aggregate measure of the ability of the classifier to distinguish between classes across all classification thresholds. Unlike other metrics, the AUROC directly considers the probabilistic output of the predictor (between 0 and 1) and also quantifies how good the model is at ranking predictions. When the AUC is 1, the model can distinguish perfectly between positive and negative class points, whereas an AUC 0.5 means that the classifier is predicting either random class or constant class for all data points.

Equation 1

$$Accuracy = \frac{t_p + t_n}{N}$$

Equation 2

$$Recall(sensitivity) = \frac{t_p}{t_p + f_n}$$

Equation 3

$$Precision(positive\ predictive\ value) = \frac{t_p}{t_p + f_p}$$

Equation 4

$$F1score = \frac{2t_p}{2t_p + f_p + f_n}$$

where tp is true positive; tn is true negative; fn is false negative; fp is false positive; N is total subjects. A major property of precision, recall, and F1 score is that, by definition, they are calculated only on the positive class (INF group), whereas accuracy and the AUROC take into account positive and negative classes equally and usually are a better choice when the dataset is balanced and there is equal interest in predicting both classes correctly. For this reason, only accuracy was applied as an evaluation metric for selecting optimal hyperparameters. Finally, the post hoc Friedman test and the Nemenyi test for multiple comparisons were performed to determine the most suitable ML classifier, in which we compared accuracy and AUROC metrics of all 6 models. Statistical significance was set alpha .05.

2.3.5 Web user interface

The model with the best average performance in the 100 repeated trials was implemented in the web application. Because each trial resulted in a different set of optimal hyperparameters, there were 100 versions of the selected model. To address this issue, we took the median value of each hyperparameter for implementation of the final model. This classifier then was retrained on the entire dataset to exploit the full capacity of the data. The web application was built using the Streamlit Python-based framework (https://streamlit.io/). The application can operate only when all input variables are given. It returns the probability of a patient with infection or inflammation of the CNS. Probabilities >50% are indicative of a CNS disorder of infectious or inflammatory origin, whereas probabilities < 50% are predictive of a CNS disorder not of infectious or inflammatory origin.

3 Results

3.1 Study sample characteristics

The study sample was 184 cattle (85/184 [46%] males and 99/184 [54%] females). The median age was 4 months (IQR, 1-9 months). Most were beef cattle (142/184, 78%), 24/184 (13%) were dairy cattle, and 18/184 (9%) belonged to breeds of both beef and dairy usage. Forebrain neurological localization was identified in 81/184 (44%), multifocal localization in 30/184 (16%), the brainstem was involved in 24/184 (13%), focal spinal localization in 22/184 (12%), the central vestibular system in 16/184 (9%), the cerebellum in 7/184 (4%), and diffuse intracranial disorder was identified in 4/184 (2%). The median TNCC was 12.5 cells/μL (IQR, 3.9-44.2) and the median TP concentration was 42.9 mg/dL (IQR, 27.5-95.9). The final CSF analysis showed mononuclear PL in 76/184 (41%), unremarkable results in 63/184 (34%), neutrophilic PL in 27/184 (15%), mixed PL in 7/184 (4%), AC dissociation in 7/184 (4%), and lymphocytic PL in 4/184 (2%). An infectious or inflammatory disorder was diagnosed in 98/184 (53%) animals (INF group) and a CNS disorder of other origin in the remaining 86/184 (47%; NON INF group). Among the latter, a metabolic-toxic disorder was diagnosed in 50/86 (58%), an anomalous congenital condition in 14/86 (16%), trauma in 12/86 (14%), degenerative disease in 6/86 (7%), vascular disorder in 3/86 (4%), and CNS neoplasm in 1/86 (1%). Table 2 presents the characteristics of the two groups.

Table 2: Demographic, clinical and diagnostic attributes of INF group and NON-INF group. AC = albucminocytologic ; CSF = cerebrospinal fluid ; NL = neurolocalization ; PL = pleocytosis ; TNCC = total nucleated cells count; TP = total protein.

Clinical attributes	**INF group (n = 98)**	**NON INF group (n= 86)**
Age	4 (IQR 0-12)	4 (IQR 1.50-6.50)
Sex		
Female	57/98 (58%)	42/86 (49%)
Male	41/98 (42%)	44/86 (51%)
Breed aptitude		
Beef	75/98 (77%)	67/86 (78%)
Dairy	13/98 (13%)	11/86 (13%)
Duplex	10/98 (10%)	8/86 (9%)
NL		
Forebrain	27/98 (28%)	54/86 (63%)
Multifocal	24/98 (24%)	6/86 (7%)
Brainstem	23/98 (24%)	1/86 (1%)
Focal spinal	3/98 (3%)	19/86 (22%)
Central vestibular system	16/98 (16%)	0
Cerebellum	3/98 (3%)	4/86 (5%)
Diffuse intracranic disorder	2/98 (2%)	2/86 (2%)
CSF: TNCC (cells/uL)	33.2 (IQR 12.20-107.4)	6.50 (IQR 2.10-12.15)
CSF: TP (mg/dl)	61.00 (IQR 38.85-198.31)	30.00 (IQR 22.85-48.09)
CSF: interpretation		
Mononuclear PL	51/98 (52%)	25/86 (29%)
Unremarkable	10/98 (10%)	53/86 (62%)
Neutrophilic PL	27/98 (28%)	0
Mixed PL	5/98 (5%)	2/86 (2%)
AC dissociation	4/98 (4%)	3/86 (3.5%)
Lymphocytic PL	1/98 (1%)	3/86 (3.5%)

3.2 Algorithms

We trained and evaluated the binary classifiers: LR, SVM, RF, MLP, KNN, and GB. The dataset was balanced between the two groups: 53% in the INF group and 47% in the NON INF group. Table 3 presents the average evaluation metrics obtained from the 6 classification algorithms trained on the training set and evaluated on the test set. The LR classifier had the highest average accuracy and AUROC (0.843 ± 0.005 and 0.907 ± 0.005, respectively) whereas the RF classifier returned the lowest average accuracy and AUROC (0.802 ± 0.005 and 0.801 ± 0.005, respectively). The Friedman test and the post hoc Nemenyi comparisons were performed to compare the AUROC and the accuracy metrics of

the six models. The accuracy of the LR classifier was statistically superior to the other models ($P \leq .01$), except for the SVM ($P = .28$); the AUROC of the LR classifier was statistically higher than that of all the other models ($P = .001$). Figures 1 and 2 present the results of the AUROC and the accuracy for each model.

Table 3: Performances of the classification algorithms in predicting the diagnostic class, in terms of accuracy, precision, recall, F1 score and AUROC metrics, computed on the test set. The average values with respect to 100 repeated experiments and the related standard error of the mean (±SEM) are reported. LR = Logistic Regression; SVM = Support Vector Machine; RF = Random Forest; MLP = Multi-Layer Perceptron; KNN = K-Nearest Neighbors; GB = Gradient Boosting.

Model	**Accuracy** ± SEM	**Precision** ± SEM	**Recall** ± SEM	**F1-score** ± SEM	**AUROC** ± SEM
LR	**0.843±0.005**	**0.904±0.006**	0.794±0.007	**0.843±0.005**	**0.907±0.004**
SVM	0.832±0.005	0.890±0.006	0.788±0.006	0.833±0.005	0.835±0.005
RF	0.802±0.005	0.817±0.006	0.818±0.007	0.814±0.005	0.801±0.005
MLP	0.810±0.006	0.847±0.008	0.797±0.007	0.818±0.005	0.811±0.006
KNN	0.823±0.004	0.887±0.006	0.772±0.008	0.822±0.005	0.827±0.004
GB	0.805±0.005	0.820±0.006	**0.821±0.008**	0.817±0.005	0.804±0.005

Figure 1: Comparison of the average accuracies of the 6 ML methods (LR = Logistic Regression; SVM = Support Vector Machine; RF = Random Forest; MLP = Multi-Layer Perceptron; KNN = K-Nearest Neighbors; GB = Gradient Boosting) run on the test set, in prediction of the diagnostic class (INF group or NON INF group).

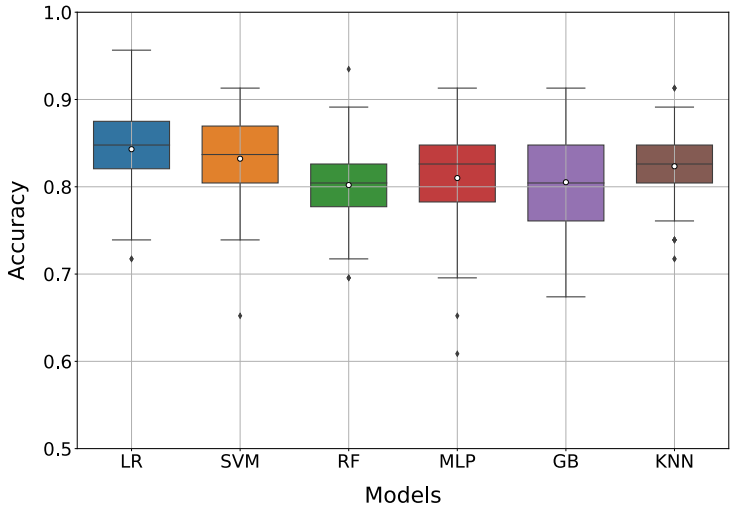

Figure 2: Comparing Receiver Operating Characteristic (ROC) curves of the six ML methods (LR = Logistic Regression; SVM = Support Vector Machine; RF = Random Forest; MLP = Multi-Layer Perceptron; KNN = K-Nearest Neighbors; GB = Gradient Boosting), computed on the test set, in prediction of the diagnostic class (INF group or NON INF group).

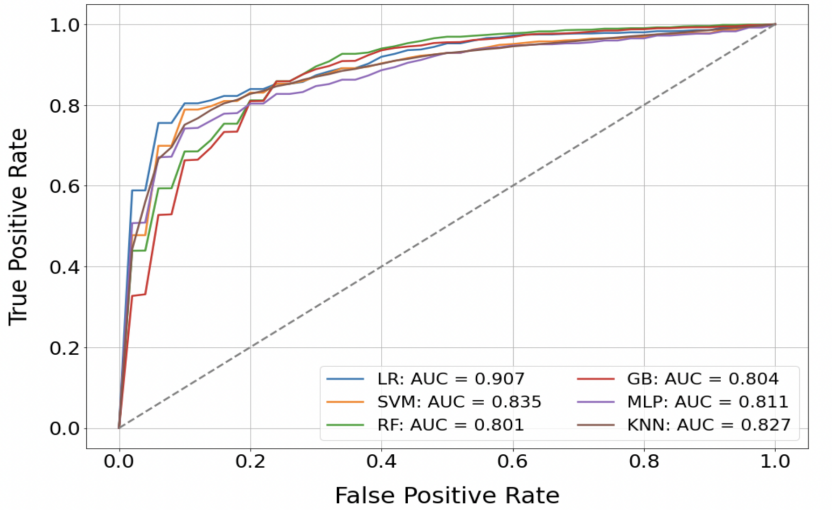

Based on these results, the LR algorithm was implemented in a free-use web application (https://cnsprediction.streamlit.app/) in the Streamlit Python-based framework (Figure 3).

Figure 3: Web-app Graphic Interface. From the website https://cnsprediction.streamlitapp.com

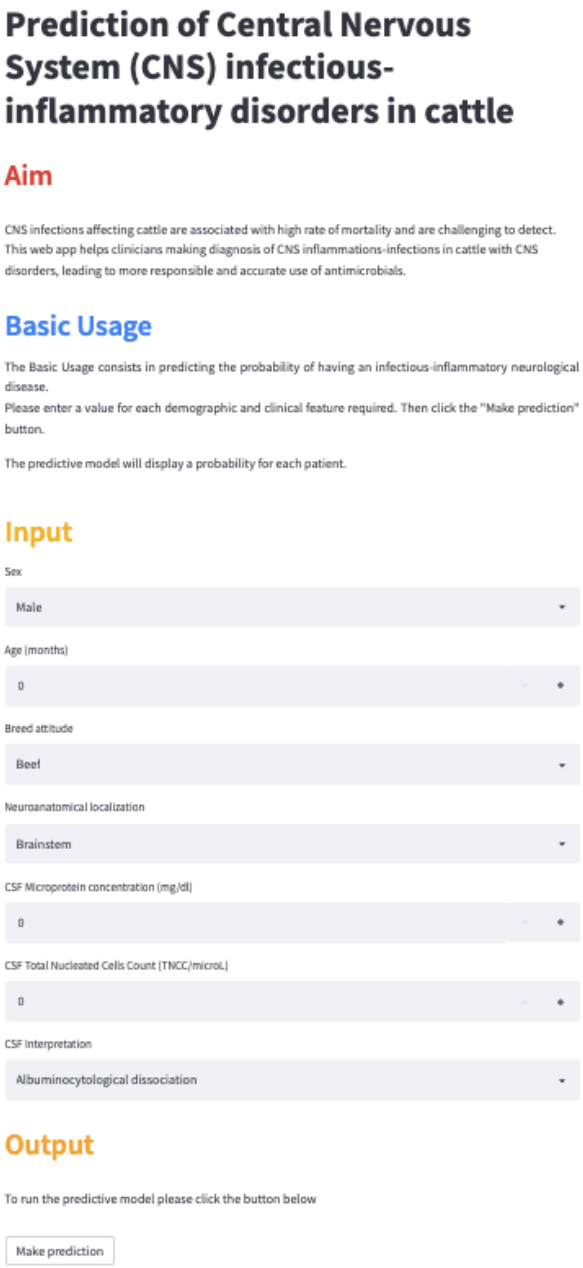

3.3 Importance of clinical attributes

We identified the major factors predicting the diagnostic class and their contributions to prediction. Indeed, not all features contributed equally to the decision-making process in the classification models. We examined the LR coefficients to explain the relative contribution of each feature. Figure 4 reports the LR coefficients attributed to the top 10 encoded features. Those associated with the INF group were neutrophilic PL in CSF and NL: brainstem, central vestibular system, and multifocal localization. Patient age was positively associated with this group as well. The features associated with the NON INF group were unremarkable CSF analysis and NL: spinal, forebrain, diffuse intracranial and cerebellar localization. Other CSF results, TNCC, TP concentration, sex, and breed usage were retained as being less informative by the model for prediction.

Figure 4: Plot of the logistic regression coefficients' ranking for the prediction of the diagnostic class. Coefficients with positive weights are associated with the INF group, coefficients with negative weights are associated with the NON-INF group. CSF = cerebrospinal fluid; NL = neurolocalization.

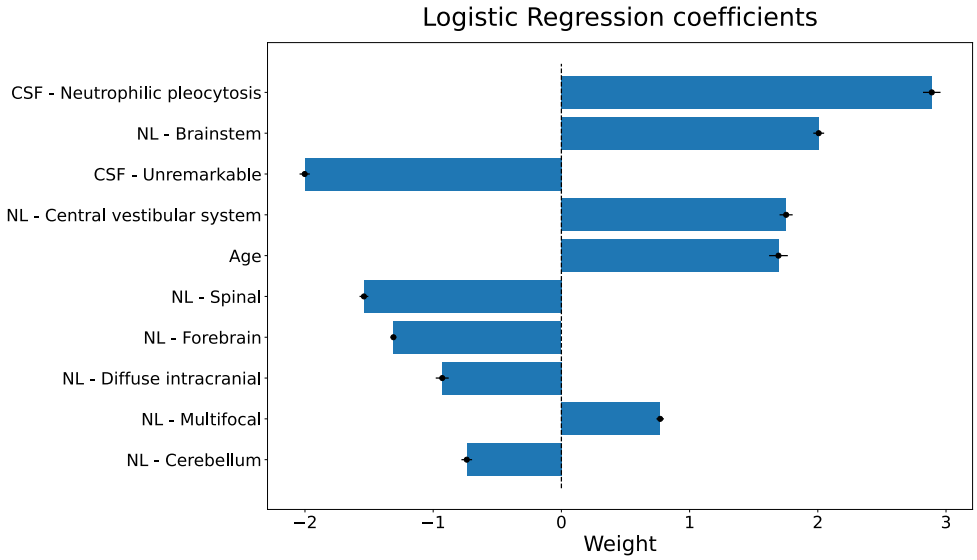

4 Discussion

We applied advanced computational modeling to predict the diagnostic class in cattle with CNS disorders. The large dataset size and balance in diagnostic classes allowed us to perform robust predictive analyses using ML techniques. One of the advantages of using ML is that, by dividing the dataset into training and test groups, the learned model can be validated on unseen data, thus decreasing the risk of overfitting and improving generalizability as a result. In our study, all six ML models performed well to predict diagnostic class (approximately 80%) according to the evaluation metrics. The average precision was higher than (LR, SVM, MLP, KNN) or equal to (RF and GB) the recall scores. Higher precision indicates that the classifier is better able to minimize false positives than false negatives. Two points were evaluated for selecting which metrics to consider. The study dataset was balanced for the number of patients in each of the two diagnostic classes, and thus accuracy and AUROC were robust and reliable metrics. Also, we were interested in accurate classification of both positive (INF group) and negative (NON INF group) cases. This information potentially decreases inappropriate use of antimicrobials, thus helping control the spread of antibiotic resistance without compromising animal health. For these reasons, neutral metrics such as accuracy and AUROC were chosen to determine the optimal model. Comparison of these 2 metrics showed that LR outperformed all of the others and therefore was selected for implementation in the web application. The reason why LR, which unlike the other models is linear, showed the best performances may be related to dataset size and the possibility that complex and nonlinear interaction between variables was not sufficiently intense. In fact, because all of the other models were intrinsically built to learn nonlinear functions for outcome prediction, their performance could suffer if the available dataset is not large enough to encompass the potential complexity. The variables used to train the model and their coefficients were consistent with the current literature and our clinical experience. The LR coefficient most strongly associated with the INF group was

neutrophilic PL in the CSF. Indeed, detection of neutrophilic PL usually is interpreted as indicating a bacterial CNS infection in cattle (8,29). Brainstem, central vestibular and multifocal NL also were strongly associated with the INF group. In ruminants, the main differential diagnoses for brainstem disease are listeriosis and brainstem abscess. Similarly, central vestibular system involvement often occurs consequent to the spread of otogenic intracranial infection (59). Multifocal localization is considered highly suspicious of infectious or inflammatory disease in both human and veterinary medicine (34). Older age was associated with increased risk of belonging to the INF group. Infectious and inflammatory diseases of the CNS can occur in animals of any age (34). The NON INF group consisted mostly of animals with metabolic disease (60% of those in the NON INF group), which affects animals of any age (207). However, our study population included several patients with congenital anomalies (16% of the NON INF group), which usually are referred in the first days of life, which partially could explain this result. In contrast, the LR coefficient most often associated with the NON INF group was unremarkable CSF analysis, as noted in previous studies (8). Spinal localization associated with the NON INF group may be explained by the fact that neurological disorders of the spine often are of traumatic origin, (208) whereas CNS infection or inflammation frequently is associated with intracranial signs (34). In addition, neoplasia was reported to be the most common cause of spinal cord lesions in a recent study on recumbent dairy cows (209). Forebrain localization was associated with the NON INF group. It is a common in metabolic-toxic disorders in young and adult cattle, (207) which made up approximately 60% of diagnoses in the NON INF group. Hypocalcemia and hypomagnesemia have been reported as the most common causes of seizures in cattle, (210) whereas seizures caused by infection occurred in <9% of cases. Finally, the main differential diagnosis of diffuse intracranial and cerebellar localization, which was associated with the NON INF group, includes congenital and genetic anomalies and metabolic-toxic disorders (211,212). Variables that were less useful for the predictive model were TNCC

and microprotein concentration. Although this finding was somewhat unexpected because CSF analysis for infectious and inflammatory conditions usually is characterized by a moderate to marked increase in both TNCC and TP concentration, most cases of infection in our study had only mild or moderate PL, which does not rule out other neurological disorders (8,213). Our study had some limitations. The predicted diagnostic class was either infectious inflammatory or noninfectious inflammatory because sample size did not allow for differentiation of the predictive output for all classes of the VITAMIN D mnemonic. A larger representation of each etiological class and a larger dataset would be necessary to train the model adequately to predict such classes with reasonable confidence. Similarly, our dataset size did not allow the models to sub-differentiate each infectious case from the others. Increasing sample size by involving other study centres with strict inclusion criteria to minimize bias could overcome this problem and allow for higher predictive power. Finally, we cannot exclude a geographical bias that could influence the prevalence of different disease pathogens because all cases came from a particular Italian area (Piedmont). The inclusion of other research centres in different geographical areas could help achieve more representative disease prevalence, potentially making our model more effective worldwide. Overall, our findings and user-friendly web application may be a useful tool in the clinical decision-making process. Although the web application cannot replace the experience of a veterinarian, it can serve as a guide to diagnosis, with the added benefit of promoting more responsible use of antimicrobials.

Additional information

The present study has recently been published as:

Ferrini S, Rollo C, Bellino C, et al. A novel machine learning-based web application for field identification of infectious and inflammatory disorders of the central nervous system in cattle. J Vet Intern Med. 2023;37(2): 766-773. doi:10.1111/jvim.16664

PROJECT 2 - Feasibility of 16S rRNA sequencing for cerebrospinal fluid microbiome analysis in cattle with neurological disorders: a pilot study

1 Introduction

CNS infection in cattle incurs economic losses due to livestock mortality, neurological impairment, and reduction of animal performance and productivity. Neurological diseases may also be zoonotic (35). CNS infection can be caused by bacteria, viruses, fungi, and parasites, among which bacteria are the most common cause in cattle and are characterized by a rapid course, high morbidity and mortality unless treated with antimicrobials. Some of the leading bacterial agents reported are *Escherichia coli*, *Trueperella pyogenes*, *Histophilus somni*, *Pasteurella multocida* and *Listeria monocytogenes*; mixed aerobic-anaerobic bacterial infections are reported as well (214). Prompt etiological diagnosis is key to the initiation of appropriate antibiotic treatment and the adoption of control and prevention measures. This can be difficult, however, because clinical signs and blood test results are often nonspecific. CSF collection can be easily and safely performed in field conditions; it is the most direct antemortem method of diagnosing CNS disease, in which advanced diagnostic imaging in large animals is much less feasible (26). Infectious-inflammatory disease of the CNS can usually be distinguished by abnormal increases in TP concentration and total and differential nucleated cell counts in the CSF (8). Bacterial culture of the CSF is currently the gold standard for etiological antemortem diagnosis of bacterial CNS infection (215), but culture results may not be available for at least 24–48 h and are reported to be false negative in 44–100% of cases (8,29). The occurrence of false negatives may be due to previous use of antibiotics or to the presence of slow-growing and fastidious microorganisms (30,31). There is increasing evidence for 16S rRNA gene sequencing in human medicine as a rapid and accurate means to detect bacteria in the CSF, thus overcoming the limitations of culture-based bacterial detection (87). 16S rRNA gene is a

universal gene highly conserved among bacteria and sequencing of its variable regions allows differentiation between organisms at the genus level. 16S rRNA sequencing has introduced some advantages for diagnostic microbiology laboratories such as accuracy, simplification of protocols and identification of unculturable and fastidious bacteria. Furthermore, the results are in electronic formats, easy to share between laboratories and useful for pathogenic surveillance and future epidemiological studies. However, the low taxonomic resolution, the price of sequencing and the need for bioinformatic knowledge to generate results represent potential disadvantages of this technique that must be overcome (216). Conventional methods for bacterial identification in the CSF highlight a microbe-free CSF in healthy individuals. While the CSF circulating in the human CNS has long been considered sterile because the BBB is thought to effectively protect against microbial invasion (217), reports of microorganisms detected in human brains and CSF have challenged this concept (89,218). Based on these premises, we hypothesized that 16S rRNA sequencing of DNA isolated from CSF samples collected in the field from cattle with neurological diseases could lead to microorganism identification and their taxonomic classification. In the present study, we described the distribution of microorganisms in the CSF of two groups of cattle (patients with an infectious/inflammatory neurological disease and patients with nervous disorders of other nature) exploring whether there were any detectable differences in the microbial distribution between the two groups.

2 Materials and methods

2.1 Study design

The study sample was obtained from animals referred to the Neurology Service of the VTH, University of Turin, because of neurological signs suggestive of a CNS disorder. All underwent general physical examination, neurologic examination by a board-certified neurologist (ADA), CSF sampling in the field and analysis within 1 h after collection, blood

biochemical analysis and necropsy when possible. CSF analysis also included CSF bacterial culture. The final diagnosis was reached based on signalment, results of the neurological examination, blood and CSF analysis, response to treatment, and postmortem histopathology when performed. Information on therapies administered before referral was recorded. Two groups were formed according to the final diagnosis expressed according to the VITAMIN D classification (206). The one group was composed of patients with infectious inflammatory disease of the CNS (INF group) and the other included patients with CNS disorders of another nature (NON INF group). This prospective pilot study was conducted in accordance with current animal welfare regulations (Directive 98/58/EC and Italian Decree Law 146/2001). Samples were collected during the routine analysis required to perform the diagnostic procedure. Written informed consent was obtained from the owners to authorize veterinary assessment and treatment of their animals. CSF was collected in the field from the lumbosacral space, as described by Mayhew (7). If necessary, the animal was sedated with 0.05 mg/kg xylazine (Rompun, Bayer HealthCare) administered intravenously. The sampling site (5 cm x 10 cm) was clipped, surgically prepared, and locally anesthetized with 2.5 ml of procaine hydrochloride 20 mg/ml (Procamidor, Richter Pharma Ag). The skin around the sampling site was disinfected by alternating application of povidone iodine and alcohol moistened gauze three times. Disposable sterile spinal needles (20G 0.9 mm x 90 mm or 21G 0.8 mm x 50 mm, Terumo) were used depending on the size of the animal. After correct positioning of the needle, the sample was obtained by gentle aspiration with a sterile syringe. The CSF sample was then divided into two aliquots and placed in empty sterile tubes. The tube cap was previously sterilized with alcohol and a new sterile hypodermic needle was used to transfer the CSF into each tube. The first aliquot, intended for routine analysis and macroscopic evaluation, TNCC, erythrocyte count, and morphological evaluation, was analyzed within 1 h of collection and the second aliquot was stored at -80 °C until 16S rRNA sequencing analysis.

2.2 DNA extraction and quantification

DNA extraction from CSF was performed by using three different extraction kits, including: QI Amp® DNA Mini Kit (Qiagen GmbH, Hilden, Germany), Bacterial Genomic DNA Isolation Kit (Norgen Biotek Corp., Thorold, Canada) and DNAzol™ (Thermo Fisher Scientific, Waltham, USA). The DNAzol™ extraction protocol was the one that led to a suitable final DNA concentration for the NGS library production. DNA concentration was determined using a NanoDrop 2000 spectrophotometer (Thermo Fisher Scientific).

2.3 Library preparation, PCR enrichment and sequencing

In order to generate a suitable library, enrichment PCR reactions were performed towards the 16S rRNA V3– V4 hypervariable region, using the forward primer (5' TCGTCGGCAGCGTCAGATGTGTATAAGAGACAGCCTACGGGNGCWGCAG) and the reverse primer (5'-GTCTCGTGGGCTCGGAGATGTGTATAAGAGACAGGACTACHVGGGTATCTAATCC). PCR Illumina standard conditions (82) were applied according to the manufacturer's instructions for an initial analysis (first phase) and then modified (second phase) to achieve a more sensitive amplification as follows: 12.5 μL of 2x KAPA HiFi HotStart ReadyMix, 10 μL of each primer and 8 μL of 12.5 ng/μL of microbial DNA underwent initial denaturation at 95 °C for 3 min, then 25 cycles at 95 °C for 30 s, at 55 °C for 30 s, at 72 °C for 30 s, at 75 °C for 5 min and then maintained at 4 °C. Controls were added in each extraction and amplification step. Samples in which no genetic material was amplified were excluded from further analysis. The enriched 16S rRNA PCR library was then sent for normalization and quantification (Biomolecular Research Genomics) before proceeding with sequencing on an Illumina iSeq100 platform (Illumina) with a PE 2×300 bp protocol.

2.4 Bioinformatic analysis

Reads were checked for sequence quality using FastQC (version 0.11.5) (219), trimmed with Trimmomatic software (release 0.39) (220), and aligned with the bovine genome (Ensembl Bos_taurus ARS-UCD 1.2.101) using the BowTie2 (version 2.3.5.1) aligner (221) to eliminate possible host genomic material. The cleaned fastq files were then processed and analyzed using QIIME2 (Quantitative Insights into Microbial Ecology, release 2020.8) (222). DADA2 (223) (via q2-dada2 implementation) has been used to quality-filter and denoise sequence data: specifically, forward and reverse reads were further cleaned by trimming off the first ten positions and by truncating at positions 290 and 250, respectively, to remove low quality portions. The resulting ASVs, cleaned from chimeric sequences, were taxonomically classified by classify-sklearn command, as in q2-feature-classifier plugin, on the SILVA 138 Small SubUnit database using a 99% identity criterion [q2-silva-138-99-nb-classifier.qza]. A confidence level (CL) of ≥97% for identification of bacteria was set. The ASVs were further taxonomically characterized by NCBI (national center for biotechnology information) BLAST (Basic Local Alignment Search Tool, release 2.11.0) by aligning them on the NCBI 16S bacterial database (2020_12_24). Only results with a single best hit and high similarity levels (>98% of identical matches and eValue <0.05) were considered. Phyla, classes, orders, families, and genera are reported as overall relative abundance, average relative abundance and SEM. Species are reported as overall relative abundance, in relation to ASVs identified at species level. Alpha diversities was evaluated by Shannon Index, Simpson Index, Faith's Phylogenetic Diversity and Observed Feature measure and their significances were analyzed by Kruskal-Wallis test; beta diversity was calculated with Unweighted UniFrac and Normalized Weighted UniFrac distances, and with Bray-Curtis dissimilarity and their significances were analyzed by Permutational multivariate analysis of

variance (PERMANOVA) test based on 1000 permutations. Rarefaction curves were produced to estimate species richness.

2.5 Statistical analysis

Standard descriptive statistics are reported as median and IQR for continuous variables and as percentage and frequency for categorical variables. Statistical analysis was performed using Excel (Microsoft, version 16.27).

3 Results

Ten animals were enrolled in this pilot study: 4 with a CNS infection and 6 with CNS disorders of other natures. The median DNA concentration in the CSF of the animals was 90 ng/µL (IQR 4.85–725). Standard PCR yielded no genetic material from any of the samples. The modified 16S rRNA PCR amplification produced no bacterial genetic material in samples from 4 out of 10 patients: 1 with CNS infection-inflammation and 3 with a noninfectious inflammatory CNS disorder. These 4 were excluded from further analysis; the remaining 6 were: 4 males (66.67%) and 2 females (33.33%) of Piemontese (N=3; 50%), Holstein Friesian (N=1; 16.67%), Blonde d'Aquitaine (N=1; 16.67%), and mixed breeds (N=1; 16.67%), ranging from 3 days to 3 years of age (median: 2 months; IQR 13 days-6 months); the neuroanatomical localisation was: forebrain (N=3; 50%), diffuse intracranial (N=1; 16.67%), lumbosacral spinal cord segments (N=1; 16.67%), and multifocal (N=1; 16.67%). The final diagnosis based on the VITAMIN D classification (206) was: infectious-inflammatory disease (N=3; 50%), metabolic/toxic (N=2; 33.3%), and anomalous (1; 16.67%). Two groups were formed: an INF group and a NON INF group. In the INF group, neonatal meningitis/meningoencephalitis(-myelitis) of suspected bacterial origin was diagnosed in 2 calves < 1 month that presented with 1–3 day history of neurological signs, which occurred following enteritis and omphalophlebitis in 1 calf (Case 1) and enteritis and

arthritis in the other (Case 2). CSF analysis revealed mononuclear PL in both cases. One older calf (Case 3) (7 months old) presented with clinical signs consistent with meningitis/meningoencephalitis and 1–3 day history of seizures. CSF analysis showed marked mixed PL and increased TP concentration. The patient was euthanized a few hours after the referral due to deterioration of neurological signs and onset of status epilepticus. Necropsy highlighted yellow-greenish thickening of the meninges at the level of the cerebellum, multifocal abscesses and mononuclear vasculitis at the level of the pons and cerebellum, edema, and inflammatory infiltrate in the brain parenchyma. All brain areas showed signs of predominantly mononuclear inflammation.

The polymicrobial growth in the culture of brain samples was a mixed flora of slow-growing bacteria that in a standard culture system resulted in a failure to identify single putative microorganisms. The NON INF group included 3 patients. A 3-month-old calf (Case 5) presented with central blindness and abnormal compulsive behavior. CSF analysis was normal. Hypovitaminosis A was suspected; vitamin A therapy resolved all the clinical signs but not the blindness. A 3-year-old (Case 6) patient presented because of recurrent epileptic seizures. CSF analysis was normal and blood analysis revealed hypocalcemia. The patient died shortly after referral; necropsy was unremarkable. Hypocalcemia was the assumed cause of the neurological signs.

A 3-day-old calf (Case 7) presented with abnormal facial conformation and inability to stand on forelimbs and hindlimbs since birth. The diagnosis was complex congenital malformation of the head consistent with hydranencephaly or holoprosencephaly associated with other congenital facial abnormalities disclosed on postmortem autopsy (224). CSF analysis was normal. CSF bacterial culture was performed in all 6 cases and resulted no-growth. Table 1 presents patients' characteristics, amplification results and number of reads.

Table 1. Clinical Characteristics.

TNCC = total nucleated cell count; TP = total protein; CSF: cerebrospinal fluid; NBSM: neonatal bacterial suppurative meningitis; BSM = bacterial suppurative meningitis; NL = neurolocalization; PL = pleocytosis

*Merged reads number is expressed in brackets.

Cases	Age (months)	NL	Previous antibiotic therapy	TNCC/ µL	TP mg/dl	CSF interpretation	Diagnosis	Outcome	Amplification and reads number*
INF									
1	1	Multifocal [forebrain, spinal ´T3-L3)]	No	18.8	24	Mononuclear PL	NBSM	Died	Amplified (21952)
2	0 (17 days)	Spinal (L4-S3)	Yes	21.7	32	Mononuclear PL	NBSM	Died	Amplified (35586)
3	7	Forebrain	No	768	330	Mixed PL	BSM	Died	Amplified (9247)
4	0 (7 days)	Multifocal (forebrain, central vestibular)	Yes	205.6	232	Neutrophilic PL	NBSM	Died	Non amplified
NON INF									
5	3	Forebrain	Yes	1.6	19	Normal	Hypovitaminosis A	Recovered	Amplified (33293)
6	36	Forebrain	Yes	1	29	Normal	Hypocalcemia	Died	Amplified (33305)
7	0 (3 days)	Diffuse intracranial	No	2	18	Normal	Holoprosencephaly/ Hydranencephaly	Died	Amplified (36386)
8	24	Spinal (T3-L3)	No	1	26	Normal	Degenerative myelopathy	Died	Not amplified
9	72	Spinal (T3-L3)	No	1.4	25	Normal	Trauma	Recovered	Not amplified
10	12	Spinal (T3-L3)	No	1.2	18	Normal	Trauma	Recovered	Not amplified

3.1 16S rRNA sequencing of DNA isolated from CSF

DADA2 denoising procedure, based on quality-based filtering, sequence inferring and merging, and chimera removal, led to 728 ASVs. Specifically, the median reads count per sample was 71750.5 (IQR 53806–76036); those obtained after elimination of host material, elimination of poor quality sequences, and pairing between forward and reverse sequences (indicated as merged) were about 70% of the starting counts (median per sample 49699; IQR 37399.5– 50474). The sequences compared to the database were about 45% of the total as only the real sequences, not the chimeric ones, were considered (median per sample 33299; IQR 24787.25–35015.75). The samples from Case 3 produced the lowest number of reads (total 20344; merged 12890; non-chimeric 9247), while the highest reads count was obtained from sample 5 (total 78084; merged 50650; non-chimeric 33305). Each ASV resulting from DADA2 denoising step was then compared to the SILVA database to obtain a classification into a microbial taxonomy. A total of 17 phyla, 27 classes, 71 orders, 115 families and 150 genera were identified and the most present are reported in Table 2. Figures 1A and 1B illustrate phylum and genera abundance and composition in the INF and NON INF groups.

Table 2. Most present phyla, classes, orders, families and genera presented in descending order. Phyla, classes, orders, families, and genera are reported as overall relative abundance, average relative abundance and standard error of the mean (SEM). *Numbers in brackets refer to the total number of phyla, classes, orders, families and genera identified.

Phyla (n = 17*)	Classes (n =27*)	Orders (n =71*)	Families (n =115*)	Genera (n =150*)
Proteobacteria (73.56%; 75.07%, ± 2.27%)	Gammaproteobacteria (64.87%; 66.03%, ± 1.91%)	Pseudomonadales (64.12%; 65.19%; ± 2.03%)	Pseudomonadaceae (44.61%; 46.11%, ± 2.43%)	Pseudomonas (45.42%; 46.10%, ± 2.44%)
Actinobacteriota (15.25%; 14.72%, ± 2.76%)	Actinobacteria (15.06%; 14.55%, ± 2.82%)	Corynebacteriales (12.69%; 12.34%, ± 2.58%)	Moraxellaceae (19.54%; 19.08%, ± 0.86%)	Acinetobacter (19.91%; 19.08%, ± 0.86%)
Firmicutes (5.06%; 4,63%, ± 1.66%)	Alphaproteobacteria (8.70%; 9.04%, ± 0.69%)	Sphingomonadales (4.47%; 4.55%, ± 0.44%)	Mycobacteriaceae (11.80%; 227 11.59%, ± 2.50%)	Mycobacterium (12.01%; 11.59%, ± 2.51%)
Bacteroidota (3.81%; 3.48%, ± 1.21%)	Bacteroidia (3.82%; 3.48%, ± 1.21%)	Rhizobiales (3.56%; 3.84%, ± 0.55%)	Sphingomonadaceae (4.47%; 4.55%, ± 0.44%)	Sphingobium (4.35%; 4.36%, ± 0.41%)
Cyanobacteria (1.30%; 1.19%, ± 0.35%)	Bacilli (2.56%; 2.58%, ±0.73)	Lactobacillales (1.85%; 1.99%, ± 0.59%)	Beijerinckiaceae (2.77%; 2.97%, ± 0.51%)	Bosea (2.56%; 2.68%, ± 0.43%)
	Clostridia (2.42%; 1.99%, ± 1.96%)	Flavobacteriales (1.71%; 1.64%, ± 0.34%)	Weeksellaceae (1.44%; 1.42%, ± 0.35%)	Cutibacterium (1.33%; 1.13%, ± 0.45%)
		Bacteroidales (1.54%; 1.31%; ± 1.03%)	Propionibacteriaceae (1.30%; 1.13%, ± 0.45%)	Chryseobacterium (1.32%; 1.30%, ± 0.38%)
		Propionibacteriales (1.32%; 1.15%, 225 ± 0.46%)	Streptococcaceae (1.12%; 1.40%, ± 0.60)	Streptococcus (1.08%; 1.35%, ± 0.60%)
		Oscillospirales (1.07%; 0.87%, ± 0.84%)		

Figure 1: Average relative abundance of phyla (A) and genera (B) in the infectious-inflammatory (INF) and non infectious-inflammatory (NON INF) samples. Only the 5 more present bacterial phyla (A) and genera (B) were represented. Blue columns represent INF (n = 3) samples, while orange columns represent NON INF (n = 3). The bars represent the standard error of the mean (SEM).

A

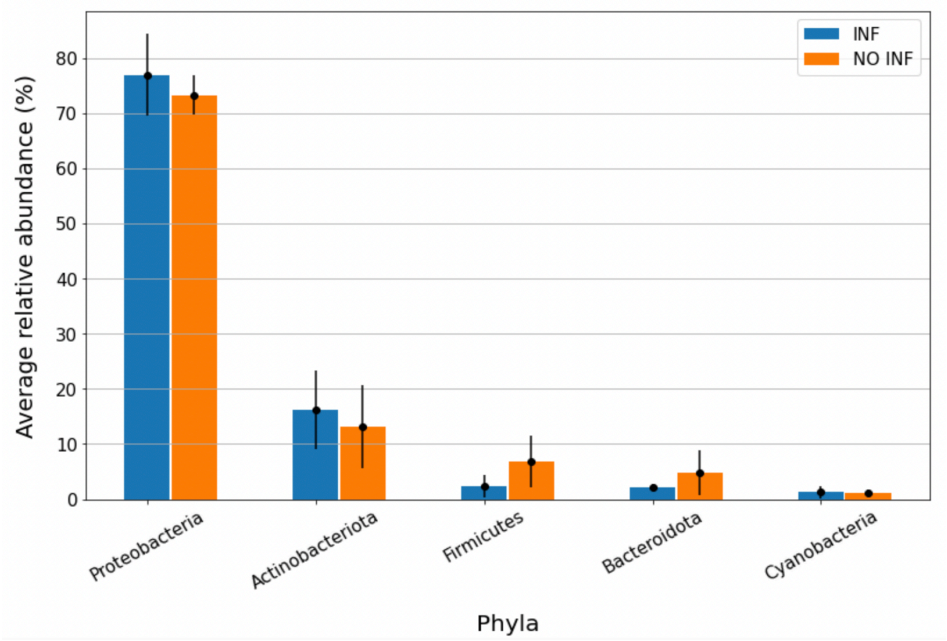

B

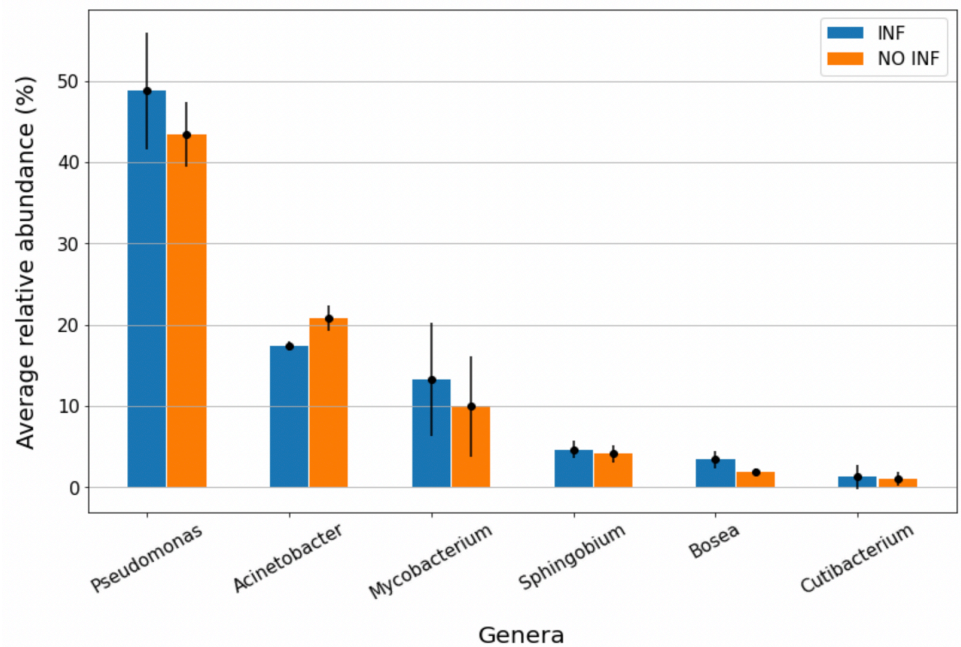

Only 11 out of 728 ASVs were identified at the species level, accounting for 1.51% of the ASVs and 0.69% of total abundance. The most abundant were: *Corynebacterium kroppenstedtii* (49.70%), *Lactobacillus algidus* (14.05%), *Pseudomonas pertucinogena* (8.50%), *Cutibacterium granulosum* (6.61%), *Bifidobacterium bifidum* (6.37%), *Treponem porcinum* (5.19%), *Corynebacterium maris* (3.07%), *Sphingobacterium jejuense* (2.71%), *Pseudomonas formosensis* (2.60%). *Negativicoccus succinicivorans* and *Peptoniphilus duerdenii* accounted for < 1% of the identified species. Both alpha and beta diversity analyses did not detect any differences between the microbial communities of the two groups. The rarefaction curves reached a plateau, indicating good representation of the microbial community. By blasting the ASVs versus the NCBI database, we assigned 169 ASVs to a species, 105 of which were ASVs previously recognized by QIIME with a CL>97% and 64 ASVs with a CL < 97%. The former accounted for 14.28% of ASVs and 11.61% of total abundance, the most abundant identified species were: *Acinetobacter johnsonii* (43.46%), *Chryseobacterium profundimaris* (10.73%), *Pseudomonas helmanticensis* (4.94%), *Psychromonas aquatilis* (4.54%), *Afipia massiliensis* (4.50%), *Carnobacterium gallinarum* (2.92%), *Staphylococcus hominis* (2.39%), *Anaerococcus nagyae* (1.64%), *Acinetobacter indicus* (1.46%), *Brevundimonas naejangsanensis* (1.37%), *Rothia endophytica* (1.21%), and *Corynebacterium pilbarens* (1.06%). Six of the 11 ASVs assigned to a species by QIIME were likewise identified by BLAST and there was correspondence between them.

4 Discussion

With the present study we evaluated for the first time the feasibility of 16S rRNA gene sequencing of DNA isolated from CSF of cattle with CNS disorders. Also, we evaluated the CSF microbiota composition in patients with CNS infection-inflammation and CNS disorders of other nature. Despite the attempt to increase sensitivity by means of modified PCR, not all samples led to bacterial genetic material detection. Possible explanations are the very

low CSF biomass, since the amount of CSF that can be collected is usually very small (a few mL) and the concentration of the genetic material in CSF is low (225). In addition, previous (before CSF collection) exposure to antimicrobials in 4 of the 10 patients could have reduced the bacterial mass even further. Other possible causes, like prolonged time between onset of clinical signs and CSF collection (65) and sample storage errors, were ruled out because CSF was collected shortly after the onset of clinical signs and the samples were correctly stored at -80 °C to prevent degradation of DNA and RNA. By gene sequencing we detected microorganisms in the CSF samples from all six patients; however, our findings did not allow us to highlight any differences in the microbial population between the two groups. Moreover, none of the more prevalent genera found were among those commonly encountered as cause of CNS infections in cattle at the present time. In other words, both groups, although they differed in their clinical features and diagnosis, presented similar microbial communities. To the authors opinion, there are different explanations of the presence of microorganisms in the CSF samples: sampling contamination or laboratory contamination, the presence of a CSF microbial community, and blood-CSF-barrier breakdown. A minimal external contamination during sample collection, despite all possible precautions taken to maintain sterility, cannot be ruled out as 16S rRNA sequencing of DNA isolated from samples from the environment was not performed. However, the microorganisms highlighted in this study do not reflect those typical of the skin microbiota of cattle (98). Laboratory contamination, which has been described in previous cases (226) was excluded by analysis of the reagent controls that was consistently negative. Alternatively, the bacteria identified could represent the microbiological community of the CSF in healthy cattle. Finally, given that the noninfectious inflammatory cases demonstrated neurological disorders, the blood-CSF-barrier might have been breached, resulting in contamination of the CSF from other body districts, as described in human medicine (217,227). The results of the present study did not allow to differentiate the microorganism

population between the two groups. Two options can be advanced to explain our results and the lack of pathogens identification in the INF group. First, classification did not reach the species level in most cases. Commensal and pathogenic bacterial species can share the same genus. For instance, the genus *Pseudomonas*, abundantly found in the samples from all patients, includes *Pseudomonas aeruginosa*, a common pathogen known to cause CNS infection in humans (228), and other *Pseudomonas spp.* that are ubiquitous in the environment but are not pathogenic (229). Another possible explanation could be that the pathogens were not present in the CSF but rather in the nervous system parenchyma. It is possible that free pathogenic bacteria in CSF are transient and that they are present only in minimal quantities in this substrate. Unfortunately, 16S rRNA gene PCR and sequencing of DNA isolated from brain and spinal cord samples were not performed in the present study to confirm this hypothesis. The issue of accurate taxonomic identification deserves consideration. The ability to identify bacteria with high taxonomic resolution depends in part on the sequencing technique. We sequenced only the V3-V4 hypervariable regions of the 16S gene (partial 16S sequencing). While it has been reported that the most variable regions are sufficient to identify genera, they are unlikely to adequately discriminate between species (230). When we blasted the ASVs versus the GenBank NCBI database, more species were identified (1.15% of ASVs versus the SILVA database and 14.28% versus the NCBI database). The reason could be related to the different update status of these database: the SILVA database was last updated in 2019, whereas the GenBank NCBI is updated every two months, which could explain the greater ability of the latter to identify microorganisms at the species level. *Acinetobacter johnsonii* was the most abundant species when we blasted the ASVs versus the NCBI database. This bacterium is a free-living, saprophytic organism that can be isolated from soil, water, sewage, and a wide variety of foods. *A. johnsoni* meningitis has been rarely reported in humans and it is usually seen in post-neurosurgical patients with nosocomial infection (231). In the present study, *A.*

johnsonii was equally found in both the INF and in the NON INF group and to the authors opinion it should not be considered a causative agent of CNS infection in cattle.

The present study has several limitations. The low number of cases included prevented us from achieving significant results. Four of the 10 cattle from the initial population were excluded, as no sufficient genetic material was obtained, although one patient was diagnosed with an infectious inflammatory CNS disease. However, despite the small sample size, this study presents the first attempt to describe the CSF microbiome composition of cattle. Further studies with larger sample size on microbiome analysis of CSF in cattle are warranted. In addition, previous unavoidable exposure to antibiotics may have created a bias. A further limitation is the lack of CSF samples from healthy animals as controls. However, the procedure, although performed by skilled veterinarians, is potentially associated with risks for the patients. Furthermore, it requires pharmacological restrictions of the animals, raising ethical concerns in healthy subjects. On the other hand, post-mortem collection at the slaughterhouse is unrealistic because of the unpreventable contamination of the CSF by the captive-bolt stunning procedure. Our finding of a microbial community in the CSF of cattle with various neurological disorders is a valid starting point for future studies, with the inclusion of an ethical approved control group of healthy animals, that aim to validate this method as a diagnostic approach, reliable in clinical setting. Finally, no etiological diagnosis was made in any of the infectious inflammatory cases. Bacterial cultures positive for one or more specific microorganisms could have aided in the interpretation of the NGS data. According to the literature, however, bacterial culture of CSF is only rarely positive (1,8). Other ways to confirm 16S rRNA sequencing findings, such as other NGS techniques, microarray analysis, PCR assay for specific pathogens or bacterial culture from brain tissue need to be investigated.

In conclusion, we evaluated the applicability and utility of 16S rRNA sequencing for the study of CSF microbial community in cattle. Our results indicate that 16S rRNA of DNA isolated

from CSF can lead to bacterial identification and taxonomic classification at the genus level. The findings of this pilot study are preliminary. Further studies, in which CSF samples from healthy animals and from the environment are included as controls, are needed in order to better evaluate CSF collection in the field. Positive culture or other innovative techniques for bacterial identification from nervous specimens could serve as positive controls. Our results indicate that a microbial community in the CSF independent of CNS infection cannot be ruled out.

Additional information

The present study has recently been published as:

Ferrini S, Grego E, Ala U, Cagnotti G, Valentini F, Di Muro G, Iulini B, Stella MC, Bellino C, D'Angelo A. Feasibility of 16S rRNA sequencing for cerebrospinal fluid microbiome analysis in cattle with neurological disorders: a pilot study. Vet Res Commun. 2023 Jun;47(2):373-383. doi: 10.1007/s11259-022-09949-w. Epub 2022 Jun 27. PMID: 35759164; PMCID: PMC10209220.

PROJECT 3 - Cerebrospinal fluid L-lactate as a diagnostic marker for acute inflammatory disorders in the central nervous system of cattle

1 Background

Bacterial infection of the CNS poses a clinical challenge and is a leading cause of neurological disorders in cattle (35). Prompt antibiotic therapy can improve outcomes in cattle with bacterial meningoencephalitis/myelitis and reduce morbidity and mortality (34). CSF analysis in the diagnosis of infection usually shows a moderate to marked increase in TNCC and TP concentration which are not specific for CNS infectious diseases, however (34). Furthermore, etiological diagnosis of bacterial infection of the CNS currently relies on the identification of bacteria by Gram staining or isolation in CSF culture (8), which is burdened by delayed diagnosis and inadequate sensitivity (29,215).

The significance of CSF L-lactate concentration as a valuable supplementary diagnostic test for acute CNS inflammation induced by bacterial infection in humans has gained recognition. Numerous studies in humans have demonstrated an increase in CSF L-lactate concentration during bacterial meningitis in the attempt to establish a cut-off (range, from 2.1 to 4.44 mmol/L) that can differentiate bacterial meningitis from other neurological disorders (177–180). Animal studies have investigated the diagnostic value of CSF lactate in neurological diseases in dogs (163,164,167,173,174,189), but the exact relationship between CSF L-lactate and bacterial infection in this species remains to be elucidated. A handheld lactate monitor has recently been validated for quantifying L-lactate in canine blood and CSF and a CSF reference interval (RI) has been established for this analyte (1.0-2.5 mmol/L) (166) in dogs.

To date, only one published study has investigated the utility of CSF L-lactate as a diagnostic biomarker in cattle, but it failed to distinguish between bacterial meningitis and other inflammatory disorders (15).

With the present study we wanted to explore the potential of CSF L-lactate as a field

diagnostic tool to help categorize the cause of CNS disorders in cattle. To do this, we thought it important to establish a RI for L-lactate in healthy bovine CSF and to determine whether CSF L-lactate can serve as a valid biomarker for detecting acute CNS inflammation in cattle with neurological disorders. Our hypothesis was that elevated CSF L-lactate concentration may indicate acute CNS inflammation induced by bacterial infection and differentiate it from other neurological disorders.

2 Materials and methods

The study population was divided into two groups: a healthy group and a sick group. CSF analysis, including measurement of L-lactate, was an inclusion criterion. Blood L-lactate levels were analyzed when available but were not required for inclusion in the study.

2.1 Healthy Group

This group included healthy cattle housed at the Department of Veterinary Science of Turin (Authorization No. 242/2020 - PR). The subjects' health was based on an unremarkable general physical examination and normal complete blood analyte panel. Blood and CSF samples were collected in the field.

2.2 Sick Group

A prospective study was conducted between April 2019 and June 2023. All cattle referred for neurological signs suggestive of a CNS disorder to the Neurology Service of the VTH, Department of Veterinary Science of Turin were considered for inclusion in the study. All

underwent general physical examination, neurologic examination by a board-certified neurologist (ADA) blood and CSF sampling in the field, and necropsy when performed. Only cases with a confirmed diagnosis of CNS disorder were included; diagnosis is expressed by the VITAMIN D mnemonic (206). The final diagnosis was based on signalment, neurological examination, blood and CSF analysis, response to treatment, and necropsy histopathology when performed.

This prospective study was conducted in accordance with current animal welfare regulations (Italian Legislative Decree 146/2001 of 26 March 2001 implementing the European Council Directive 98/58/EC of 20 July 1998). Samples were collected during routine diagnostic evaluation. Written informed consent was obtained from the animal owners before veterinary assessment and treatment of their animals.

2.3 Collection and Analysis of blood and CSF samples

Blood samples (5 mL aliquots) were obtained from the jugular vein and placed into 2 tubes containing EDTA and a coagulation activator. CSF was collected from the lumbosacral region with the animal in either sternal recumbency or standing position, as described by Mayhew (7). When necessary, an animal was sedated prior to the procedure by intravenous administration of xylazine hydrochloride (Rompun, Bayer S.p.A) at a dose of 0.05 mg/kg body weight. The collection site (5 cm x 10 cm) was shaved and surgically prepared; local anesthesia was administered by subcutaneous injection of 2.5 mL of procaine hydrochloride (Procamidor®, Richter Pharma AG). CSF was collected using spinal needles (18 G and 90 mm in length or 21 G and 50 mm) (Terumo) depending on the body size of the animal. A minimum of 5 mL of CSF was collected by attaching the syringe to the hub of the needle and applying gentle aspiration. The sample was then placed in empty sterile tubes. The L-

lactate concentration was measured immediately after collection of blood and CSF samples using a portable StatStrip Xpress© analyzer (Nova Biomedical). A drop of blood or CSF (approximately 0.6 µL) was applied to the free end of the test strip inserted into the analyzer and the result was read out by the device within 13 seconds. The samples were kept refrigerated (4°C) until transferred to the Laboratory Service of the VTH of Turin for analysis within one hour of collection, as previously described (24).

2.4 Statistical Analysis

Statistical analysis was performed using Rstudio version 4.1.3 and Prism version 9.1.1. Numerical variables were analyzed for normality distribution with the Shapiro Wilk test and are expressed as mean and standard deviation (± SD) or median and IQR, as appropriate. Categorical variables are expressed as relative frequency and percentage. The RI with 90% Confidence Interval (CI) for CSF and blood L-lactate in the healthy group was calculated using the robust bootstrap method according to published guidelines (232). Additionally, the horn method for outlier detection was applied in the analysis. The Wilcoxon rank-sum two-tailed test was used to assess differences in L- lactate concentration between CSF and blood in the healthy cattle group. Correlations between CSF L-lactate concentration and variables (i.e., blood L- lactate, CSF RBCC, CSF TNCC, CSF TP, CSF total neutrophil count, CSF total lymphocyte count, CSF total macrophage count) were examined for the sick animal group. All correlations were assessed with Spearman's rank correlation coefficient. The Wilcoxon rank-sum two-tailed test was conducted to investigate differences in CSF and blood L-lactate concentration between sick animals diagnosed with infectious-inflammatory disease (INF subgroup) and those without this disease (NON INF subgroup). Furthermore, the Kruskal-Wallis test and pairwise Mann-Whitney tests were employed to

explore differences in CSF and blood L-lactate concentrations based on the variables derived from the VITAMIN D mnemonic. The same tests were performed to evaluate differences in CSF L-lactate, blood L-lactate, CSF TNCC, and CSF TP, and the final interpretation of CSF. The Benjamini-Hochberg procedure was used to adjust the p-values. Finally, ROC analysis compared the concentration of CSF L-lactate between cases of neutrophilic PL and those with other characteristics. The Youden index was employed to determine the optimal cut-off point. Statistical significance was set at $p < 0.05$.

3 Results

3.1 Healthy Cattle group

3.1.1 Description

The healthy group was composed of 27 cattle: 9/27 (33%) females and 18/27 (67%) males. Most (24/27, 89%) were 7 months old, 2 were 6 months old, and 1 was 5 months old. All were Holstein Friesian breed. The median concentration of CSF TP was 38 mg/dL (IQR 30-46 mg/dL). The median CSF TNCC was 4.6 cells/µL (IQR 3.7-6.1 cells/µL). The median CSF RBCC was 30 cells/µL (IQR 10-385 cells/µL). The mean CSF L-lactate concentration was 1.7 mmol/L ±0.4 mmol/L. Blood L-lactate concentration for all animals was known; the median concentration was 0.7 mmol/L (IQR 0.6-0.85 mmol/L).

3.1.2 Reference Intervals for L-lactate

The RI for CSF L-lactate was 1.1-2.4 mmol/L (lower CI 0.8-1.2; upper CI of 2.1-2.6). The RI for blood L-lactate was 0.2-1.2 mmol/L (lower CI 0-0.4; upper CI 1-1.4). No outliers were identified in either analysis. The median CSF L-lactate level was significantly higher than that of blood L-lactate ($p < 0.0001$; Figure 1).

Figure 1: Difference in L-lactate concentration between CSF and blood in healthy cattle. The scatter points represent individual data points. The median and IQR are shown. Asterisks (*) indicate the level of statistical significance: *p<0.05, **p<0.01, ***p<0.001, ****p<0.0001. CSF = cerebrospinal fluid.

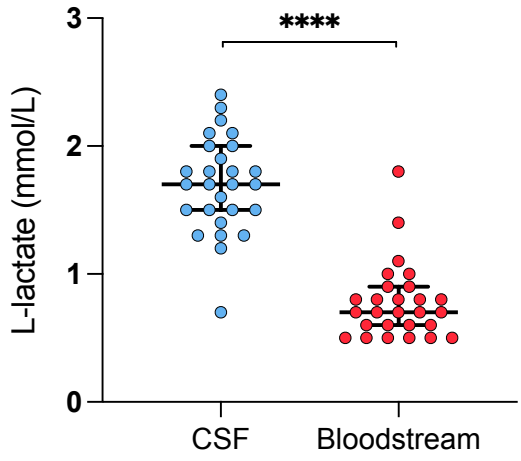

3.2 Sick Cattle group

3.2.1 Description

The sick cattle group was composed of 86 neurologically impaired cattle: 44/86 (51%) females and 42/86 (49%) males. The median age was 20 days (IQR 6-180 days). The most frequent breed was Piemontese (76/86, 89%), followed by Holstein Friesian (7/86, 8%), mixed breed (2/86, 2%), and Limousine 1/86 (1%). The most frequent neuroanatomical localization was the forebrain (24/86, 28%) or multifocal localization (15/86, 17%). Brainstem

involvement was observed in 9/86 (10%), a diffuse intracranial disorder in 9/86 (10%), L4-S3 spinal segment localization in 8/86 (9%), central vestibular system localization in 6/86 (7%), cerebellum involvement in 5/86 (6%), C6-T2 spinal segment involvement in 4/86 (5%), C1-C5 spinal segment involvement in 3/86 (4%), and T3-L3 spinal segment involvement in 3/86 (4%). The median concentration of CSF TP was 46 mg/dL (IQR 25-98 mg/dL). The median CSF TNCC was 7.8 cells/µL (IQR 2-65 cells/µL), and the median CSF RBCC was 80 cells/µL (15-1335 cells/µL). CSF interpretation was normal in 40/86 (46%). Among the remaining cases, 24/86 (28%) exhibited mononuclear PL, 14/86 (16%) neutrophilic PL, 5/86 (6%) AC dissociation, and 3/86 (4%) mixed PL, which refers to the presence of both mononuclear cells and neutrophils. The median CSF L-lactate level was 2.5 mmol/L (IQR 2-3.6 mmol/L). Blood L-lactate concentration was known for 60/86 cattle and the median level was 1.7 mmol/L (IQR 1.1-2.6 mmol/L). Over half (47/86, 55%) were diagnosed with an infectious or inflammatory CNS disorder (INF subgroup), while the remaining 39/86 (45%) had a CNS disorder of other origin (NON INF subgroup). Within the NON INF subgroup, 15/39 cattle (38%) were diagnosed with an anomalous congenital condition, 12/39 (31%) with a metabolic-toxic disorder, 9/39 (23%) had experienced trauma, and 3/39 (8%) had a vascular disorder.

3.2.2 Diagnostic Findings of CSF L-lactate

We found a significant correlation between CSF L-lactate concentration and the following variables in the sick cattle group: blood L-lactate (known for 60/86, rho = 0.34, p = 0.007); CSF TNCC (rho = 0.57, p < 0.0001); CSF TP (rho = 0.45, p < 0.0001); CSF total neutrophil count (known for 25/86, rho = 0.63, p = 0.0006); CSF total macrophage count (known for 21/86, rho = 0.66, p = 0.001). There was no significant correlation between CSF L-lactate and CSF RBCC or CSF total lymphocyte count (the latter known for 21/86). There was a statistically significant difference in CSF L-lactate concentration between the INF and the NON INF subgroup (median CSF L-lactate INF subgroup 3 mmol/L, IQR 2.2-5.95 mmol/L;

median CSF L-lactate NON INF subgroup 2.2 mmol/L, IQR 1.8-2.6 mmol/L; $p < 0.0001$). However, when the INF subgroup and each of the other VITAMIN D categories were compared and the p-values corrected, this significant difference disappeared. There were no significant differences in blood L-lactate concentration across the various diagnoses. In contrast, significant differences were observed in CSF L-lactate, CSF TNCC, and CSF TP for the final interpretations of CSF ($p < 0.0001$), with the highest CSF L-lactate, CSF TNCC, and CSF TP found in neutrophilic PL cases (median L-lactate 7 mmol/L, IQR 4.2-7.9 mmol/L; median TNCC 601.5 cells/μL, IQR 272.1-1932 cells/μL; median TP 267 mg/dL, IQR 223-348 mg/dL). The characteristics of these variables in each CSF interpretation, showing the p-values obtained from pairwise comparisons, are presented in Table 1-3; the corresponding results are illustrated in Figures 2-4. In contrast, no significant differences in blood L-lactate were observed across interpretations of CSF.

Table 1: CSF L-lactate concentration in the sick cattle for each CSF interpretation and results (p value) of pairwise multiple comparison. CSF = cerebrospinal fluid; AC = albuminocytologic dissociation; PL = pleocytosis.

	Median CSF L-lactate mmol/L (IQR)		Normal	AC dissociation	Mononuclear PL	Neutrophilic PL	Mixed PL
Normal	2.15 (1.8 – 2.6)		-	0.20	0.05	< 0.0001	0.08
AC dissociation	2 (1.6 – 2.2)		0.20	-	0.06	0.005	0.06
Mononuclear PL	2.75 (2.2 – 3.35)		0.05	0.06	-	0.0006	0.30
Neutrophilic PL	7 (4.22 – 7.92)		< 0.0001	0.005	0.0006	-	0.16
Mixed PL	4.3 (3.35 – 4.55)		0.08	0.06	0.30	0.16	-

Table 2: CSF TNCC/μL in the sick cattle for each CSF interpretation and results (p value) of pairwise

multiple comparison. CSF = cerebrospinal fluid; TNCC = total nucleated cell count; AC = albuminocytologic dissociation; PL = pleocytosis.

	Median TNCC/μL (IQR)		Normal	AC dissociation	Mononuclear PL	Neutrophilic PL	Mixed PL
Normal	2 (1.2 – 4)		-	0.32	< 0.0001	< 0.0001	0.007
AC dissociation	5.2 (1.8 – 5.4)		0.32	-	0.0003	0.0003	0.04
Mononuclear PL	18.2 (11.72 – 45.65)		< 0.0001	0.0003	-	< 0.0001	0.02
Neutrophilic PL	601.5 (272.2 – 1932)		< 0.0001	0.0003	< 0.0001	-	0.04
Mixed pl.	166.2 (123.4 – 193.6)		0.007	0.04	0.02	0.04	-

Table 3: CSF TP concentration in the sick cattle for each CSF interpretation and results (p value) of pairwise multiple comparison. CSF = cerebrospinal fluid; TP = total protein; AC = albuminocytologic dissociation; PL = pleocytosis.

	Median TP mg/dL (IQR)		Normal	AC dissociation	Mononuclear PL	Neutrophilic PL	Mixed PL
Normal	25 (20 - 32)		-	0.006	0.0002	< 0.0001	0.01
AC dissociation	62 (53 - 62)		0.006	-	0.35	0.006	0.04
Mononuclear PL	50 (37.75 – 72.5)		0.0002	0.35	-	0.0002	0.03
Neutrophilic PL	267 (223 – 348)		< 0.0001	0.006	0.0002	-	0.36
Mixed PL	178 (167 – 250)		0.01	0.04	0.03	0.36	-

Figure 2: Difference in CSF L-lactate concentration between CSF final interpretations in sick cattle. The scatter points represent individual data points. The median and IQR are shown. Asterisks (*) indicate the level of statistical significance: *p<0.05, **p<0.01, ***p<0.001, ****p<0.0001. The absence of an asterisk indicates a lack of statistically significant differences between groups. CSF = cerebrospinal fluid; AC = albuminocytologic; PL = pleocytosis.

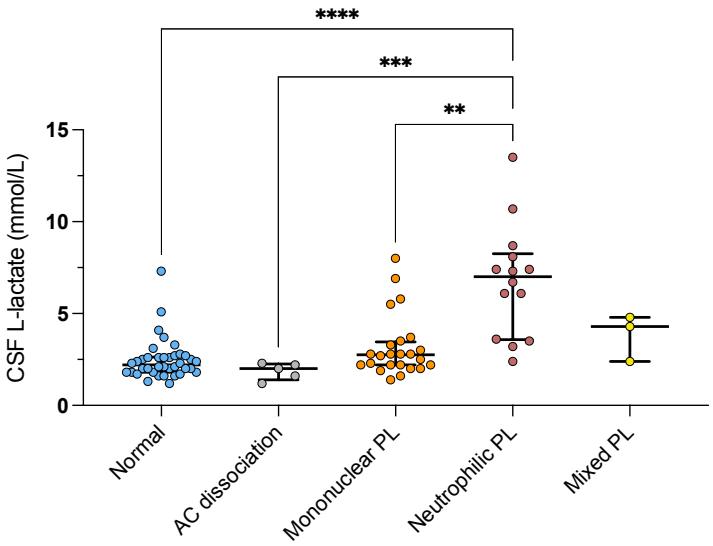

Figure 3: Difference in CSF TNCC/μL between CSF final interpretations in sick cattle. The scatter points represent individual data points. The median and IQR are shown. Asterisks (*) indicate the level of statistical significance: *p<0.05, **p<0.01, ***p<0.001, ****p<0.0001. The absence of an asterisk indicates a lack of statistically significant differences between groups. TNCC = total nucleated cell count; CSF = cerebrospinal fluid; AC = albuminocytologic; PL = pleocytosis.

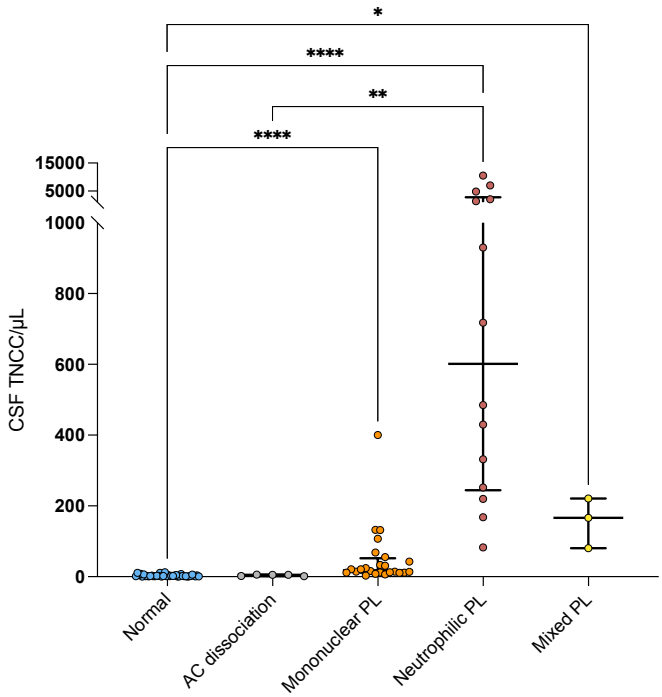

Figure 4: Difference in CSF TP concentration between CSF final interpretations in sick cattle. The scatter points represent individual data points. The median and IQR are shown. Asterisks (*) indicate the level of statistical significance: *p<0.05, **p<0.01, ***p<0.001, ****p<0.0001. The absence of an asterisk indicates a lack of statistically significant differences between groups. TP = total microprotein; CSF = cerebrospinal fluid; AC = albuminocytologic; PL = pleocytosis.

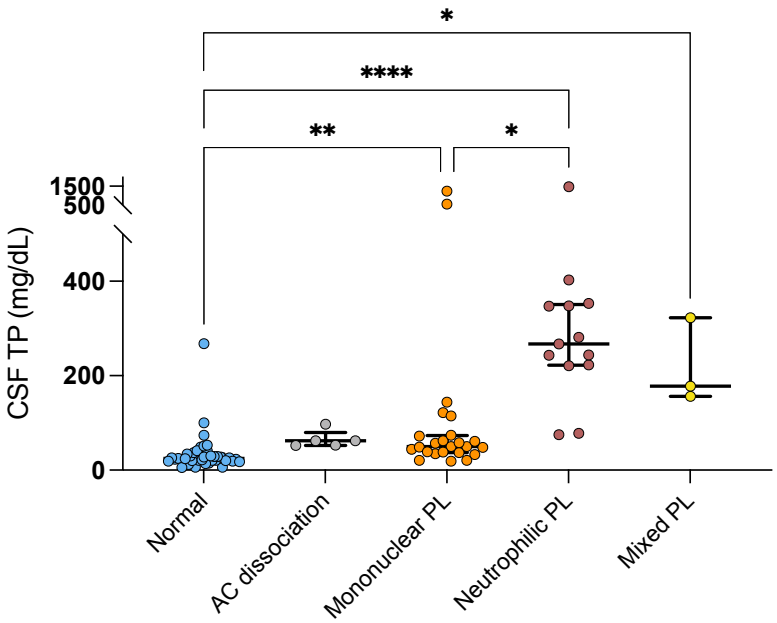

We observed higher concentration of CSF L-lactate in the cases of neutrophilic PL and analyzed the ROC curve. The AUROC for CSF L-lactate concentration in the neutrophilic PL group versus the other groups was 0.92. The Youden index method identified a threshold of 3.15 mmol/L for CSF L-lactate, which yielded a diagnostic sensitivity of 93% and a specificity of 80% in the detection of neutrophilic PL (Figure 5).

Figure 5: ROC curve for predicting neutrophilic PL based on CSF L-lactate concentration. The x-axis represents the false positive rate (1-Specificity), and the y-axis represents the true positive rate (Sensitivity).

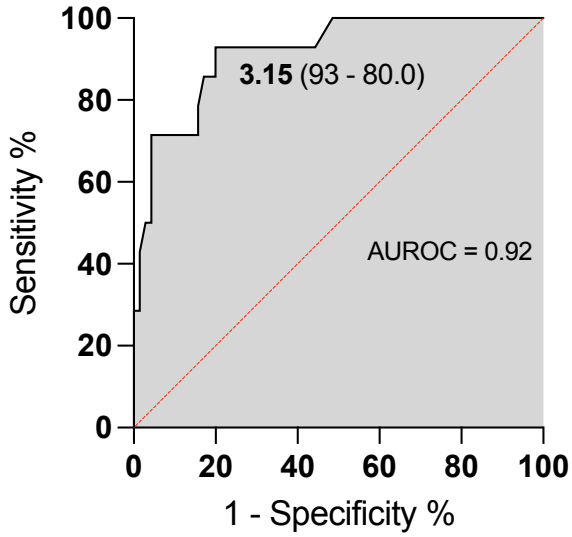

4 Discussion

To our best knowledge, this is the first study to determine a RI for CSF L-lactate in cattle. In a recent study, CSF L-lactate levels were assessed in healthy cattle however, the authors could not establish a RI for health due to the small sample size (15). We noted significantly higher L-lactate concentration in the CSF than in the blood in the healthy cattle group. This observation is shared by Posner et al(161) and further supports the notion that blood and CSF L-lactate levels are independent of each other. Several factors may contribute to this difference, including processes influencing the production and the clearance of L-lactate in the CSF. Lactate is produced primarily by astrocytes in the brain in response to neuronal activity by aerobic glycolysis. This metabolic pathway is specific to astrocytes and is regulated by a gene expression profile that promotes lactate production from pyruvate rather than its utilization in the tricarboxylic acid cycle. This distinctive process might lead to elevated lactate production within the brain and subsequently in the CSF (158). Additionally, lactate clearance from the CSF may be slower than its clearance from the bloodstream, further contributing to the higher concentration in CSF compared to blood (170).

When we compared the CSF L-lactate levels in the sick cattle group, we identified relatively weak differences between the INF and the NON INF subgroup. This is evident from the overlapping distribution of values between the two subgroups, with a few higher values in the INF subgroup contributing to the observed statistical significance. Elevated CSF L-lactate concentration has been documented in humans with bacterial infections of the CNS, and cut-off values have been proposed as a way to distinguish them from aseptic inflammations (179). Based on this notion, we sought a more accurate method to differentiate bacterial infections, particularly in the acute phase, from other disorders. Following this idea, we observed significant differences in L-lactate concentration together with alterations in the CSF. Notably, the highest L-lactate concentration was observed in the subjects with neutrophilic PL, and a CSF L-lactate above 3.15 mmol/l was highly predictive of this condition.

Neutrophilic PL is commonly encountered in acute bacterial infection of the CNS in cattle and it is considered specific for such disease. Neutrophils are the first cells to be recruited to the site of infection where they participate in anti-microbial host defense as regulators of both innate and adaptive immunity. Activated neutrophils display diverse effector mechanisms, including phagocytosis, activation of NADPH oxidase, release of granular contents, and release of neutrophil extracellular traps (NETs). These NETs consist of DNA, histones, microbicidal peptides, and antimicrobial enzymes and are associated with L-lactate formation via the Warburg effect (127,181,182).

Accordingly, we examined the relationship between total neutrophilic count and CSF L-lactate concentration and found a moderate-to-strong correlation between the two. Although our analysis was performed on a small subgroup, potentially limiting the external validity of the results, our findings align with studies in human medicine (127,181,182). Of note, our study does not provide conclusive evidence about whether lactate concentration is more closely linked to the functional state of neutrophils or their absolute numbers. Moreover, we

found similar correlations between total macrophage count and L-lactate, which suggests that L-lactate might be secondary to general differences in CNS inflammation. Further studies are needed to develop this hypothesis and determine the production rate of L-lactate from neutrophils and other immune cells isolated from the CSF in relation to their activation status.

Significant correlations were observed between CSF L-lactate concentration and CSF TNCC and TP. The cases of neutrophilic PL exhibited elevated TNCC and TP, which might explain the correlation. Additional studies are needed to investigate the functional relationship between these variables and CSF L-lactate concentration.

We did not to exclude samples with blood contamination since it is widely believed in both human and veterinary medicine that iatrogenic blood contamination of the CSF does not alter L-lactate concentration (167,171–173). Our results further support this notion, as no correlation was observed between CSF L-lactate and RBCC.

We noted a weak correlation between CSF L-lactate and blood L-lactate concentration in the sick cattle group. This finding contradicts the current literature, which states that CSF and blood lactate levels are independent of one another (161,162). A plausible explanation for our observation is that the integrity of the BBB may be altered in disease, with a partial effect of blood L-lactate concentration on CSF L-lactate concentration (163,164). No significant differences in blood L-lactate concentration were observed across diagnoses or CSF interpretations. This underlines the importance of measuring L-lactate in CSF rather than in blood to accurately detect acute bacterial infection of the CNS.

This study has some limitations. There were differences in the demographics between the healthy cattle, on which the RI of CSF L-lactate was calculated, and the sick cattle, particularly for age and breed. The healthy group consisted exclusively of young Holstein Friesian cattle. Slight differences in the RI of CSF L-lactate have been reported between human neonates and adults (175). Thus, caution is warranted when applying the RI obtained

in this study to evaluate CSF L-lactate in animals differing in age. The bacterial agents of infection were not identified, which precluded investigating correlations between specific types of bacteria and lactate concentration. Bacterial metabolism is known to play a relatively minor role in lactate production, with the host's immune response being the primary determinant (181). Furthermore, our focus was solely on the measurement of L-lactate, without taking into account the other isotype, D-lactate, which is produced by bacteria [35]. This decision was based on the fact that D-lactate is typically found in low concentrations, accounting for 1–5% of L-lactate (233). Commonly used lactate measurement methods primarily target L-lactate.

In conclusion, our findings underscore a strong association between CSF L-lactate concentration and neutrophilic PL, marker of acute CNS inflammation induced by bacterial infection in cattle. A CSF L-lactate cut-off value of 3.15 mmol/L for identifying this kind of disease appears therefore reasonable. Measuring CSF L-lactate in field conditions requires only a small volume of CSF, less than one drop, and yields results within a few seconds. The quick turnaround time, along with the high sensitivity and specificity (93% and 80% respectively in our population) in detecting acute inflammatory disorders, can provide veterinarians with the advantage of obtaining prompt results and the opportunity to initiate antimicrobial treatments as needed, thus promoting a more rational use of antimicrobials in farm animal practice.

Additional information

The present study has recently been submitted as a research article to BMC Veterinary Research journal as:

Ferrini S, Cagnotti G, Ala U, Avilii E, Bellino C, Biasibetti E, Borriello G, Corona C, Di Muro G, Iamone G, Iulini B, Pezzolato M, Bozzetta E, D'Angelo A. Cerebrospinal fluid L-lactate as a diagnostic marker for acute inflammatory disorders in the central nervous system of

cattle. BMC Veterinary Reseach (2023), under revision.

PROJECT 4 - A study on the utility of Idexx ProCyte Dx® for bovine cerebrospinal fluid evaluation

1 Introduction

CSF analysis holds significant importance in the diagnosis of disorders of the CNS, especially in identifying infectious-inflammatory conditions. Among cattle, infections and inflammatory conditions of the CNS are the primary contributors to neurological disorders (29). For this species, CSF analysis serves as the most direct antemortem diagnostic method for CNS diseases, as advanced diagnostic imaging is less practical compared to companion animals (26). Gold standard for CSF analysis relies on the use of a haemocytometer chamber for cell counting and cytologic evaluation to differentiate cell types. These procedures are manually performed and demand specialized expertise and facilities that may not be readily available on-site (67,203). A significant disadvantage of this is the resultant delay in analysis, which has been observed to adversely affect cell integrity, and delayed therapeutic intervention possibilities. Automated analyzers for CSF are currently studied in human medicine as an alternative to the gold standard manual analysis, and these methods serve as alternatives to manual techniques (67,200,201). In the field of veterinary medicine, limited research has explored the application of haematology analyzer for CSF in dogs (199,202,203) and demonstrated that automated CSF analysis can be performed in canine species. Some limitations were observed, particularly in samples with low cellularity and in differential cell count analysis. Among haematology analyzers, the Idexx ProCyte Dx® Haematology Analyzer (IDEXX Laboratories, Inc.) is the most accurate and comprehensive complete blood counting machine available. It is currently in use at numerous veterinary hospitals. A recent study assessed the ProCyte Dx® Hematology

Analyzer's performance in analyzing CSF in dogs (199). The findings revealed a strong correlation between the analyzer and the gold standard laboratory analysis in detecting TNCC, but suggested software modifications to improve the analyzer's sensitivity in detecting smaller cell increments.

Based on these premises, the objectives of this prospective study were to assess the Idexx ProCyte Dx® hematology analyzer's capability in determining total and differential CSF nucleated cell counts in cattle and to compare it with the gold standard laboratory analysis. Specifically, we established a RI for TNCC in bovine CSF analyzed with the Idexx ProCyte Dx® and investigated the performance of the instrument in delivering TNCC and differential cell counts that exhibited comparability to the gold standard laboratory analysis.

2 Materials and methods

2.1 Samples

CSF samples were prospectively collected from a healthy cattle group (Authorization No. 242/2020 - PR) housed at the VTH of Turin and from a sick cattle group. The latter presented to the VTH Neurology Service for neurological signs suggestive of a CNS disorder, where CSF analysis was performed as a part of the clinical evaluation. CSF samples where then categorized into two groups: CSF samples with normal TNCC (normal TNCC group) and CSF samples with PL (increased TNCC group). The normal TNCC group was composed of samples from all the healthy cattle and from part of the cattle included in the sick group when the laboratory CSF analysis would confirm a normal TNCC. The remaining sick cattle samples were included in the increased TNCC group. For the purpose of the present study, cases exhibiting AC dissociation were considered in the normal TNCC group.

Animals were excluded from the study if the collected sample volume was insufficient for both internal gold standard laboratory analysis and automated analysis using the Idexx ProCyte Dx®.

This prospective study was conducted in accordance with current animal welfare regulations (Directive 98/58/EC and Italian Decree Law 146/2001). Pathological samples were collected during routine diagnostic evaluation. Written informed consent was obtained from the owners before veterinary assessment and treatment of their animals.

2.2 CSF collection

CSF was collected from the lumbosacral region of animals using the procedure described by Mayhew (7). The animals were positioned either in sternal recumbency or standing position, and when necessary, sedation was administered using xylazine hydrochloride.

The CSF collection site was shaved, surgically prepared, and local anesthesia was provided by subcutaneously injecting 2.5 mL of procaine hydrochloride (Procamidor®). Spinal needles of either 18 G and 90 mm in length or 21 G and 50 mm (Terumo) were used for the CSF collection, based on the body size of the animal.

The CSF was collected by gently aspirating it into a syringe attached to the needle hub. The collected samples were then divided into sterile empty tubes for gold standard analysis (minimum volume 800 µL) and EDTA tubes for automated analysis (minimum volume 300 µL).

2.3 Gold standard laboratory CSF analysis

The freshly collected CSF samples were transferred to the Laboratory Service of the VTH of Turin and analyzed within one hour of collection. For the assessment of the TNCC, 100 µl of CSF were mixed with 100 µl of Turks stain and placed on a Nageotte haemacytometer. The number of cells in an eight by ten rectangle was counted. Cytospin slides were prepared using 250 µl of CSF, which was centrifuged at 150 g for six minutes using a Cytospin2 (Shandon). The slides were then stained with May-Grünwald Giemsa for both the differential

cell count and morphological evaluation. Only samples with a minimum of 10 cells per slide were included in the differential cell count. A certified clinical pathologist evaluated the cytocentrifuge preparations providing a comment regarding the types of cells observed and their respective proportions. The total protein concentration of the samples was measured using a spectrophotometer (Sentinel Diagnostics) with a pyrogallol red assay. Based on the characteristics of the sample, CSF possible final interpretations included: normal CSF or CSF with one of the following: mononuclear PL, neutrophilic PL, mixed PL or AC dissociation.

PL was defined when the TNCC was > 10 cells/ µL. Cases with increased TNCC were further divided into mildly increased when TNCC < 50 cells/ µL, moderately increased when TNCC > 50 and < 100 cells/ µL, markedly increased when TNCC > 100 cells/ µL.

2.4 Automated CSF analysis with Idexx Procyte Dx®

To perform automated CSF analysis, the CSF sample collected in an EDTA tube was inserted into the Idexx Procyte Dx® machine. After collection the sample was gently rotated to resuspend any sedimented cells and the analysis was always performed within one hour of collection. A specific cycle was selected, choosing the substrate "other fluid". The analysis produced a TNCC per liter (TNCC/L), and a red blood cell count per liter (RBCC/L) which were subsequently converted to TNCC/µL and RBCC/µL respectively for further examination. Furthermore, a scatter plot was generated to visually represent the distribution of cells in the sample. In cases where the sample exhibited sufficient cellularity (TNCC > 1000/µL), the automated analysis also provided a differential cell count, distinguishing between granulocytes (polymorphonucleate cells) and agranulocytes (mononuclear cells).

In cases where the preceding sample that was analyzed by the machine was blood, the analysis of the CSF was conducted twice. The first analysis was performed without any additional steps, while the second analysis was preceded by a cleaning cycle was carried

out using 2 mL of IDEXX Hydro-Clean solution (a manufacturer-provided cleansing agent containing 5.25% active chlorine). However, if consecutive CSF samples were being analyzed, the cleaning cycle was only performed for the first sample.

2.5 Statistical Analysis

All analyses were performed using Rstudio version 4.1.3 and Prism version 9.1.1. Numerical variables were analyzed for normality distribution with the Shapiro Wilk test and described as mean SD or median and IQR as appropriate. Categorical variables were described as relative frequency and percentage. A preliminary RI for Procyte Dx® CSF TNCC was identified with the percentile method by the 2.5th and 97.5th percentiles within the normal TNCC group. The correlation and discrepancies between the pre- and post-cleaning cycle for Procyte Dx® TNCC were evaluated using the Spearman rank test coefficient and Wilcoxon signed rank test, respectively.

The correlation between TNCC performed by Procyte Dx® and laboratory analysis were assessed with Spearman rank test coefficient. The agreement between the two methods were assessed using Bland-Altman plots. All the aforementioned analyses were performed for the combined data and separately for the normal TNCC and increased TNCC groups.

The Wilcoxon rank sum test was employed to examine the TNCC provided by the Procyte Dx® between cases classified as with normal TNCC and those with increased TNCC, as determined by the laboratory analysis. A ROC analysis was conducted to compare the TNCC obtained through the Procyte Dx® analysis between cases within the increased TNCC group and those within the normal TNCC group, as determined by the laboratory analysis. The Youden index was used to identify the optimal cut-off point for distinguishing between the two groups based on the Procyte Dx® analysis. Statistical significance was defined as $p < 0.05$.

In the increased TNCC group, the correlation in differential cell count between the Procyte Dx® and the laboratory was conducted using the Spearman rank test coefficient when the data were available. Moreover, scatter plots were subjected to visual analysis and assessment by one of the authors who was unaware of the interpretation of the laboratory. This process involved determining the number of cell types present in the plot and identifying the predominant cell type. Instances where the observer identified predominantly mononuclear cells were categorized as mononuclear PL, cases where both mononuclear cells and polymorphonucleated cells were equally present were classified as mixed PL, and finally, when polymorphonucleated cells were the most prevalent, it indicated neutrophilic PL. The agreement between the Procyte Dx® scatter plot interpretation compared to the laboratory CSF interpretation was subsequently calculated according to the K Cohen statistic.

3. Results

3.1 Study population

113 cattle were included in this prospective study. 25/113 (22%) cattle belonged to healthy group while 88/113 (78%) to the sick cattle group. The normal TNCC group was composed of 76/113 (67%) bovine CSF samples. The increased TNCC group was composed of 37/113 (33%) bovine CSF samples. Nineteen out of 37 (51%) presented a mild PL (median cells/µL 14, IQR 12.2 – 20.9), 3/37 (8%) a moderate PL (median cells/µL 80.6, IQR 73.8 – 88.6) and 15/37 (41%) a marked PL (median cells/µL 221, IQR 133.2 – 824).

3.2 Comparison pre- and post- cleansing cycle

There was significant correlation between TNCC counted by the Procyte Dx® pre and post cleansing cycle in both the normal TNCC group (TNCC: rho = 0.48; p = 0.002), the increased TNCC group (TNCC: rho = 0.98; p < 0.0001) and when groups were combined (TNCC: rho

= 83; p < 0.0001). The median of the differences in TNCC between pre and post cleansing cycle was not significantly different from zero in both the normal TNCC group, the increased TNCC group, and when the groups were combined.

3.3 Procyte Dx® RI for CSF TNCC

Median Procyte Dx® CSF TNCC in the normal TNCC group was 10 cells/μL (IQR 0-10 cells/μL). The RI for CSF TNCC was 0-20 cells/μL.

3.4 Comparison between Procyte Dx® and laboratory TNCC

We found a significant difference in median Procyte Dx® TNCC between the increased TNCC group and the normal TNCC group. Specifically, the increased TNCC group had a substantially higher median of 70 cells/μL (IQR 30-410 cells/μL), (p-value < 0.0001; Figure 1). When we compared Procyte Dx® TNCC between the normal TNCC group and the mildly increased TNCC subgroup, a higher median TNCC was observed within the mildly increased TNCC subgroup (median for the mildly increased TNCC subgroup: 20 cells/μL, IQR 20-30 cells/μL; p < 0.0001).

Figure 1: Difference in Procyte Dx® TNCC/μL between the normal TNCC group and the increased TNCC group. The scatter points represent individual data points. The median and IQR are shown. Asterisks (*) indicate the level of statistical significance: *p<0.05, **p<0.01, ***p<0.001, ****p<0.0001. The absence of an asterisk indicates a lack of statistically significant differences between groups. TNCC = total nucleated cell count.

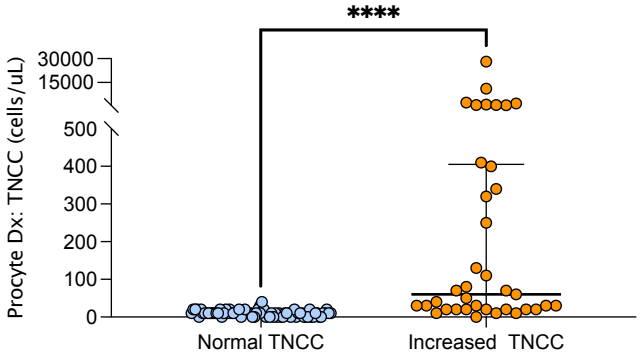

The AUROC for Procyte Dx® in distinguishing between the increased TNCC group and the normal TNCC group was 0.93. Using the Youden index method, we determined a cutoff value of 15 cells/ µL, which corresponded to a diagnostic sensitivity of 79% and specificity of 89% in detecting CSF PL (Figure 2).

Figure 2. ROC curve for predicting the presence of PL based on Procyte Dx® TNCC/µL. The x-axis represents the false positive rate (1-Specificity), and the y-axis represents the true positive rate (Sensitivity).

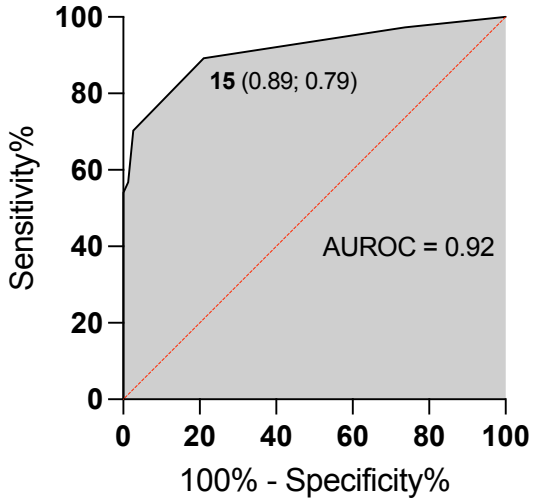

A strong and significant correlation was observed between Procyte Dx® and laboratory TNCC, in the increased TNCC group (rho = 0.89; p < 0.0001; Figure 3), as well as when considering both groups together (rho = 0.68; p < 0.0001). Within the normal TNCC group, there was no significant correlation observed (rho = 0.19; p = 0.09).

Figure 3: Correlation between Procyte Dx® and Laboratory TNCC in the increased TNCC group. Scatter points represent individual data points. The X-axis represents Procyte Dx TNCC/uL and the Y-axis represents Laboratory TNCC/µL. The correlation coefficient (rho 0.89; p < 0.0001) indicates the strength and the direction of the correlation between the variables. TNCC = total nucleated cell count.

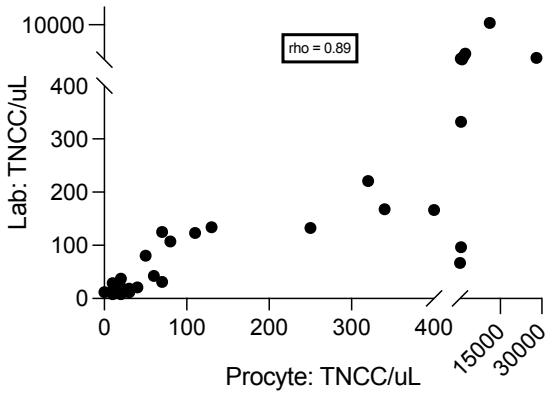

The Bland-Altman plot, when focusing solely on the normal TNCC group, showed 95% limits of agreement ranging from -8.45 to 21.11 cells/µL, with a bias of 6.33 ± 7.54 µL. For the increased TNCC group, the 95% limits of agreement spanned from -311.7 to 548.5 cells/µL, with a bias of 42.35 ± 134.1 µL. When examining the combined data, the Bland-Altman plot showed 95% limits of agreement ranging from -200.5 to 305.2 cells/µL, with a bias of 118.4 ± 119.5 µL (Figure 4).

Figure 4: Bland-Altman plot showing the difference between the TNCC of various CSF samples determined with the Idexx ProCyte Dx® against the mean of the two methods evaluated (N = 113). The dotted lines represent the mean ± 2SD difference between the methods. TNCC = total nucleated cell count.

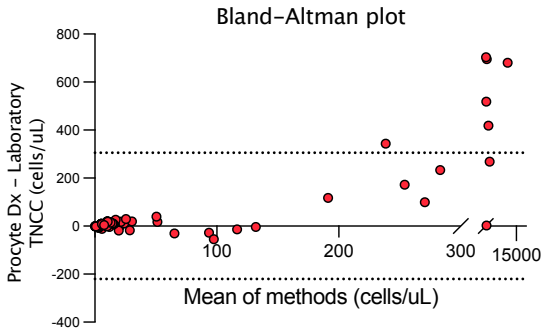

3.5 Comparison between Procyte Dx® and laboratory differential cell count

For differential cell count comparison, we focused exclusively on the increased TNCC group. For 4/37 (11%) subjects in this group, we had access to differential cell counts from both Procyte Dx® and laboratory analyses. In this limited sample, the Spearman rank test

coefficient (rho) was 0.8, indicating a strong correlation. However, due to the small sample size, we were unable to make any meaningful population-wide inferences.

For 27/37 (73%) subjects, we compared the Procyte Dx® scatter plot interpretation with the CSF interpretation conducted by the laboratory, revealing a K-Cohen coefficient of agreement of 0.69.

4. Discussion

In the present study, the Procyte Dx® analyzer performed well in measuring CSF TNCC and could distinguish samples with normal TNCC from those with increased TNCC, with a cutoff of 15 cells/ µL. By analyzing samples with normal TNCC, we defined a RI for Procyte Dx® TNCC. The upper RI cut off (20 cells/µL) was higher than the laboratory cut off for normal TNCC (10/µL). This finding might reflect the Procyte Dx® tendency to produce slightly higher values compared to the laboratory or might depend on the limited sensitivity and precision of the instrument. Procyte Dx® in fact can only provide TNCC in 10 cell/µL increments.

When assessing Procyte Dx® TNCC against the laboratory values, a strong and significant correlation was observed within the increased TNCC group. Conversely, within the normal TNCC group, we identified only a weak and non-significant correlation, supporting the hypothesis that Procyte Dx® lacks capabilities at low cellularity levels. We performed further analysis to evaluate Procyte Dx® abilities in distinguishing mildly increased TNCC from normal TNCC and disclosed an overlapping distribution of values, with a few higher values in the mildly increased TNCC subgroup contributing to the observed statistical significance. Bland-Altman analysis revealed that measurement differences tended to increase with higher TNCC values. This finding was deemed clinically insignificant. Elevated differences were observed solely when TNCC exceeded 200 cells/µL, a threshold at which TNCC does not provide additional meaningful information for clinical interpretation of a disease process.

Upon analyzing the bias in this analysis, we indeed confirmed a consistent trend in Procyte Dx® to produce slightly higher values compared to the laboratory method.

Regarding differential cell count, our ability to obtain significant results was hindered by the limited sample size due to Procyte Dx®'s high threshold for providing differential cell count. Nevertheless, we observed a substantial agreement between the evaluation of the scatter plot and the laboratory CSF interpretation.

Our findings are consistent with a previous study that applied the same procedure in dogs (199). Notably, ProCyte Dx® analysis, based on 10 cells/µL increments, may be well-suited for bovine species, given that the normal range for TNCC in this species extends up to 10 cells/µL (5), whereas in dogs, it is 5 cells/µL (12). Additionally, we observed a strong and statistically significant correlation in TNCC between the pre- and post-cleansing cycle samples. This finding suggests that Procyte Dx® CSF analysis is not influenced by prior samples with higher cellularity, such as blood.

The main limitation of this study was the lack of CSF samples with a TNCC exceeding 1000 cells/µL. This would have enabled ProCyte Dx® to perform differential cell counting, facilitating a direct comparison with laboratory values. Nevertheless, it is worth noting that such severe PL cases are infrequent in clinical practice.

In conclusion, CSF Procyte Dx® analysis can be conducted rapidly without being preceded by a cleansing cycle, with results available just a few minutes after CSF collection. Based on our study, this analysis can effectively detect increased TNCC in bovine CSF, and values ≥20 cells/µL indicate CSF PL. However, the instrument may not accurately detect mild increases in TNCC. Moreover, it is important to acknowledge that the high threshold of the instrument for providing a differential cell count is a limitation in its clinical application. To enhance accuracy in CSF differential cell counting, the software implementation with a tailored panel for CSF would be beneficial.

Additional information

The present study will be submitted to a peer-reviewed scientific journal shortly.

DISCUSSION

With the thesis presented here we investigated different approaches to overcome challenges in interpretation of CSF analysis and bacterial CNS infection diagnosis:

- We created a ML based web-app that can help predict the probability of infectious and inflammatory disorders of the CNS in cattle.
- We applied 16S gene sequencing to investigate the presence of bacteria in the CSF of cattle with neurological disorders.
- We identified that high concentration of CSF L-lactate indicates acute CNS inflammation.
- We assessed the performance of an automated and rapid CSF analysis tool.

By applying 16S gene sequencing we highlighted difficulties in distinguishing microbial communities in samples with infections from those associated with other neurological disorders. We hypothesized that this challenge was dependent on the inadvertent retrieval of contaminant bacterial DNA during sampling or lab processing. Furthermore, as our analysis typically yielded results on the genus level, we were unable to definitively identify different species present within the samples. To address these limitations, the following adjustments to the sample workflow should be considered:

- Incorporating negative controls, including 16S gene sequencing of CSF samples from healthy subjects, farm environment samples, skin samples from the CSF collection site, and DNA extraction and PCR blank controls. This approach can identify potential

contaminants and enable the subtraction of contaminants to detect genuine bacteria originating from CSF samples in infected cattle.

- Conducting orthogonal tests on the CSF/subject to confirm the presence of infection agents, which may involve bacterial isolation through culturomics, 16S qPCR, 16S FISH, and IHC staining for bacterial components (LPS for gram-negative and LTA for gram-positive).
- Implementing a higher level of sterility, such as processing samples under biological hoods and using buffers with certified levels of sterility.
- Exploring innovative 16S gene sequencing techniques that expand the number of sequenced regions, enhancing sequencing depth and improving taxonomic classification, potentially allowing the differentiation between pathological and environmental species within the same genus (75,81).

If these improvements lead to further pathogen characterization, the association between L-lactate and neutrophils provides insights into the role of the host immune system during bacterial infection (181). Additional research could expand on this hypothesis by analyzing the composition of the CSF immune system during inflammation through flow cytometry. Furthermore, fluorescent activated cell sorting (FACS) could be utilized to isolate different immune system cells and measure their L-lactate production rates.

The study of the composition and function of immune system cells in the CSF of cattle with CNS infection, integrated with further pathogen characterization provided by 16S gene sequencing, will provide a wealth of additional information, defining a large and complex dataset. ML models can then be trained to identify the intricate relationships between these features, with the ultimate goal of developing an algorithm capable of predicting precise etiological diagnoses, aiding in the correct use of antimicrobial drugs.

CONCLUSION

In conclusion, with the present studies we advanced our understanding of CSF analysis and the diagnosis of bacterial CNS infections in cattle. Key accomplishments include the development of a ML-based web app to assist with making clinical diagnoses and the identification of CSF L-lactate as an indicator of inflammation. However, challenges persist, such as microbial community differentiation and contamination issues during 16S gene sequencing. To address these challenges, we propose a comprehensive approach involving improved workflow, sterility measures, and innovative sequencing techniques. Additionally, the study highlights the potential for further research into the host immune response and pathogen characterization, aiming to create a complex dataset for ML algorithms to enhance diagnostic precision. This work represents a further step forward in veterinary diagnostics and the understanding of CNS infections in cattle.

REFERENCES

1. de Lahunta A, Glass E, Kent M. Development of the nervous system and malformations. In: Veterinary neuroanatonomy and clinical neurology. 5th ed. Elsevier; 2021. p. 45–78.
2. Ceccarelli P, Ferrandi B. Sistema nervoso centrale e occhio. In: Embriologia degli Animali Domestici. edi-ermes; 1996. p. 96–109.
3. Evans H, de Lahunta A. The Brain. In: Miller's anatomy of the dog. 4th ed. Saunders; 2013. p. 658–707.
4. Bortolami R, Callegari E, Clavenzani P, Beghelli V. Sistema Nervoso. In: Anatomia e fisiologia degli animali domestici. 3rd ed. Edagricole; 2017. p. 467–546.
5. Welles EG, Tyler JW, Sorjonen DC, Whatley EM. Composition and analysis of cerebrospinal fluid in clinically normal adult cattle. Am J Vet Res. 1992 Nov;53(11):2050–7.
6. Smith B, Van Metre D, Pusterla N. Disease of the nervous system. In: Large Animal Internal Medicine. 6th ed. Elsevier; 2020. p. 1006–117.
7. Mayhew J, MacKay R. Ancillary diagnostic aids. In: Large Animal Neurology. 3rd ed. Wiley Blackwell; 2022. p. 55–74.
8. Scott R. Diagnostic techniques and clinicopathologic findings in ruminant neurologic disease. Vet Clin Nth Amer Food Anim Pract. 2004 Jul;20(2):215–30.
9. Mayhew I, Beal C. Techniques of Analysis of Cerebrospinal Fluid. Vet Clin Nth Amer Food Anim Pract. 1980 Feb;10(1):155–76.
10. Bailey CS, Higgins RJ. Comparison of total white blood cell count and total protein content of lumbar and cisternal cerebrospinal fluid of healthy dogs. Am J Vet Res. 1985 May;46(5):1162–5.
11. Scott PR. Analysis of cerebrospinal fluid from field cases of some common ovine neurological diseases. British Vet J. 1992 Jan;148(1):15–22.

12. Platt S, Olby N. Clinical pathology. In: BSAVA Manual of Canine and Feline Neurology. 4th ed. British Small Animal Veterinary Association; 2015. p. 36–58.
13. Di Terlizzi R, Platt S. The function, composition and analysis of cerebrospinal fluid in companion animals: Part I – Function and composition. Vet J. 2006 Nov;172(3):422–31.
14. de Lahunta A, Glass E, Kent M. Cerebrospinal fluid and hydrocephalus. In: Veterinary neuroanatonomy and clinical neurology. 5th ed. Elsevier; 2021. p. 79–105.
15. Curti J, Queiroz G, Pereira P, Anjos M, Flaiban K, Lisbôa J. L-lactate in cerebrospinal fluid can be used as a biomarker of encephalitis in cattle. Can J Vet Res . 2020 Apr;84(2):146–52.
16. Jackson C, Lahunta A, Divers T, Ainsworth D. The Diagnostic Utility of Cerebrospinal Fluid Creatine Kinase Activity in the Horse. J Vet Intern Med. 1996 Jul;10(4):246–51.
17. Jackson C, de Lahunta A, Divers T, Ainsworth D. The Diagnostic Utility of Cerebrospinal Fluid Creatine Kinase Activity in the Horse. J Vet Intern Med. 1996 Jul 28;10(4):246–51.
18. Pollay M, Welch K. The function and structure of canine arachnoid villi. J Surg Res. 1962 Sep;2(5):307–11.
19. Fry M, Vernau W, Kass P, Vernau K. Effects of time, initial composition, and stabilizing agents on the results of canine cerebrospinal fluid analysis. Vet Clin Pathol. 2006 Mar;35(1):72–7.
20. Steele R, Marmer D, O'Brien M, Tyson S, Steele C. Leukocyte survival in cerebrospinal fluid. J Clin Invest. 1986 May;23(5):965–6.
21. Bellino C, Miniscalco B, Bertone I, Cagnasso A, Occhiena E, Gianella P, et al. Analysis of cerebrospinal fluid from cattle with central nervous system disorders after storage for 24 hours with autologous serum. BMC Vet Res. 2015 Dec 13;11(1):201.
22. Kjeldsberg C, Knight J. Body Fluids: Laboratory Examination of Cerebrospinal, Synovial, and Serous Fluids : a Textbook Atlas. 3rd ed. Vol. Chapter 2. Amer Society of Clinical; 2010.
23. Bienzle D, McDonnell J, Stanton J. Analysis of cerebrospinal fluid from dogs and cats after 24 and 48 hours of storage. J Am Vet Med Ass. 2000 Jun 1;216(11):1761–4.
24. D'Angelo A, Miniscalco B, Bellino C, Bormida S, Borrelli A, Maurella C, et al. Analysis of cerebrospinal fluid from 20 calves after storage for 24 hours. Vet Rec. 2009 Apr 18;164(16):491–3.
25. Di Terlizzi R, Platt S. The function, composition and analysis of cerebrospinal fluid in companion animals: Part II – Analysis. Vet J. 2009 Apr;180(1):15–32.
26. Nagy D. Diagnostics and Ancillary Tests of Neurologic Dysfunction in the Ruminant. Vet Clin Nth Amer Food Anim Pract. 2017 Mar;33(1):9–18.
27. Marshall T, Williams K. Protein determination in cerebrospinal fluid by protein dye-binding assay. British J biomed sci. 2000;57(4):281–6.
28. Jacobs R, Cochrane S, Lumsden J, Norris A. Relationship of cerebrospinal fluid protein concentration determined by dye-binding and urinary dipstick methodologies. Can Vet J. 1990 Aug;31(8):587–8.
29. Stokol T, Divers TJ, Arrigan JW, McDonough SP. Cerebrospinal fluid findings in cattle with central nervous system disorders: A retrospective study of 102 cases (1990-2008). Vet Clin Pathol. 2009 Mar;38(1):103–12.
30. Leber A, Everhart K, Balada-Llasat J, Cullison J, Daly J, Holt S, et al. Multicenter Evaluation of BioFire FilmArray Meningitis/Encephalitis Panel for Detection of Bacteria, Viruses, and Yeast in Cerebrospinal Fluid Specimens. J Clin Microbiol. 2016 Sep;54(9):2251–61.
31. Salipante S, Sengupta D, Rosenthal C, Costa G, Spangler J, Sims E, et al. Rapid 16S rRNA Next-Generation Sequencing of Polymicrobial Clinical Samples for Diagnosis of Complex Bacterial Infections. PLoS One. 2013 May 29;8(5):e65226.

32. Tetsuo M, Matsuno K, Tamura T, Fukuhara T, Kim T, Okamatsu M, et al. Development of a High-Throughput Serum Neutralization Test Using Recombinant Pestiviruses Possessing a Small Reporter Tag. Pathogens. 2020 Mar 4;9(3):188.
33. Allsop T, Pauli J. Magnesium concentrations in the ventricular and lumbar cerebrospinal fluid of hypomagnesaemic cows. Res Vet Sci. 1985 Jan;38(1):61–4.
34. Fecteau G, George L. Bacterial meningitis and encephalitis in ruminants. Vet Clin Nth Amer Food Anim Pract. 2004 Jul;20(2):363–77.
35. Clarke L, Hawkins I, Rissi D. Central nervous system diseases of cattle in Georgia, 2001–2017. J of Vet Diagn Invest. 2019 Jul 10;31(4):588–93.
36. Truchet L, Walland J, Wüthrich D, Boujon C, Posthaus H, Bruggmann R, et al. Neuropathological survey reveals underestimation of the prevalence of neuroinfectious diseases in cattle in Switzerland. Vet Microbiol. 2017 Sep;208:137–45.
37. Giles L, Orr J, Viora L, Gutierrez-Quintana R, Logue D, Guevar J. Ruminant neurological disease: a retrospective cohort study. Vet Rec. 2017 Oct 7;181(14):372–3.
38. Aldridge B, Garry F, Adams R. Neonatal septicemia in calves: 25 cases (1985-1990). J Am Vet Med Ass. 1993 Nov 1;203(9):1324–9.
39. Fecteau G, Smith B, George L. Septicemia and Meningitis in the Newborn Calf. Vet Clin Nth Amer Food Anim Pract. 2009 Mar;25(1):195–208.
40. Câmara A, Vale A, Batista J, Feijó F, Soto-Blanco B. Suppurative intracranial processes in 15 domestic ruminants. Pesq Vet Brasil. 2014 May;34(5):421–6.
41. Lofstedt J, Dohoo IR, Duizer G. Model to predict septicemia in diarrheic calves. J Vet Intern Med. 1999;13(2):81–8.
42. Smith B, Van Metre D, Pusterla N. Manifestation and management of disease in the neonate ruminants. In: Large Animal Internal Medicine. 6th ed. Elsevier; 2020. p. 335–81.
43. Simiya Y, Ohshima K, Itoh H, Ogasawara N, Okutomo M, Tanaka S. Clinicopathology of Meningoventriculitis due to Streptococcus bovis Infection in Neonatal Calves. J Vet Med . 1992;54(5):871–4.
44. Kim K. Pathogenesis of bacterial meningitis: from bacteraemia to neuronal injury. Nat Rev Neurosci. 2003 May;4(5):376–85.
45. Kessell A, Finnie J, Windsor P. Neurological diseases of ruminant livestock in Australia. III: bacterial and protozoal infections. Aust Vet J. 2011 Aug;89(8):289–96.
46. Mayhew J, Mackay R. Infectious, inflammatory and immune diseases. In: Large Animal Neurology . 3rd ed. John Wiley & Sons; 2022. p. 292–373.
47. Cordy D. Pathomorphology and Pathogenesis of Bacterial Meningoventriculitis of Neonatal Ungulates. Vet Pathol. 1984 Nov 26;21(6):587–91.
48. Green S, Smith L. Meningitis in neonatal calves: 32 cases (1983-1990). J Am Vet Med Ass. 1992 Jul 1;201(1):125–8.
49. Dore V, Smith G. Cerebral Disorders of Calves. Vet Clin Nth Amer Food Anim Pract. 2017 Mar;33(1):27–41.
50. Arrigoni N, Bassi P, Bursi E, Casadio C, Luppi A, Padovani A, et al. Linee guida Uso prudente dell'antibiotico nell'allevamento bovino da latte. 2022.
51. Jensen R, Maki L, Lauerman L, Raths W, Swift B, Flack D, et al. Cause and pathogenesis of middle ear infection in young feedlot cattle. J Am Vet Med Ass. 1983 May 1;182(9):967–72.
52. Yeruham I, Elad D, Liberboim M. Clinical and Microbiological Study of an Otitis Media Outbreak in Calves in a Dairy Herd. J Vet Med. 1999 Apr;46(3):145–50.
53. Foster A, Naylor R, Howie N, Nicholas R, Ayling R. Mycoplasma bovis and otitis in dairy calves in the United Kingdom. Vet J. 2009 Mar;179(3):455–7.
54. Bertone I, Bellino C, Alborali G, Cagnasso A, Cagnotti G, Dappiano E, et al. Clinical-pathological findings of otitis media and media-interna in calves and (clinical) evaluation of a standardized therapeutic protocol. BMC Vet Res. 2015 Dec 3;11(1):297.

55. Lamm C, Munson L, Thurmond M, Barr B, George L. Mycoplasma Otitis in California Calves. J of Vet Diagn Invest. 2004 Sep 25;16(5):397–402.
56. Boileau M, Gilliam J. Brainstem and Cranial Nerve Disorders of Ruminants. Vet Clin Nth Amer Food Anim Pract. 2017 Mar;33(1):67–99.
57. Bernier Gosselin V, Francoz D, Babkine M, Desrochers A, Nichols S, Doré E, et al. A retrospective study of 29 cases of otitis media/interna in dairy calves. Can Vet J. 2012 Sep;53(9):957–62.
58. Duarte E, Hamdan J. Otitis in Cattle, an Aetiological Review. J Vet Med . 2004 Feb;51(1):1–7.
59. Morin D. Brainstem and cranial nerve abnormalities: listeriosis, otitis media/interna, and pituitary abscess syndrome. Vet Clin Nth Amer Food Anim Pract. 2004 Jul;20(2):243–73.
60. Nation P, Frelier P, Gifford G, Carnat B. Otitis in feedlot cattle. Can Vet J. 1983 Jul;24(7):238.
61. Peters M, Pohlenz J, Jaton K, Ninet B, Bille J. Studies of the Detection of Listeria monocytogenes by Culture and PCR in Cerebrospinal Fluid Samples from Ruminants with Listeric Encephalitis. J Vet Med . 1995 Jan 12;42(1–10):84–8.
62. Konradt G, Bassuino D, Prates K, Bianchi M, Snel G, Sonne L, et al. Suppurative infectious diseases of the central nervous system in domestic ruminants. Pesq Vet Brasil. 2017 Aug;37(8):820–8.
63. D'Angelo A, Bellino C, Alborali G, Borrelli A, Capucchio M, Casalone C, et al. Aortic Thrombosis in Three Calves with *Escherichia coli* Sepsis. J Vet Intern Med. 2006 Sep;20(5):1261–3.
64. Myszczynska M, Ojamies P, Lacoste A, Neil D, Saffari A, Mead R, et al. Applications of machine learning to diagnosis and treatment of neurodegenerative diseases. Nat Rev Neurol. 2020 Aug 15;16(8):440–56.
65. Ramachandran P, Wilson M. Metagenomics for neurological infections — expanding our imagination. Nat Rev Neurol. 2020 Oct 13;16(10):547–56.
66. Lleó A. Biomarkers in neurological disorders: a fast-growing market. Brain Commun. 2021 Apr 5;3(2).
67. Wick M, Gross C, Tumani H, Wildemann B, Stangel M. Automated Analysis of Cerebrospinal Fluid Cells Using Commercially Available Blood Cell Analysis Devices—A Critical Appraisal. Cells. 2021 May 18;10(5):1232.
68. May M. Eight ways machine learning is assisting medicine. Nat Med. 2021 Jan 13;27(1):2–3.
69. Adlung L, Cohen Y, Mor U, Elinav E. Machine learning in clinical decision making. Med. 2021 Jun;2(6):642–65.
70. Bakator M, Radosav D. Deep Learning and Medical Diagnosis: A Review of Literature. Multimod Technol Interact. 2018 Aug 17;2(3):47.
71. Fraiwan M, Abutarbush S. Using Artificial Intelligence to Predict Survivability Likelihood and Need for Surgery in Horses Presented With Acute Abdomen (Colic). J Equine Vet Sci. 2020 Jul;90:102973.
72. Bradley R, Tagkopoulos I, Kim M, Kokkinos Y, Panagiotakos T, Kennedy J, et al. Predicting early risk of chronic kidney disease in cats using routine clinical laboratory tests and machine learning. J Vet Intern Med. 2019 Nov 26;33(6):2644–56.
73. Barge P, Oevermann A, Maiolini A, Durand A. Machine learning predicts histologic type and grade of canine gliomas based on MRI texture analysis. Vet Radiol Ultrasound. 2023 Jul 3;64(4):724–32.
74. Boudreau E, Otamendi A, Levine J, Griffin J, Gilmour L, Jeffery N. Relationship between Machine-Learning Image Classification of T_2 -Weighted Intramedullary Hypointensity on 3 Tesla Magnetic Resonance Imaging and Clinical Outcome in Dogs with Severe Spinal Cord Injury. J Neurotrauma. 2021 Mar 15;38(6):725–33.

75. Wensel C, Pluznick J, Salzberg S, Sears C. Next-generation sequencing: insights to advance clinical investigations of the microbiome. J Clin Invest. 2022 Apr 1;132(7).
76. Goldberg B, Sichtig H, Geyer C, Ledeboer N, Weinstock G. Making the Leap from Research Laboratory to Clinic: Challenges and Opportunities for Next-Generation Sequencing in Infectious Disease Diagnostics. mBio. 2015 Dec 31;6(6).
77. Chiu C, Miller S. Clinical metagenomics. Nat Rev Genet. 2019 Jun 27;20(6):341–55.
78. Kennedy K, de Goffau M, Perez-Muñoz M, Arrieta M, Bäckhed F, Bork P, et al. Questioning the fetal microbiome illustrates pitfalls of low-biomass microbial studies. Nature. 2023 Jan 26;613(7945):639–49.
79. Chirgwin J, Przybyla A, MacDonald R, Rutter W. Isolation of biologically active ribonucleic acid from sources enriched in ribonuclease. Biochemistry. 1979 Nov 1;18(24):5294–9.
80. Kazantseva J, Malv E, Kaleda A, Kallastu A, Meikas A. Optimisation of sample storage and DNA extraction for human gut microbiota studies. BMC Microbiol. 2021 Dec 29;21(1):158.
81. Nejman D, Livyatan I, Fuks G, Gavert N, Zwang Y, Geller L, et al. The human tumor microbiome is composed of tumor type–specific intracellular bacteria. Science (1979). 2020 May 29;368(6494):973–80.
82. Preparing 16S Ribosomal RNA Gene Amplicons for the Illumina MiSeq System. 16S Metagenomic Sequencing Library Preparation.
83. Goodwin S, McPherson J, McCombie W. Coming of age: ten years of next-generation sequencing technologies. Nat Rev Genet. 2016 Jun 17;17(6):333–51.
84. Liu Y, Qin Y, Chen T, Lu M, Qian X, Guo X, et al. A practical guide to amplicon and metagenomic analysis of microbiome data. Protein Cell. 2021 May 11;12(5):315–30.
85. Prodan A, Tremaroli V, Brolin H, Zwinderman A, Nieuwdorp M, Levin E. Comparing bioinformatic pipelines for microbial 16S rRNA amplicon sequencing. PLoS One. 2020 Jan 16;15(1):e0227434.
86. Hasbun R. Progress and Challenges in Bacterial Meningitis. J Amer Vet Med Assoc. 2022 Dec 6;328(21):2147.
87. Zhou S, Liu A, Wang C, Liang Z, Zhou Z, Wang L, et al. High-throughput sequencing of 16S rDNA amplicons characterizes bacterial composition in cerebrospinal fluid samples from patients with purulent meningitis. Drug Des Devel Ther. 2015 Aug;4417.
88. Wilson M, Sample H, Zorn K, Arevalo S, Yu G, Neuhaus J, et al. Clinical Metagenomic Sequencing for Diagnosis of Meningitis and Encephalitis. N Eng J Med. 2019 Jun 13;380(24):2327–40.
89. Dominy S, Lynch C, Ermini F, Benedyk M, Marczyk A, Konradi A, et al. Porphyromonas gingivalis in Alzheimer's disease brains: Evidence for disease causation and treatment with small-molecule inhibitors. Sci Adv. 2019 Jan 4;5(1).
90. Kang Y, Ji X, Guo L, Xia H, Yang X, Xie Z, et al. Cerebrospinal Fluid from Healthy Pregnant Women Does Not Harbor a Detectable Microbial Community. Microbiol Spectr. 2021 Dec 22;9(3).
91. Hoon-Hanks L, McGrath S, Tyler K, Owen C, Stenglein M. Metagenomic Investigation of Idiopathic Meningoencephalomyelitis in Dogs. J Vet Intern Med. 2018 Jan 2;32(1):324–30.
92. Nessler J, Jo W, Osterhaus A, Ludlow M, Tipold A. Canine Meningoencephalitis of Unknown Origin—The Search for Infectious Agents in the Cerebrospinal Fluid via Deep Sequencing. Front Vet Sci. 2021 Dec 7;8.
93. Barber R, Li Q, Levine J, Ruone S, Levine G, Kenny P, et al. Screening for Viral Nucleic Acids in the Cerebrospinal Fluid of Dogs With Central Nervous System Inflammation. Front Vet Sci. 2022 Mar 24;9.
94. Ozutsumi Y, Tajima K, Takenaka A, Itabashi H. The Effect of Protozoa on the Composition of Rumen Bacteria in Cattle Using 16S rRNA Gene Clone Libraries. Biosci Biotechnol Biochem. 2005 Jan 22;69(3):499–506.

95. Thoetkiattikul H, Mhuantong W, Laothanachareon T, Tangphatsornruang S, Pattarajinda V, Eurwilaichitr L, et al. Comparative Analysis of Microbial Profiles in Cow Rumen Fed with Different Dietary Fiber by Tagged 16S rRNA Gene Pyrosequencing. Curr Microbiol. 2013 Aug 8;67(2):130–7.
96. Nicola I, Cerutti F, Grego E, Bertone I, Gianella P, D'Angelo A, et al. Characterization of the upper and lower respiratory tract microbiota in Piedmontese calves. Microbiome. 2017 Dec 21;5(1):152.
97. Zeineldin M, Lowe J, Aldridge B. Contribution of the Mucosal Microbiota to Bovine Respiratory Health. Trends Microbiol. 2019 Sep;27(9):753–70.
98. Bay V, Griffiths B, Carter S, Evans N, Lenzi L, Bicalho R, et al. 16S rRNA amplicon sequencing reveals a polymicrobial nature of complicated claw horn disruption lesions and interdigital phlegmon in dairy cattle. Sci Rep. 2018 Oct 19;8(1):15529.
99. Bartolomaeus T, Birkner T, Bartolomaeus H, Löber U, Avery E, Mähler A, et al. Quantifying technical confounders in microbiome studies. Cardiovasc Res. 2021 Feb 22;117(3):863–75.
100. Hallmaier-Wacker L, Lueert S, Roos C, Knauf S. The impact of storage buffer, DNA extraction method, and polymerase on microbial analysis. Sci Rep. 2018 Apr 19;8(1):6292.
101. Karstens L, Asquith M, Davin S, Fair D, Gregory W, Wolfe A, et al. Controlling for Contaminants in Low-Biomass 16S rRNA Gene Sequencing Experiments. mSystems. 2019 Jun 4;4(4).
102. Gillespie Í, Rosenstein P, Hughes D. Update: Clinical Use of Plasma Lactate. Vet Clin Nth Amer Small Anim Pract. 2017 Mar;47(2):325–42.
103. Ewaschuk J, Naylor J, Zello G. D-Lactate in Human and Ruminant Metabolism. J Nutri. 2005 Jul;135(7):1619–25.
104. McLellan A, Phillips S, Thornalley P. Fluorimetric assay of d-lactate. Anal Biochem. 1992 Oct;206(1):12–6.
105. Pang D, Boysen S. Lactate in Veterinary Critical Care: Pathophysiology and Management. J Am Anim Hosp Ass. 2007 Sep 1;43(5):270–9.
106. Adeva-Andany M, López-Ojén M, Funcasta-Calderón R, Ameneiros-Rodríguez E, Donapetry-García C, Vila-Altesor M, et al. Comprehensive review on lactate metabolism in human health. Mitochondrion. 2014 Jul;17:76–100.
107. Andersen L, Mackenhauer J, Roberts J, Berg K, Cocchi M, Donnino M. Etiology and Therapeutic Approach to Elevated Lactate Levels. Mayo Clin Proc. 2013 Oct;88(10):1127–40.
108. Haji-Michael P, Ladrière L, Sener A, Vincent J, Malaisse W. Leukocyte glycolysis and lactate output in animal sepsis and ex vivo human blood. Metabolism. 1999 Jun;48(6):779–85.
109. Mészáros K, Lang C, Bagby G, Spitzer J. Contribution of different organs to increased glucose consumption after endotoxin administration. Journal of Biological Chemistry. 1987 Aug;262(23):10965–70.
110. Ruggieri A, Levy R, Deutschman C. Mitochondrial Dysfunction and Resuscitation in Sepsis. Crit Care Clin. 2010 Jul;26(3):567–75.
111. Madias N. Lactic acidosis. Kidney Int. 1986 Mar;29(3):752–74.
112. Kopanke J, Chen A, Brune J, Brenna A, Thomovsky S. Reference intervals for the activity of lactate dehydrogenase and its isoenzymes in the serum and cerebrospinal fluid of healthy canines. Vet Clin Pathol. 2018 Jun 5;47(2):267–74.
113. Bakker J, Nijsten M, Jansen T. Clinical use of lactate monitoring in critically ill patients. Ann Intensive Care. 2013;3(1):12.
114. van Hall G. Lactate kinetics in human tissues at rest and during exercise. Acta Physiologica. 2010 Aug;199(4):499–508.
115. Brooks G. What does glycolysis make and why is it important? J Appl Physiol. 2010 Jun;108(6):1450–1.

116. Rosenstein P, Tennent-Brown B, Hughes D. Clinical use of plasma lactate concentration. Part 1: Physiology, pathophysiology, and measurement. J Vet Emerg Crit Care. 2018 Mar 13;28(2):85–105.
117. Brooks G. The Science and Translation of Lactate Shuttle Theory. Cell Metab. 2018 Apr;27(4):757–85.
118. Thornalley P. The glyoxalase system: new developments towards functional characterization of a metabolic pathway fundamental to biological life. Biochemical Journal. 1990 Jul 1;269(1):1–11.
119. Halperin M, Kamel K. D-lactic acidosis: Turning sugar into acids in the gastrointestinal tract. Kidney Int. 1996 Jan;49(1):1–8.
120. Hove H. Lactate and short chain fatty acid production in the human colon: implications for D-lactic acidosis, short-bowel syndrome, antibiotic-associated diarrhoea, colonic cancer, and inflammatory bowel disease. Dan Med Bull. 1998 Feb;45(1):15–33.
121. Flick M, Konieczny S. Identification of putative mammalian d-lactate dehydrogenase enzymes. Biochem Biophys Res Commun. 2002 Jul;295(4):910–6.
122. Uribarri J, Oh M, Carroll H. D-Lactic Acidosis: A Review of Clinical Presentation, Biochemical Features, and Pathophysiologic Mechanisms. Medicine. 1998 Mar;77(2):73–82.
123. Christopher M, Broussard J, Fallin C, Drost N, Peterson M. Increased serum d-lactate associated with diabetic ketoacidosis. Metabolism. 1995 Mar;44(3):287–90.
124. Christopher M, Eckfeldt J, Eaton J. Propylene glycol ingestion causes D-lactic acidosis. Lab Invest. 1990 Jan;62(1):114–8.
125. Packer R, Cohn L, Wohlstadter D, Shelton G, Naylor J, Zello G, et al. d-Lactic Acidosis Secondary to Exocrine Pancreatic Insufficiency in a Cat. J Vet Intern Med. 2005;19(1):106.
126. Packer R, Moore G, Chang C, Zello G, Abeysekara S, Naylor J, et al. Serum D-Lactate Concentrations in Cats with Gastrointestinal Disease. J Vet Intern Med. 2012 Jul;26(4):905–10.
127. Palsson-Mcdermott EM, O'Neill LAJ. The Warburg effect then and now: From cancer to inflammatory diseases. BioEssays. 2013 Nov;35(11):965–73.
128. Lagutchik M, Ogilvie G, Hackett T, Wingfield W. Increased Lactate Concentrations in III and Injured Dogs. J Vet Emerg Crit Care. 1998 May;8(2):117–27.
129. Hughes D, Rozanski E, Shofer F, Laster L, Drobatz K. Effect of sampling site, repeated sampling, pH, and PCO2 on plasma lactate concentration in healthy dogs. Am J Vet Res. 1999 Apr;60(4):521–4.
130. Rand J, Kinnaird E, Baglioni A, Blackshaw J, Priest J. Acute Stress Hyperglycemia in Cats Is Associated with Struggling and Increased Concentrations of Lactate and Norepinephrine. J Vet Intern Med. 2002;16(2):123.
131. Figueiredo M, Nydam D, Perkins G, Mitchell H, Divers T. Prognostic Value of Plasma L-Lactate Concentration Measured Cow-Side with a Portable Clinical Analyzer in Holstein Dairy Cattle with Abomasal Disorders. J Vet Intern Med. 2006 Nov;20(6):1463–70.
132. Benzon H, Toleikis J, Meagher L, Shapiro B, Ts'ao C, Avram M. Changes in Venous Blood Lactate, Venous Blood Gases, and Somatosensory Evoked Potentials after Tourniquet Application. Anesthesiology. 1988 Nov 1;69(5):677–82.
133. Jones A, Leonard M, Hernandez-Nino J, Kline J. Determination of the Effect of In Vitro Time, Temperature, and Tourniquet Use on Whole Blood Venous Point-of-care Lactate Concentrations. Academic Emergency Medicine. 2007 May 18;14(7):587–91.
134. Christopher M, O'Neill S. Effect of Specimen Collection and Storage on Blood Glucose and Lactate Concentrations in Healthy, Hyperthyroid and Diabetic Cats. Vet Clin Pathol. 2000 Mar;29(1):22–8.
135. Margaria R, Edwards H, Dill D. The possible mechanism of contracting and paying the oxygen debt and the role of lactic acid in muscular contraction. American Journal of Physiology-Legacy Content. 1933 Nov 30;106(3):689–715.

136. Vincent J, De Backer D. Circulatory Shock. N Eng J Med. 2013 Oct 31;369(18):1726–34.
137. Elbers P, Ince C. Mechanisms of critical illness-classifying microcirculatory flow abnormalities in distributive shock. Crit Care. 2006;10(4):221.
138. Durocher L, Hinchcliff K, DiBartola S, Johnson S. Acid-base and hormonal abnormalities in dogs with naturally occurring diabetes mellitus. J Am Vet Med Ass. 2008 May 1;232(9):1310–20.
139. Mcmahon M, Gerich J, Rizza R. Effects of glucocorticoids on carbohydrate metabolism. Diabetes / Metabolism Reviews. 1988 Feb;4(1):17–30.
140. Shah A, Wood D, Dargan P. Understanding lactic acidosis in paracetamol (acetaminophen) poisoning. British J Clin Pharm. 2011 Jan;71(1):20–8.
141. Verelst S, Vermeersch P, Desmet K. Ethylene glycol poisoning presenting with a falsely elevated lactate level. Clin Toxicol. 2009 Mar 7;47(3):236–8.
142. Hopper K, Epstein S. Falsely increased plasma lactate concentration due to ethylene glycol poisoning in 2 dogs. J Vet Emerg Crit Care. 2013 Jan;23(1):63–7.
143. Claus M, Jandrey K, Poppenga R. Propylene glycol intoxication in a dog. J Vet Emerg Crit Care. 2011 Dec;21(6):679–83.
144. Levin G, Bonczynski J, Ludwig L, Barton L, Loar A. Lactate as a Diagnostic Test for Septic Peritoneal Effusions in Dogs and Cats. J Am Anim Hosp Ass. 2004 Sep 1;40(5):364–71.
145. Nestor D, McCullough S, Schaeffer D. Biochemical Analysis of Neoplastic Versus Nonneoplastic Abdominal Effusions in Dogs. J Am Anim Hosp Ass. 2004 Sep 1;40(5):372–5.
146. DeLaurier G, Cannon R, Johnson R, Sisley J, Baisden C, Mansberger A. Increased peritoneal fluid lactic acid values and progressive bowel strangulation in dogs. Am J Surg. 1989 Jul;158(1):32–5.
147. Latson K, Nieto J, Beldomenico P, Snyder J. Evaluation of peritoneal fluid lactate as a marker of intestinal ischaemia in equine colic. Equine Vet J. 2010 Jan 5;37(4):342–6.
148. Peloso J, Cohen N. Use of serial measurements of peritoneal fluid lactate concentration to identify strangulating intestinal lesions in referred horses with signs of colic. J Am Vet Med Ass. 2012 May 15;240(10):1208–17.
149. Delesalle C, Dewulf J, Lefebvre R, Schuurkes J, Proot J, Lefere L, et al. Determination of Lactate Concentrations in Blood Plasma and Peritoneal Fluid in Horses with Colic by an Accusport Analyzer. J Vet Intern Med. 2007 Mar;21(2):293–301.
150. de Laforcade A, Freeman LM, Rozanski E, Rush J. Biochemical analysis of pericardial fluid and whole blood in dogs with pericardial effusion. J Vet Intern Med. 2005;19(6):833–6.
151. Wolak J, Esther C, O'Connell T. Metabolomic analysis of bronchoalveolar lavage fluid from cystic fibrosis patients. Biomarkers. 2009 Feb;14(1):55–60.
152. Chavalittamrong B, Angsusingha K, Tuchinda M, Habanananda S, Pidatcha P, Tuchinda C. Diagnostic Significance of pH, Lactic Acid Dehydrogenase, Lactate and Glucose in Pleural Fluid. Respiration. 1979;38(2):112–20.
153. Curtis G, Newman R, Slack M. Synovial fluid lactate and the diagnosis of septic arthritis. J Inf. 1983 May;6(3):239–46.
154. Gobelet C, Gerster J. Synovial fluid lactate levels in septic and non-septic arthritides. Ann Rheum Dis. 1984 Oct;43(5):742–5.
155. Proot J, Vicente F, Sheahan D. Analysis of lactate concentrations in canine synovial fluid. Veterinary and Comparative Orthopaedics and Traumatology. 2015 Dec 28;28(05):301–5.
156. Dechant J, Symm W, Nieto J. Comparison of pH, Lactate, and Glucose Analysis of Equine Synovial Fluid using a Portable Clinical Analyzer with a Bench-Top Blood Gas Analyzer. Vet Surg. 2011 Jul;no-no.
157. Tulamo R, Bramlage L, Gabel A. Sequential clinical and synovial fluid changes associated with acute infectious arthritis in the horse. Equine Vet J. 1989 Sep 23;21(5):325–31.

158. Magistretti PJ, Allaman I. Lactate in the brain: From metabolic end-product to signalling molecule. Vol. 19, Nature Reviews Neuroscience. Nature Publishing Group; 2018. p. 235–49.
159. Izumi Y, Benz A, Katsuki H, Zorumski C. Endogenous Monocarboxylates Sustain Hippocampal Synaptic Function and Morphological Integrity during Energy Deprivation. J Neurosci. 1997 Dec 15;17(24):9448–57.
160. Chow S. The significance of elevated CSF lactate. Arch Dis Child. 2005 Nov 1;90(11):1188–9.
161. Posner JB, Plum F, York N. Independence of Blood and Cerebrospinal Fluid Lactate. Arch Neurol [Internet]. 1967;16(5):451–564. Available from: http://archneur.jamanetwork.com/
162. Alexander SC, Workman RD, Lambertsen CJ. Hyperthermia, lactic acid infusion, and the composition of arterial blood and cerebrospinal fluid. Am J Physiol. 1961;
163. Cainnes Deanne, Sinclair Melissa, Wood Darren, Valverde Alexander, Dyson Doris, Gaitero Luis, et al. Evaluation of cerebrospinal fluid lactate and plasma lactate concentrations in anesthetized dogs with and without intracranial disease. Can J Vet Res. 2013;(77):297–302.
164. Benedicenti Leontine, Gianotti Giacomo, Evelyin M. Galban. Comparison between cerebrospinal fluid and serum lactate concentrations in neurologic dogs with and without structural intracranial disease. Can J Vet Res. 2018;82–97.
165. Pundir C, Narwal V, Batra B. Determination of lactic acid with special emphasis on biosensing methods: A review. Biosens Bioelectron. 2016 Dec;86:777–90.
166. Nye CJ, Mariani CL. Validation of a portable monitor for assessment of cerebrospinal fluid lactate in dogs. Vet Clin Pathol. 2018 Mar 1;47(1):108–14.
167. Portero M, Martínez de Merlo E, Pérez C, Benito M, Daza MA, Fragio C. Cerebrospinal fluid and blood lactate concentrations as prognostic biomarkers in dogs with meningoencephalitis of unknown origin. Vet J. 2019 Dec 1;254.
168. Shannon D, Shore N, Kazemi H. Acid-base balance in hemorrhagic cerebrospinal fluid. Neurology. 1972 Jun 1;22(6):585–585.
169. Venkatesh B, Morgan T, Boots R, Hall J, Siebert D. Interpreting CSF lactic acidosis: effect of erythrocytes and air exposure. Crit Care Resusc. 2003 Sep;5(3):177–81.
170. Inao S, Marmarou A, Clarke GD, Andersen BJ, Fatouros PP, Young HF, et al. Production and clearance of lactate from brain tissue, cerebrospinal fluid, and serum following experimental brain injury. J Neurosurg. 1988;69:736–44.
171. Begovac J, Baće A, Soldo I, Lehpamer B. Lactate and glucose in cerebrospinal fluid heavily contaminated with blood. Acta Med Croatica. 1991;45(4–5):341–5.
172. Hurtt AE, Smith MO. Effects of iatrogenic blood contamination on results of cerebrospinal fluid analysis in clinically normal dogs and dogs with neurologic disease. J Am Vet Med Ass. 1997 Oct 1;211(7):866–7.
173. Mariani CL, Nye CJ, Tokarz DA, Green L, Lau J, Zidan N, et al. Cerebrospinal fluid lactate in dogs with inflammatory central nervous system disorders. J Vet Intern Med. 2019 Nov 1;33(6):2701–8.
174. Mariani CL, Nye CJ, Ruterbories L, Tokarz DA, Green L, Lau J, et al. Cerebrospinal fluid lactate concentrations in dogs with seizure disorders. J Vet Intern Med. 2020 Nov;34(6):2562–70.
175. Baheerathan A, Pitceathly RDS, Curtis C, Davies NWS. CSF lactate. Pract Neurol. 2020 Aug 1;20(4):322–5.
176. Grille P, Torres J, Porcires F, Bagnulo H. Value of cerebrospinal fluid lactate for the diagnosis of bacterial meningitis in postoperative neurosurgical patients. Neurocirugia. 2012 Jul;23(4):131–5.
177. Mekitarian Filho E, Horita SM, Gilio AE, Nigrovic LE. Cerebrospinal fluid lactate level as a diagnostic biomarker for bacterial meningitis in children. Int J Emerg Med. 2014 Dec 1;7(1):1–4.

178. Huy NT, Thao NTH, Diep DTN, Kikuchi M, Zamora J, Hirayama K. Cerebrospinal fluid lactate concentration to distinguish bacterial from aseptic meningitis: A systemic review and meta-analysis. Crit Care. 2010 Dec 31;14(6).
179. Sakushima K, Hayashino Y, Sc DM, Kawaguchi T, Jackson JL, Fukuhara S. Diagnostic accuracy of cerebrospinal fluid lactate for differentiating bacterial meningitis from aseptic meningitis: A meta-analysis. J Inf. 2011;62(4):255–62.
180. Leib SL, Boscacci R, Gratzl O, Zimmerli W. Predictive Value of Cerebrospinal Fluid (CSF) Lactate Level Versus CSF/Blood Glucose Ratio for the Diagnosis of Bacterial Meningitis Following Neurosurgery. Clinical Infectious Diseases [Internet]. 1999;(29):69–74. Available from: https://doi.org/10.7892/boris.52776
181. Manosalva C, Quiroga J, Hidalgo AI, Alarcón P, Anseoleaga N, Hidalgo MA, et al. Role of Lactate in Inflammatory Processes: Friend or Foe. Vol. 12, Front Immunol. Frontiers Media S.A.; 2022.
182. Awasthi D, Nagarkoti S, Sadaf S, Chandra T, Kumar S, Dikshit M. Glycolysis dependent lactate formation in neutrophils: A metabolic link between NOX-dependent and independent NETosis. Biochim Biophys Acta Mol Basis Dis. 2019 Dec 1;1865(12).
183. Calabrese V, Gruemer H, James K, Hranowsky N, DeLorenzo R. Cerebrospinal Fluid Lactate Levels and Prognosis in Status Epilepticus. Epilepsia. 1991 Dec;32(6):816–21.
184. Parnetti L, Gaiti A, Polidori M, Brunetti M, Palumbo B, Chionne F, et al. Increased cerebrospinal fluid pyruvate levels in Alzheimer's disease. Neurosci Lett. 1995 Oct;199(3):231–3.
185. Su K, Bourdette D, Forte M. Mitochondrial dysfunction and neurodegeneration in multiple sclerosis. Front Physiol. 2013;4.
186. Albanese M, Zagaglia S, Landi D, Boffa L, Nicoletti C, Marciani M, et al. Cerebrospinal fluid lactate is associated with multiple sclerosis disease progression. J Neuroinflamm. 2016 Dec 10;13(1):36.
187. Renfrow J, Frey C, Arnel M, Wolfe S, McLouth C, Datar S. Utility of cerebrospinal fluid lactate in aneurysmal subarachnoid hemorrhage. Surg Neurol Int. 2018;9(1):155.
188. Yamada K, Toribe Y, Yanagihara K, Mano T, Akagi M, Suzuki Y. Diagnostic accuracy of blood and CSF lactate in identifying children with mitochondrial diseases affecting the central nervous system. Brain Dev. 2012 Feb;34(2):92–7.
189. Fitz FR, Reese M. Association between cerebrospinal fluid lactate concentration and central nervous system disease in dogs. Vet Clin Pathol. 2020 Dec 1;49(4):583–9.
190. Plum F, Posner J, Troy B. Cerebral Metabolic and Circulatory Responses to Induced Convulsions in Animals. Arch Neurol. 1968 Jan 1;18(1):1–13.
191. Meldrum B, Nilsson B. Cerebral blood flow and metabolic rate early and late in prolonged epileptic seizures induced in rats by bicuculline. Brain. 1976;99(3):523–42.
192. Oses J, Müller A, Strogulski N, Moreira J, Böhmer A, Hansel G, et al. Sustained elevation of cerebrospinal fluid glucose and lactate after a single seizure does not parallel with mitochondria energy production. Epilepsy Res. 2019 May;152:35–41.
193. Seisdedos A, Galán A, Carletti B, Quirós S, Funes F, Martín E, et al. Anesthetic effects of isoflurane and propofol on cerebrospinal fluid biochemical markers in healthy dogs. Vet Clin Pathol. 2019 Jun 9;48(2):270–5.
194. Anderson D, Prockop L, Means E, Hartley L. Cerebrospinal fluid lactate and electrolyte levels following experimental spinal cord injury. J Neurosurg. 1976 Jun;44(6):715–22.
195. Witsberger T, Levine J, Fosgate G, Slater M, Kerwin S, Russell K, et al. Associations between cerebrospinal fluid biomarkers and long-term neurologic outcome in dogs with acute intervertebral disk herniation. J Am Vet Med Ass. 2012 Mar 1;240(5):555–62.
196. Vander Heiden M, Cantley L, Thompson C. Understanding the Warburg Effect: The Metabolic Requirements of Cell Proliferation. Science (1979). 2009 May 22;324(5930):1029–33.

197. Sugi T, Fujishima M, Omae T. Lactate and Pyruvate Concentrations, and Acid-Base Balance of Cerebrospinal Fluid in Experimentally Induced Intracerebral and Subarachnoid Hemorrhage in Dogs. Stroke. 1975 Nov;6(6):715–9.
198. Pugliese M, Carrasco J, Andrade C, Mas E, Mascort J, Mahy N. Severe cognitive impairment correlates with higher cerebrospinal fluid levels of lactate and pyruvate in a canine model of senile dementia. Prog Neuropsychopharmacol Biol Psychiatry. 2005 May;29(4):603–10.
199. Romero-Fernandez N, Ives E, Fraser A, Williams T, Paul A. Evaluation of the Idexx ProCyte Dx® for analysis of canine cerebrospinal fluid. J Sm Anim Pract. 2020 Feb 25;61(2):110–5.
200. Hoffmann J, Janssen W. Automated Counting of Cells in Cerebrospinal Fluid Using the CellDyn-4000 Haematology Analyser. Clin Chem Lab Med. 2002 Jan 2;40(11).
201. Boer K, Deufel T, Reinhoefer M. Evaluation of the XE-5000 for the automated analysis of blood cells in cerebrospinal fluid. Clin Biochem. 2009 May;42(7–8):684–91.
202. Becker M, Bauer N, Moritz A. Automated flow cytometric cell count and differentiation of canine cerebrospinal fluid cells using the ADVIA 2120. Vet Clin Pathol. 2008 Sep;37(3):344–52.
203. Ruotsalo K, Poma R, da Costa R, Bienzle D. Evaluation of the ADVIA 120 for analysis of canine cerebrospinal fluid. Vet Clin Pathol. 2008 Jun;37(2):242–8.
204. Biercher A, Meller S, Wendt J, Caspari N, Schmidt-Mosig J, De Decker S, et al. Using Deep Learning to Detect Spinal Cord Diseases on Thoracolumbar Magnetic Resonance Images of Dogs. Front Vet Sci. 2021 Nov 2;8.
205. Cihan P, Gokce E, Kalipsiz O. Veterinerlik Alanında Makine Öğrenmesi Uygulamaları Üzerine Bir Derleme. Kafkas Univ Vet Fak Derg. 2017;
206. Jaggy Andrè. Classification of neurological diseases: VITAMIN D. In: Small Animal Neurology, An Illustrated Text. 2010. p. 48–52.
207. Cebra C, Cebra M. Altered mentation caused by polioencephalomalacia, hypernatremia, and lead poisoning. Vet Clin Nth Amer Food Anim Pract. 2004 Jul;20(2):287–302.
208. Divers T. Acquired spinal cord and peripheral nerve disease. Vet Clin Nth Amer Food Anim Pract. 2004 Jul;20(2):231–42.
209. Achard D, Francoz D, Grimes C, Desrochers A, Nichols S, Babkine M, et al. Cerebrospinal Fluid Analysis in Recumbent Adult Dairy Cows With or Without Spinal Cord Lesions. J Vet Intern Med. 2017 May 6;31(3):940–5.
210. D'Angelo A, Bellino C, Bertone I, Cagnotti G, Iulini B, Miniscalco B, et al. Seizure Disorders in 43 Cattle. J Vet Intern Med. 2015 May;29(3):967–71.
211. Washburn K, Streeter R. Congenital defects of the ruminant nervous system. Vet Clin Nth Amer Food Anim Pract. 2004 Jul;20(2):413–34.
212. Scarratt W. Cerebellar disease and disease characterized by dysmetria or tremors. Vet Clin Nth Amer Food Anim Pract. 2004 Jul;20(2):275–86.
213. Tvedten H. Clinical Pathology of Bovine Neurologic Disease. Vet Clin Nth Amer Food Anim Pract. 1987 Mar;3(1):25–44.
214. Fecteau G, Parent J, George L. Neurologic Examination of the Ruminant. Vet Clin Nth Amer Food Anim Pract. 2017 Mar;33(1):1–8.
215. Benninger F, Steiner I. CSF in acute and chronic infectious diseases. In: Handbook of clinical neurology. 2017. p. 187–206.
216. Muhamad Rizal N, Neoh H, Ramli R, A/L K Periyasamy P, Hanafiah A, Abdul Samat M, et al. Advantages and Limitations of 16S rRNA Next-Generation Sequencing for Pathogen Identification in the Diagnostic Microbiology Laboratory: Perspectives from a Middle-Income Country. Diagnostics. 2020 Oct 14;10(10):816.
217. Sweeney M, Sagare A, Zlokovic B. Blood–brain barrier breakdown in Alzheimer disease and other neurodegenerative disorders. Nat Rev Neurol. 2018 Mar 29;14(3):133–50.
218. Ghose C, Ly M, Schwanemann L, Shin J, Atab K, Barr J, et al. The Virome of Cerebrospinal Fluid: Viruses Where We Once Thought There Were None. Front Microbiol. 2019 Sep 6;10.

219. Andrews S. Fast QC, A quality control tool for high throughput sequence data [Internet]. 2010 [cited 2023 Oct 1]. Available from: https://www.bioinformatics.babraham.ac.uk/projects/fastqc/
220. Bolger A, Lohse M, Usadel B. Trimmomatic: a flexible trimmer for Illumina sequence data. Bioinformatics. 2014 Aug 1;30(15):2114–20.
221. Langmead B, Salzberg S. Fast gapped-read alignment with Bowtie 2. Nat Methods. 2012 Apr 4;9(4):357–9.
222. Bolyen E, Rideout J, Dillon M, Bokulich N, Abnet C, Al-Ghalith G, et al. Reproducible, interactive, scalable and extensible microbiome data science using QIIME 2. Nat Biotechnol. 2019 Aug 24;37(8):852–7.
223. Callahan B, McMurdie P, Rosen M, Han A, Johnson A, Holmes S. DADA2: High-resolution sample inference from Illumina amplicon data. Nat Methods. 2016 Jul 23;13(7):581–3.
224. Di Muro G, Cagnotti G, Bellino C, Capucchio M, Colombino E, D'Angelo A. Multiple Cephalic Malformations in a Calf. Animals. 2020 Aug 30;10(9):1532.
225. Moon J, Kim N, Kim T, Jun J, Lee H, Shin H, et al. Rapid diagnosis of bacterial meningitis by nanopore 16S amplicon sequencing: A pilot study. International Journal of Medical Microbiology. 2019 Sep;309(6):151338.
226. Salter S, Cox M, Turek E, Calus S, Cookson W, Moffatt M, et al. Reagent and laboratory contamination can critically impact sequence-based microbiome analyses. BMC Biol. 2014 Dec 12;12(1):87.
227. Van Dyken P, Lacoste B. Impact of Metabolic Syndrome on Neuroinflammation and the Blood–Brain Barrier. Front in Neurosci. 2018 Dec 11;12.
228. Huang C, Lu C, Chuang Y, Tsai N, Chang C, Chen S, et al. Adult Pseudomonas aeruginosa meningitis: high incidence of underlying medical and/or postneurosurgical conditions and high mortality rate. Jpn J Infect Dis. 2007 Nov;60(6):397–9.
229. Gomila M, Pena A, Mulet M, Lalucat J, Garcia-Valdes E. Phylogenomics and systematics in Pseudomonas. Front Microbiol. 2015 Mar 18;6.
230. Johnson J, Spakowicz D, Hong B, Petersen L, Demkowicz P, Chen L, et al. Evaluation of 16S rRNA gene sequencing for species and strain-level microbiome analysis. Nat Commun. 2019 Nov 6;10(1):5029.
231. Chang W, Lu C, Huang C, Chuang Y. Community-Acquired Acinetobacter Meningitis in Adults. Infection. 2000 Dec 1;28(6):395–7.
232. Friedrichs KR, Harr KE, Freeman KP, Szladovits B, Walton RM, Barnhart KF, et al. ASVCP reference interval guidelines: Determination of de novo reference intervals in veterinary species and other related topics. Vet Clin Pathol. 2012 Dec;41(4):441–53.
233. Chen Z, Wang Y, Zeng A, Chen L, Wu R, Chen B, et al. The clinical diagnostic significance of cerebrospinal fluid d-lactate for bacterial meningitis. Clinica Chimica Acta. 2012 Oct 9;413(19–20):1512–5.

AKNOWLEDGMENTS

I wish to express my gratitude to my supervisors Prof Antonio D'Angelo and Dr Giulia Cagnotti for all the support and guidance throughout the challenging journey of these past three years.

I want to thank my colleagues and fellow PhDs Dr Giorgia Di Muro and Dr Eleonora Avilii whose companionship has not only lightened the load but also enriched this academic journey in ways I could not have imagined.

A special note of gratitude goes out to Prof Ugo Ala, whose enlightening and stimulating scientific discussions have been instrumental in shaping my perspective and driving my passion for research.

I would also like to acknowledge the assistance of Prof Elena Grego and Dr Maria Cristina Stella, who patiently supported me during my initial foray into the wet lab, offering guidance and encouragement that were pivotal to my growth as a researcher.

Starting this PhD as a freshly graduated veterinarian, I embarked on a challenging and uncertain journey with passion and determination. Today, I finish my PhD as a scientist, driven by a deep commitment to contribute meaningfully to the advancement of knowledge in the fields of human and veterinary neurological disorders.